Exon Definition Facilitates Reliable Control of Alternative Splicing in the *RON* Proto-Oncogene

Mihaela Enculescu,[1,*] Simon Braun,[1] Samarth Thonta Setty,[2] Anke Busch,[1] Kathi Zarnack,[2] Julian König,[1,*] and Stefan Legewie[1,*]

[1]Institute of Molecular Biology, Mainz, Germany and [2]Buchmann Institute for Molecular Life Sciences, Goethe University Frankfurt, Frankfurt am Main, Germany

ABSTRACT   Alternative splicing is a key step in eukaryotic gene expression that allows for the production of multiple transcript and protein isoforms from the same gene. Even though splicing is perturbed in many diseases, we currently lack insights into regulatory mechanisms promoting its precision and efficiency. We analyze high-throughput mutagenesis data obtained for an alternatively spliced exon in the proto-oncogene *RON* and determine the functional units that control this splicing event. Using mathematical modeling of distinct splicing mechanisms, we show that alternative splicing is based in *RON* on a so-called "exon definition" mechanism. Here, the recognition of the adjacent exons by the spliceosome is required for removal of an intron. We use our model to analyze the differences between the exon and intron definition scenarios and find that exon definition prevents the accumulation of deleterious, partially spliced retention products during alternative splicing regulation. Furthermore, it modularizes splicing control, as multiple regulatory inputs are integrated into a common net input, irrespective of the location and nature of the corresponding *cis*-regulatory elements in the pre-messenger RNA. Our analysis suggests that exon definition promotes robust and reliable splicing outcomes in *RON* splicing.

SIGNIFICANCE   During messenger RNA (mRNA) maturation, pieces of the pre-mRNA (introns) are removed during splicing, and the remaining parts (exons) are joined together. In alternative splicing, certain exons are either included or excluded, resulting in different splice products. Inclusion of *RON* alternative exon 11 leads to a functional receptor tyrosine kinase, whereas skipping results in a constitutively active receptor that promotes epithelial-to-mesenchymal transition and contributes to tumor invasiveness. Intron retention results in deleterious isoforms that cannot be translated properly. Using kinetic modeling, we investigate the combinatorial regulation of this important splicing decision and find that the experimental data support a so-called exon definition mechanism. We show that this mechanism enhances the precision of alternative splicing regulation and prevents the retention of introns in the mature mRNA.

INTRODUCTION

Eukaryotic gene expression is controlled at multiple levels. One important step in eukaryotic gene regulation is splicing, the removal of intronic sequences from pre-messenger RNA (mRNA) precursors to yield mature mRNAs. Spliced mRNAs are then exported from the nucleus and translated into protein. In alternative splicing, certain exons are either included or excluded (skipped) to yield distinct mRNA and potentially protein isoforms. Additional isoforms can arise from intron retention, meaning that one or more introns are not removed during splicing. Alternative splicing is thought to be key to transcriptome and proteome complexity in higher eukaryotes and is perturbed in multiple diseases, including cancer (1–5). The analysis of specific alternative splicing events potentially allows for the identification of new targets for cancer immunotherapy (6,7) and may provide strategies to combat cancer therapy resistance (8).

Mis-splicing involving intron retention usually leads to deleterious isoforms containing stop codons or frameshifts that disrupt the open reading frame. Intron retention thus should be in most cases avoided in alternative splicing regulation because it reduces the amount of functional protein resulting by translation. This is also the case in *RON* because

the intron upstream of alternative exon (AE) 11 contains a stop codon, and the downstream intron shifts the open reading frame. Expression of functional RON protein therefore requires the prevention of intron retention isoforms.

Splicing is catalyzed by a complex molecular machine, the spliceosome, which recognizes splice consensus sequences in nascent pre-mRNAs. The resulting splicing reaction generates mature mRNAs by removing intronic and joining exonic sequences. The catalytic cycle is initiated by recruitment of the U1 and U2 small nuclear ribonucleoprotein (snRNP) subunits to the 5′ splice site and the branch point upstream of the 3′ splice site, respectively. Upon joining of further subunits (U4-U5-U6 snRNPs) and extensive remodeling, a catalytically active higher-order complex is formed. Alternative splicing is commonly regulated by differential recruitment of the U1 and U2 snRNPs. In most cases, such modulation occurs by auxiliary RNA-binding proteins (RBPs), which promote or inhibit U1 or U2 snRNP recruitment by binding to intronic or exonic *cis*-regulatory elements (1,4,9,10).

Spliceosome assembly may occur by two conceptually different mechanisms: in "intron definition," the U1 and U2 snRNPs directly assemble across the intron to form a catalytically competent spliceosome. Alternatively, a cross-exon complex of U1 and U2 snRNPs forms first in a process termed "exon definition" and is then converted into the catalytic cross-intron complex. The simpler intron definition scenario is thought to be the default splicing mechanism for short introns (<200 bp) that allows for efficient cross-intron spliceosome complex formation (11,12). Accordingly, intron definition is prevalent in lower organisms such as *Saccharomyces cerevisiae* and *Drosophila melanogaster* that often display just one or few short introns per gene (12–14). In contrast, exon definition seems to be required for splicing of most mammalian genes because these typically contain long introns and short exons (12–14). The predominant role of exon definition in mammals is supported by splice-site mutation effects on splicing outcomes and by the coevolution of *cis*-regulatory elements across exons (12,14,15). Furthermore, mathematical models accurately described human splicing kinetics when assuming an exon definition mechanism (16,17).

Here, we study how intron and exon definition affect the precision and efficiency of alternative splicing regulation. We compare both mechanisms using mathematical modeling, study their functional implications, and test the models against comprehensive high-throughput mutagenesis data. As a model system, we use a cancer-relevant human alternatively spliced exon in the RON receptor tyrosine kinase gene (*MST1R*), in which the flanking introns are short (87 and 80 nt), implying that both intron and exon definition scenarios are possible (11,12,15). Notably, our data include measurements of all arising isoforms, including the ones that exhibit retention of one or both introns. We find that only exon definition quantitatively explains concerted isoform changes upon sequence mutations. The measured changes in the intron retention isoforms are crucial to distinguish between the two splicing scenarios. This evidences once more the importance of quantifying all present alternative isoforms for the understanding of a specific splicing event (18). We further show that the more complex exon definition pathway provides additional benefits beyond spliceosome assembly across long introns. Our analysis indicates that exon definition greatly simplifies alternative splicing regulation compared to intron definition and efficiently prevents the generation of intron retention products, which are potentially toxic to cells. The presented model provides a framework for the systems-level analysis of complex splice isoform patterns and offers insights into the mechanistic principles of alternative splicing regulation.

METHODS

Extraction and clustering of single point mutation effects on splicing from random mutagenesis screen

We recently established a high-throughput screen of randomly mutated minigenes to decode the *cis*-regulatory landscape that determines splicing of the AE 11 in the proto-oncogene *RON* (*MST1R*). Experimental details and data have been published in (19). Here, we briefly summarize the linear regression model that we used in this previous work to identify single point mutation effects. Furthermore, we describe new, to our knowledge, data analyses performed in this work.

Most mutated minigenes in the random mutagenesis screen contained more than one point mutation. As a result, for most mutations only a combined effect on five splice isoforms (AE inclusion, AE skipping, first intron retention (IR), second IR, and full IR; see Fig. 1 *A*) was measured. Linear regression modeling allowed us to infer the effect of single mutations on the splicing outcomes (see Fig. 1 *B*). The key assumption of the model was that mutation effects on isoform ratios (e.g., skipping/inclusion) add up in logarithmic space (or, equivalently, that mutations have multiplicative effects on isoform ratios). The predictive power of the regression model for individual point mutation effects on the five splice isoforms was confirmed in two ways: 1) RT-PCR measurements of single mutation effects that were not part of the model training data set showed an excellent agreement with the model predictions (Fig. 2 *d* in (19)), and 2) in a cross-validation approach, we found that a model fitted to subsets of the original data could accurately predict single mutation minigenes excluded from the training data set, as soon as the corresponding mutation occurred in at least five minigenes (in combination with other mutations) in the training data set (Fig. 2 *c* in (19)). Based on these findings, we concluded that single point mutation effects on splice isoforms as inferred by regression can be used as a basis for kinetic modeling of splicing decisions. Given the high reproducibility of mutation effects in the initial screen (19), we restricted all analyses described below to the first RNA sequencing replicate in human embryonic kidney (HEK) 293T cells (19).

In Fig. 1 *C*, single point mutation effects on the frequencies of five canonical isoforms (AE inclusion, AE skipping, first IR, second IR, and full IR) were clustered to identify recurrent patterns in mutation-induced splicing changes. In total, 1942 single mutation effects on splicing were inferred from the random mutagenesis screen (and the splice isoform distributions of all these mutation effects are shown in Fig. 1 *B*). The
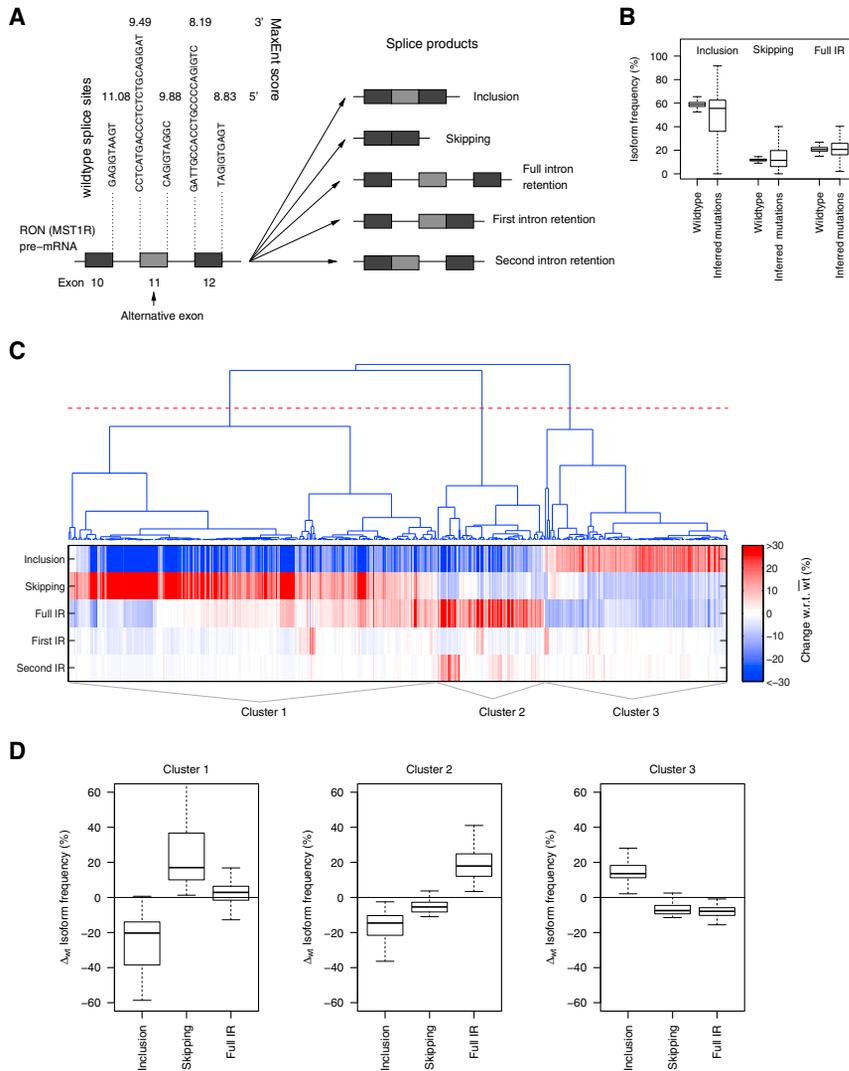
FIGURE 1 Sequence mutations in a three-exon minigene containing *RON* AE 11 induce concerted changes in the distribution of splice isoforms. (*A*) The studied three-exon-minigene (704 bp) contains *RON* AE 11 and the complete adjacent introns and constitutive exons 10 and 12. The wild-type (wt) sequences of the 3′ and 5′ splice sites included in the minigene are shown together with the corresponding MaxEnt splice site scores. Using next-generation sequencing, five different splice products were quantified (as percent of all splice products) for wt minigenes as well as for single point mutations (see Methods and (19)). (*B*) Point mutations induce strong changes in the splice isoform distribution, as visible by the much broader isoform frequency distributions of the mutated minigenes compared to the population of 500 unmutated wt minigenes. Full IR: full intron retention. (*C*) A heat map of splice isoform difference between mutant and wt is plotted for 510 point mutations (*columns*) with a strong effect on the splicing (more than 10% change in at least one isoform frequency with respect to wt). Mutations are sorted using hierarchical clustering (cosine distance), and three main clusters are defined (using the *red line* in the dendrogram as a threshold). (*D*) The same data as in (*C*) are given, represented as boxplots summarizing the isoform distribution of each cluster for the three main isoforms. Mutations in clusters 1 and 3 induce anticorrelated changes in inclusion and skipping. In cluster 1, these changes are most pronounced in absolute terms, and IR is only slightly changed compared to wt. Cluster 3 shows weaker changes and altered IR, though in opposite direction. Mutations assigned to cluster 2 decrease both inclusion and skipping and simultaneously increase full IR.

majority of these mutations, however, induce only small changes in the isoform distribution compared to the wild-type. We therefore selected mutations that induce more than 10% change in at least one of the five canonical isoforms. For each of these 510 mutations, the vector of changes with regards to the wild-type for the five canonical isoforms was built. These vectors were classified using complete linkage hierarchical clustering and the cosine distance as a similarity measure. Note that for clustering and plotting of Fig. 1 *C*, isoform changes of larger than ±30% were bounded to ±30%, whereas the isoform distributions in Fig. 1 *D* do not include such bounding and therefore show larger maximal changes in isoform frequencies.

Kinetic model of binding and steady-state distribution of binding states

Alternative splicing is commonly regulated by differential recruitment of the U1 and U2 snRNPs to the 5′ and 3′ splice sites. Such differential recruitment affects splicing decisions and thus splice isoform distributions (see Fig. 1). To mechanistically understand the emergence of the splice outcome from the binding kinetics, we built an ordinary differential equation (ODE)-based mathematical model (sketched in Fig. 2). We described the U1 and U2 binding kinetics and derived the resulting steady-state distribution of

binding states. Two different splice mechanisms (intron and exon definition; see Fig. 3 *A*) were implemented to connect the binding states to splicing decision and measured splice outcomes.

The minigene analyzed in the work contains three exons and corresponding introns (see Fig. 1). For completion, we also include the 5′ end of the first exon in the model (altogether six splice sites), even though mutations of the first splice site were not present in the data set. Combinatorial binding of spliceosome subunits (U1 or U2 snRNP) to these sites results in a total of 2^6 possible binding states. Fig. 2 shows the considered binding states and examples of possible transitions between them. We can assign each binding state a binary vector with entries 1 at the bound sites and 0 at unbound positions. The completely unbound state (000000) is produced by transcription and can be bound by the spliceosome. Each state can turn into another state by binding of the spliceosome at free splice sites or unbinding of the occupied splice sites. Because we have six binding positions, each state can switch to one of six other states by binding or unbinding. Additionally, we assume splicing can take place and that spliced transcripts are not available for further binding/unbinding. A set of linear ODEs describing the kinetics of the concentration of transcripts in each binding state can be derived. For example, if we denote by n_{001100} the concentration of transcripts in which only both splice sites of the AE are bound, the temporal evolution of n_{001100} will follow
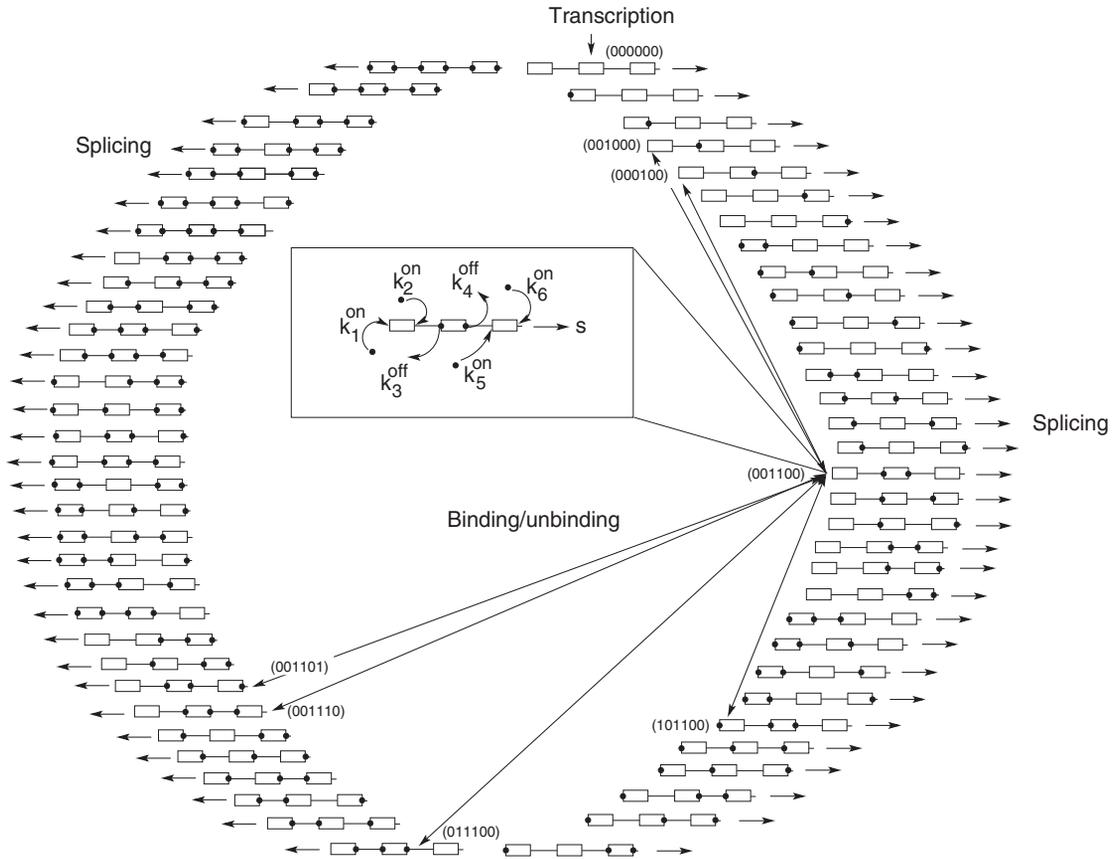
FIGURE 2 Kinetic model for the derivation of the steady-state spliceosome binding probabilities. Each of the six splice sites present in the minigene can be bound (1, *black circles* on pre-mRNA schematic) or unbound (0) by spliceosomal subunits, leading to a total of 2^6 binding states on the pre-mRNA. The unbound pre-mRNA, denoted by (000000), is produced by transcription, and then spliceosome binding reactions eventually take place. An unbound splice site i can be bound at a rate k_i^{on} by the spliceosome, and a bound site i can unbind again at a rate k_i^{off}. For a better overview, these binding reactions are mostly omitted from the scheme, and only exemplary transitions reflecting the possible reactions for the state (001100), in which only both sites of the AE are bound, are shown in the inset and by arrows. Generally, each binding state interacts with six different other states in the kinetic reaction scheme. Additionally, splicing of all binding states occurs at rate s.

$$\frac{dn_{001100}}{dt} = k_1^{off} n_{101100} + k_2^{off} n_{011100} + k_3^{on} n_{000100}$$
$$+ k_4^{on} n_{001000} + k_5^{off} n_{001110} + k_6^{off} n_{001101}$$
$$- \left(k_1^{on} + k_2^{on} + k_3^{off} + k_4^{off} + k_5^{on} + k_6^{on} \right) n_{001100} - s n_{001100},$$

(1)

where k_i^{on} and k_i^{off} are the binding and unbinding rates at splice site i and s is the splicing rate (see Fig. 2 and *inset*). If splicing is slow relative to spliceosome binding and unbinding ($s \ll k_i^{on}, k_i^{off}$, $i = 1, ..., 6$, rapid equilibrium assumption), we can neglect the splicing term in Eq. 1 and simplify the steady-state solution of the ODE system to

$$p_i = \frac{k_i^{on}}{k_i^{on} + k_i^{off}}, i = 1, ..., 6 \tag{3}$$

for each splice site i and express the general steady-state solution in the form

$$\frac{n_k}{premRNA} = \prod_{i,bound} p_i \prod_{j,unbound} \left(1 - p_j \right), \tag{4}$$

where the first product is taken over all bound sites in state k and the second product over all unbound sites in state k.

$$n_{001100} = \frac{k_1^{off}}{k_1^{on} + k_1^{off}} \frac{k_2^{off}}{k_2^{on} + k_2^{off}} \frac{k_3^{on}}{k_3^{on} + k_3^{off}} \frac{k_4^{on}}{k_4^{on} + k_4^{off}} \frac{k_5^{off}}{k_5^{on} + k_5^{off}} \frac{k_6^{off}}{k_6^{on} + k_6^{off}} premRNA \tag{2}$$

and similar structured terms for all other binding states, where *premRNA* = $\sum n_k$ is the total amount of the unspliced transcripts. The special solution 2 can be verified by substitution in Eq. 1 and neglecting splicing terms. We therefore introduce a steady-state recognition probability

Equation 4 states that the probability for the transcript to end in a certain spliceosome binding state is a product of the single probabilities that the splice sites are bound or unbound. In the above derivation for the spliceosome binding states, we assume that binding and unbinding
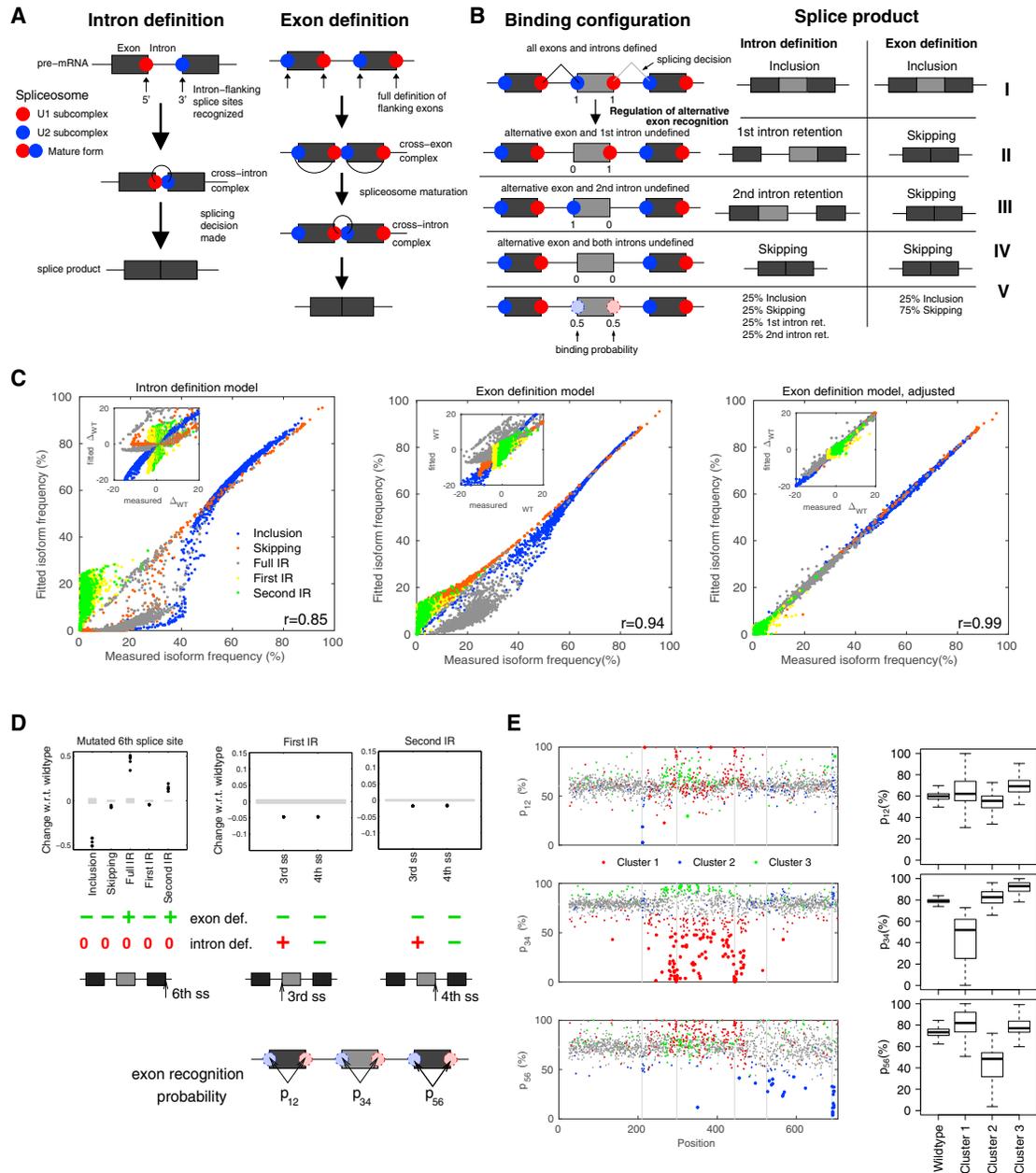
FIGURE 3 The exon definition model quantitatively explains isoform changes in the mutagenesis screen. (*A*) Intron definition model: an intron is spliced out as soon as its 3′ and 5′ splice sites are simultaneously bound by the U1 and U2 snRNP spliceosomal subcomplexes. Exon definition model: full definition of flanking exons is additionally required for the splicing of an intron, as transitory cross-exon complexes are involved in spliceosome maturation. (*B*) Different spliceosome binding configurations (*I–IV*) of the U1 and U2 subcomplexes may result in distinct splice products in the intron and exon definition models. In configuration V, binding at the 3′ and 5′ splice sites of the AE is assumed to take place with 50% probability, giving rise to an equimolar mixture of binding states I–IV. (*C*) The exon definition model (*middle*) shows a better quantitative agreement with the mutagenesis data when compared to the intron definition model (*left*), as judged by the scatter of model fit against measurements of all five splice isoforms for 1854 point mutations. The performance of the exon definition model is further improved by allowing five global parameters (common to all point mutations) to model under-representation of long IR products due to metabolic instability and/or sequencing biases (*right*). The insets compare model fit (*y* axis) versus data (*x* axis) as the difference in splicing outcomes between point mutations and wt (zero: no change relative to wt). In terms of directionality of changes, the exon definition model provides a better match to the measured mutation effects. (*D*) Defined point mutations in the third, fourth, and sixth splice sites (see *bottom sketches*) allow for a categorical discrimination between the intron and exon definition mechanisms. Shown are measured splice isoform differences (relative to wt) for minigenes harboring individual point mutations in the indicated splice sites (*dots*) alongside with the wt standard deviation (*gray shadows*). Directionalities of mutation effects according to the intron and exon definition models—as derived from analytical calculations (Supporting Materials and Methods, Section S1)—are indicated below (*green* for matches with the data, *red* for contradicting results). (*E*) Landscapes and corresponding boxplots showing the exon recognition probabilities (p_{12}, p_{34}, and p_{56}; see scheme) expressed as percent recognition for point mutations along the minigene sequence (*x* axis) according to the best-fit adjusted exon definition model. The dot color indicates to which cluster a mutation was assigned (see legend and Fig.1; mutations with weak effects not included in

(legend continued on next page)

of the spliceosome to the pre-mRNA occur post-transcriptionally. However, as discussed in the following, Eq. 4 is also obtained in the case of co-transcriptional binding and unbinding of the spliceosome, as long as the splicing reaction only occurs once all six relevant splice sites are present in the nascent pre-mRNA. By considering the binding of the spliceosome to a particular splice site i during the process of transcription, we get

$$\frac{dn_0}{dt} = -k_i^{on} n_0 + k_i^{off} n_1, \frac{dn_1}{dt} = +k_i^{on} n_0 - k_i^{off} n_1, \quad (5)$$

where $n_0(t)$ and $n_1(t)$ are the number of transcripts with the splice site i unbound or bound, respectively, and we neglect possible co-transcriptional splicing reactions. During transcription, elongating RNA polymerase II may deposit the spliceosome and associated factors on the nascent transcript (20). Therefore, spliceosome assembly will occur most efficiently in a short time window of opportunity just after splice-site transcription (and, for simplicity, we neglect later spliceosome assembly in our model). If we assume that the time window of opportunity for recognition of this splice site starts at $t = 0$ and ends at $t = \tau_i$, we can solve the corresponding initial value problem with $n_0(0) = N_i, n_1(0) = 0, N_i$ being the total number of transcripts considered. Because we have $n_0(t) + n_1(t) = const. = N_i$, we get, by substituting $n_1 = N_i - n_0$ in Eq. 5,

$$\frac{dn_0}{dt} = k_i^{off} N_i - \left(k_i^{on} + k_i^{off}\right) n_0, \quad n_0(0) = N_i. \quad (6)$$

Equation 6 can be solved by variation of the constants, leading to the solution

$$n_0(t) = N_i \frac{k_i^{off} + k_i^{on} e^{-\left(k_i^{on} + k_i^{off}\right)t}}{k_i^{on} + k_i^{off}}, \quad t \in [0, \tau_i] \quad (7)$$

and subsequently

$$p_i = \frac{n_1(\tau)}{N_i} = \frac{k_i^{on}}{k_i^{on} + k_i^{off}} \left[1 - e^{-\left(k_i^{on} + k_i^{off}\right)\tau_i}\right]. \quad (8)$$

Thus, in the co-transcriptional case, the final probability for a splice site to be bound has the same structure as in the post-transcriptional case but additionally depends on the length of the corresponding time window of opportunity (τ_i). Co-transcriptional spliceosome binding or unbinding therefore introduces a correction term in Eq. 3.

Owing to the rapid equilibrium assumption, Eq. 4 does not hold true in the general case when splicing is not slow compared to binding or unbinding and especially if splicing reactions can take place before downstream exons are transcribed. A more complex model considering the competition of splicing reactions and spliceosome binding and unbinding would include a higher number of model parameters and could not be calibrated properly based on these experimental mutagenesis data. The approximations made above, however, seem to be reasonable for the particular splicing decision considered in this work because the resulting model quantitatively describes our data. Moreover, the minigene under consideration is short (705 bp), so RNA polymerase II with a typical speed of 2 kb/min (21) should complete transcription within less than 20 s, which is well below the reported timescale of splicing (22).

Splice outcome distribution for the intron definition and exon definition mechanisms

To connect the measured splicing outcome to the binding rates k_i^{on} and k_i^{off}, the splice isoform generated from each binding state (i.e., the splicing decision) has to be identified. For six states (see Fig. S1 A), the splicing outcome is identical for both intron and exon definition mechanisms. For example, when all sites are recognized (state 111111), both introns are spliced out, leading to the inclusion isoform. Similarly, if all except the two flanking splice sites of the alternative exon are recognized, the only possible outcome is skipping. Furthermore, for 32 other binding states, no splicing can occur because no matching 3′ and 5′ splice sites are recognized (see Fig. S1 B). Thus, the only possible splicing outcome of these states is full intron retention. For the remaining 26 partially bound states in Fig. S1 C, the splicing outcome depends of the splicing mechanism considered. We have tested two different model variants based on intron and exon recognition mechanisms of splicing (Fig. 3 A). For the intron recognition mechanism, we assume that an intron is spliced out as soon as its 3′ and 5′ sites are recognized. If splicing could occur either across an intron or across a longer sequence containing both introns and the alternative exon (skipping), we assume that the former reaction is much more efficient and neglect the latter. In the exon definition mechanism, an intron is spliced out only if the adjacent exons are also fully defined. The resulting splicing reactions for both mechanisms are indicated in Fig. S1 C. The color codes the splice outcome for each binding state. By adding the steady-state probabilities $n_k/premRNA$ for all binding states leading to a certain splice isoform and using Eq. 4, we get the splice isoform distribution in both models. For the intron definition model, we find the following splice isoform frequencies

$$\begin{aligned} p_{inclusion}^{ID} &= \frac{\text{inclusion}}{\text{all isoforms}} = p_2 p_3 p_4 p_5, \\ p_{skipping}^{ID} &= p_2(1 - p_3)(1 - p_4)p_5, \\ p_{first\ IR}^{ID} &= (1 - p_2 p_3)p_4 p_5, \\ p_{second\ IR}^{ID} &= p_2 p_3(1 - p_4 p_5), \end{aligned} \quad (9)$$

where $p_i, i = 1, \ldots, 6$ are the recognition probabilities of the different splice sites defined in Eq. 3. The splice isoform distribution resulting for the exon definition model reads

$$\begin{aligned} p_{inclusion}^{ED} &= p_1 p_2 p_3 p_4 p_5 p_6, \\ p_{skipping}^{ED} &= p_1 p_2(1 - p_3 p_4)p_5 p_6, \\ p_{first\ IR}^{ED} &= (1 - p_1 p_2)p_3 p_4 p_5 p_6, \\ p_{second\ IR}^{ED} &= p_1 p_2 p_3 p_4(1 - p_5 p_6). \end{aligned} \quad (10)$$

For both models, all frequencies add up to one, implying that the full intron retention probability can be calculated as

$$p_{full\ IR} = 1 - p_{inclusion} - p_{skipping} - p_{first\ IR} - p_{second\ IR}. \quad (11)$$

Note that in the exon definition model, p_1 and p_2 and p_3 and p_4, as well as p_5 and p_6, appear in all formulae only together. We can therefore introduce

$$p_{12} = p_1 p_2, p_{34} = p_3 p_4, p_{56} = p_5 p_6, \quad (12)$$

clustering are plotted in *gray*). Mutations with a recognition probability shift of more than 20% relative to wt are highlighted in bold (only the strongest effect being highlighted for each mutation). Mutations in cluster 2 mainly affect the recognition probability of constitutive exons (p_{12} or p_{56}), whereas mutations in the other two clusters mainly affect alternative exon recognition (p_{34}), although in different directions and to a different extent.

which give the steady-state recognition probabilities of the three exons, and reformulate Eq. 10:

$$p_{\text{inclusion}}^{ED} = p_{12}p_{34}p_{56},$$
$$p_{\text{skipping}}^{ED} = p_{12}(1 - p_{34})p_{56},$$
$$p_{\text{first IR}}^{ED} = (1 - p_{12})p_{34}p_{56}, \quad (13)$$
$$p_{\text{second IR}}^{ED} = p_{12}p_{34}(1 - p_{56}).$$

Remarkably, these splice isoform distributions are robust to the precise implementation of the exon definition mechanism: in our model, we assume that the U1 and U2 snRNPs independently recognize splice sites and that cross-exon and cross-intron complexes form only later, during spliceosome maturation (i.e., they influence only the splicing decision made for a given binding configuration). Alternatively, exon definition may already occur at the level of initial U1 and U2 snRNPs binding because both subunits cooperate across exons during splice-site recognition (14,23). Interestingly, the same isoform distribution formulae as derived above are obtained if we assume highly cooperative binding of U1 and U2 snRNPs across exons; then, the binding space in Fig. 2 reduces to only 2^3 states, in which each of the three exons is either completely bound or completely unbound, each exon having the overall recognition probability given in Eq. 12. The binding state distribution is found as above in Eq. 4, now depending on the recognition probabilities of the exons as a whole given in Eq. 12. Assuming that splicing can occur between two bound exons, the distribution of the splice outcome in Eq. 13 is recovered.

RESULTS

Mutations in the *RON* minigene induce concerted splice isoform changes

Using high-throughput mutagenesis and next-generation sequencing, we recently quantified the splice products originating from a splicing reporter minigene of the *RON* gene for 1942 single point mutations (19). The three-exon minigene covers *RON* alternative exon 11 (147 nt) and the two flanking introns (87 and 80 nt), as well as constitutive exons 10 and 12 (210 and 166 nt, respectively; Fig. 1 *A*). All five splice sites included in the minigene had a comparable wild-type strength, as judged by the MaxEnt 5′ and 3′ scores (Fig. 1 *A*; (24)). The wild-type splice-site scores have an average value when compared to a MaxEnt scan across all GENCODE annotated exons (25).

In HEK293T cells, the major splice product for the unmutated wild-type minigene is exon 11 inclusion (59%), followed by full intron retention (21%), exon 11 skipping (12%), first intron retention (4%), and second intron retention (4%) (Fig. 1, *A* and *B*). 510 out of the 1942 single point mutations quantified in our study induced significant changes of >10% in the relative abundance of any isoform with regard to the wild-type (Fig. 1 *C*). Using hierarchical clustering, we sorted these mutations according to their effect on all isoform frequencies and found three types of splice isoform changes (Fig. 1 *D*): in cluster 1, mutations induced anticorrelated changes in exon 11 inclusion and skipping, with little change in intron retention isoforms. The remaining mutations additionally affected intron retention, either together with correlated changes in exon 11

inclusion and skipping (cluster 2) or with anticorrelated changes in inclusion and skipping (cluster 3). Taken together, these results indicate that mutation effects in *RON* converge on a small set of splice isoform patterns and may contain information about the underlying regulatory mechanisms.

Mathematical modeling discriminates intron and exon definition

We turned to mathematical modeling to mechanistically explain mutation-induced changes in splice isoforms. We assumed that mutations influence the splice-site recognition by the spliceosome and modeled the binding of spliceosomes to the pre-mRNA (Figs. 2 and 3, *A* and *B*). For simplicity, we only described the initial binding events, i.e., U1 and U2 snRNP binding to the 5′ and 3′ splice sites, respectively. Subsequent spliceosome maturation steps were not modeled explicitly, and it was assumed that splicing decisions are made based on the initial U1 and U2 snRNP recognition patterns (see below). In our model, each U1 or U2 snRNP binding step to one of the six splice sites in the three-exon minigene is characterized by a recognition probability p_i. Note that the experimentally measured *RON* minigene lacked the first splice site of exon 10. In the model, we assumed a recognition probability $p_1 = 1$ to mimic that an exon definition complex forms between mRNA cap structure and second splice site. We assumed that U1 and U2 snRNP binding is fast compared to the subsequent spliceosome maturation and splicing catalysis. Then, the probabilities p_i are given by $k_i^{\text{on}}/(k_i^{\text{on}} + k_i^{\text{off}})$, where k_i^{on} and k_i^{off} are the binding and unbinding rates of U1 or U2 snRNP to splice site i (see Methods). For each pre-mRNA molecule, multiple splice sites can be occupied at a time, and depending on the individual recognition probabilities (p_i), such simultaneous binding may occur in different combinations. We describe the combinatorial nature of spliceosome binding by combining the individual recognition probabilities p_i into joint probabilities, one for each of the 64 (2^6) possible U1 and U2 snRNP binding configurations (Fig. 2). For instance, the joint probability of all six splice sites being simultaneously occupied is given by the product $p_1...p_6$, and this term changes to $(1 - p_1)p_2...p_6$ if the first splice site is not occupied.

In the next step, we assigned a splicing outcome to each of the 64 binding states and summed up the probabilities over all binding states yielding the same splicing outcome (Methods and Fig. S1). We thereby describe the frequency of five splice isoforms as a function of six splice-site recognition parameters (p_i). By fitting this model to the measured mutation-induced isoform changes, we infer how mutations affect spliceosomal recognition of splice sites (see below).

In two alternative model variants, we implemented splicing decisions based on intron definition and exon definition mechanisms (Fig. 3, *A* and *B*): for the intron definition

model, it was assumed that an intron can be spliced out as soon as its flanking 5′ and 3′ splice sites are simultaneously occupied by U1 and U2 snRNPs (Fig. 3 A, left). If multiple competing splicing reactions are possible in a binding configuration, we assumed that splicing occurs across the shortest distance (Figs. 3 B and S1). The exon definition model involves an additional layer of regulation: before catalytic cross-intron complexes can form, transitory cross-exon U1-U2 snRNP complexes are required to stabilize initial U1/U2 snRNP binding to splice sites (Fig. 3 A, right). We implemented this additional requirement for cross-exon complexes by assuming that an intron can only be spliced if all splice sites flanking the adjacent exons are occupied ("defined"). For example, splicing of the first intron requires full definition of neighboring exons 10 and 11, i.e., simultaneous recognition of splice sites 1–4 in the three-exon minigene (Figs. 3 B and S1). Importantly, 26 out of 64 binding configurations generate distinct splicing outcomes in the exon and intron definition models (Fig. S1). Hence, we expect that concerted isoform changes in our mutagenesis data set (Fig. 1) will discriminate between intron and exon definition mechanisms.

High-throughput mutagenesis data support the exon definition model

To investigate whether our mutagenesis data evidence intron and/or exon definition, we separately fitted these model variants to the measured frequencies of five splice isoforms for the wild-type sequence and 1854 out of 1942 single point mutations. We excluded 88 that resulted in >5% noncanonical isoforms, e.g., when mutations generate or activate additional splice sites in the minigene sequence (see Table S1). During fitting, we assumed that mutations affect the recognition of one or multiple splice sites. In exon definition, the U1 and U2 snRNPs affect splicing only if they are simultaneously bound to both splice sites of an exon. Therefore, splicing outcomes depend only on three effective parameters (p_{12}, p_{34}, p_{56}), each reflecting the recognition probability of the complete exon. Thus, in exon definition, there are three free parameters per mutation variant, whereas intron definition results in four independent parameters (see Methods and Supporting Materials and Methods, Section S2).

Despite its lower degree of freedom, the exon definition model provides an overall better fit to the mutagenesis data when compared to the intron definition model (Pearson correlation coefficients = 0.94 vs. 0.85, respectively; Fig. 3 C, left and middle panels). The fit quality can be further improved if we additionally allow five global parameters (shared between all mutation variants) to accommodate that long intron retention products may be under-represented in the RNA sequencing library because of metabolic instability (faster degradation of unspliced transcripts (26)) and/or sequencing biases (such as PCR amplification or clustering problems for long fragments on the Illumina

flow cell (San Diego, CA)). Taken together, these quantitative results favor exon definition as the predominant mechanism of RON splicing.

Qualitative arguments based on the algebraic sign of mutation-induced splice isoform changes further disfavor the intron definition model: first, isoform changes in the best-fit intron definition model frequently occur in the opposite direction compared with the data, whereas this is not the case for the best-fit exon definition model (Fig. 3 C, insets). Second, using analytical calculations, we show that the direction of isoform changes for splice-site mutations completely abolishing spliceosome binding is fully consistent with exon definition but frequently disagrees with intron definition (Figs. 3 D and S2 and Supporting Materials and Methods, Section S1). This is particularly evident for mutations of the last splice site (5′ splice site of exon 12), which induce characteristic changes in all splice isoforms (Fig. 3 D, left panel). Here, the exon definition model perfectly describes the isoform changes observed in the data, whereas the intron definition model predicts that the sixth splice site does not contribute at all. Notably, the measurement of partial and full intron retention isoforms turns out to be essential for the discrimination of intron and exon definition because it increases considerably the number of experimentally accessible opposite splice-site mutation effects.

Taken together, these results strongly support that RON exons 10–12 are spliced via the exon definition mechanism, even though they are flanked by two short introns. Thus, in human cells, exon definition may be the preferred and more efficient splicing mechanism, even if the gene structure (intron length) permits the simpler intron definition mode. Currently, it is difficult to generalize this finding to other human genes because mutagenesis data including quantification of intron retention isoforms are not available in the literature.

Notably, our conclusions concerning RON splicing are robust to the precise implementation of the exon definition mechanism: in our model, we assume that the U1 and U2 snRNPs independently recognize splice sites and that cross-exon and cross-intron complexes form only later, during spliceosome maturation. Alternatively, exon definition may already occur at the level of initial U1 and U2 snRNP binding because both subunits cooperate across exons during splice-site recognition (16,23). We find that both scenarios lead to the same splice isoform probability equations, implying that our fitting results also apply for strong cross-exon cooperation of U1 and U2 snRNP binding (see Methods).

Modeling infers spliceosome relocation upon mutations and RBP knockdowns

To further validate the biological plausibility of the exon definition model, we analyzed how the exon recognition probabilities (p_{12}, p_{34}, p_{56}) are perturbed by point mutations

in the best-fit model. In line with the intuitive expectation, we find that strong changes in exon recognition require point mutations to be located either within or in close vicinity to the respective exon (Fig. 3 *E*). For the outer constitutive exons, strong mutation effects are mostly confined to the corresponding splice sites, whereas the alternative exon is additionally regulated by a large number of non-splice-site mutations. This reflects the extensive regulation of alternative (but not constitutive) exons by nearby *cis*-regulatory elements. The recognition probability landscapes also provide plausible explanations for the concerted splice isoform changes we had identified by clustering (Fig. 1): concerted changes in exon 11 inclusion and skipping (cluster 2) are explained by changes in constitutive exon recognition (p_{12} and p_{56}). On the contrary, any type of anticorrelated change in exon 11 inclusion and skipping (clusters 1 and 3) is assigned to perturbed AE recognition (parameter p_{34}), p_{34} being affected with opposing directionality in each of the clusters (decreased p_{34} in cluster 1 and increased p_{34} in cluster 3).

In Fig. S3, we relate positive and negative mutation effects on the three exon recognition probabilities (model fit) to the presence of binding motifs of *trans*-acting RBPs in the minigene sequence. The positions with the strongest splicing effects in the model are found within the alternative exon and are related to strengthening or weakening AE recognition due to affected heterogeneous nuclear ribonucleoprotein H (HNRNPH) binding sites, as we showed in detail in Fig. S3 *A* (19). We further analyzed the minigene sequence with the Human Splicing Finder, Version 3.1 (27) and found a multitude of putative exonic splicing enhancers and silencers, as summarized in Fig. S3 *B* and Table S2

Next, we asked whether our model allows us to quantify the effects of knockdowns of *trans*-acting RBPs that control *RON* splicing. Using capillary electrophoresis-based quantification of exon 11 inclusion and skipping, we confirmed previously reported effects of 13 RBP knockdowns on alternative splicing of our minigene and endogenous *RON* transcripts in HEK293T cells (see Fig. S4 *A*; (28)). This result further supported that our minigene accurately resembles endogenous regulation of *RON* exon 11 splicing. For five of these knockdowns (*HNRNPH*, *PRPF6*, *PUF60*, *SMU1*, and *SRSF2*), we performed in-depth RNA sequencing of the full minigene library and found characteristic patterns of exon 11 inclusion and skipping and first and second as well as full intron retention for each perturbation in the population of wild-type minigenes (Fig. S4 *B*). To infer how the three exon recognition probabilities are affected by RBP knockdowns, we fitted the exon definition model to the knockdown data (Fig. S4 *C*). We find that *HNRNPH* knockdown selectively enhances the recognition of the alternative exon (p_{34}), implying that this RBP is a specific inhibitor of exon 11 inclusion. This agrees with our previous finding in human MCF7 cells that although HNRNPH binds throughout the *RON* minigene sequence, splicing control is mainly executed via a cluster of binding sites within the alternative exon (19). In Fig. S4 *D*, we confirm that in HEK293T cells, HNRNPH similarly affects splicing outcomes by binding to the alternative exon. For PUF60, the model predicts a similar mode of action as for HNRNPH, i.e., specific inhibition of the alternative exon, reflected in increased inclusion in the knockdown (Fig. S4, *B* and *C*). Conversely, *PRPF6* knockdown drastically reduced the AE recognition probability, resulting in more than 70% exon skipping. Despite being an integral spliceosome component, a specific regulation of distinct target exons by *PRPF6* has been observed before (29). Finally, knockdown of *SMU1* and *SRSF2* seems to more generally impair splicing efficiency, as evidenced by a marked increase in full intron retention, by lowering the recognition probability of two or all three exons, respectively. This is in line with the idea that SR proteins are splicing activators that promote both constitutive and alternative splicing (30). Moreover, SMU1 was shown to be specifically required for spliceosome activation on short introns as present in our minigene (31). Taken together, the alternative exon is affected by all RBP knockdowns and thus seems to be more heavily regulated, as expected, when compared with the flanking constitutive exons.

Hence, fitting the exon definition model to perturbation conditions allows us to reconstruct how RBPs affect the splice-site recognition by the spliceosome. This constitutes a first step toward reconstruction and mechanistic modeling of combinatorial splicing networks, in which many RBPs jointly control splicing.

Benefits of splicing regulation by an exon definition mechanism

To explore the biological benefits of exon definition beyond the recognition of exons flanked by long introns, we performed simulations using our splicing models. Interestingly, these simulations revealed that exon definition facilitates alternative splicing control when compared to intron definition. In our models, we simulate alternative splicing regulation by modulating the recognition probability of exon 11 at its 3′ or 5′ splice site. This mimics point mutations or the binding of regulatory RBPs near these splice sites. In the intron definition mechanism, splicing outcomes are very distinct, depending on whether p_3 and p_4 are separately or jointly regulated (Fig. 4 *A*, *left* and Supporting Materials and Methods). In contrast, in the exon definition model, splicing outcomes are identical, irrespective of how the recognition of the 3′ and 5′ splice site of the alternative exon is regulated (Fig. 4 *A*, *right*). Thus, only for exon definition, the alternative exon serves as a regulatory module that integrates inputs on both exon-flanking splice sites into a joint recognition probability p_{34} of the alternative exon 11. This modularization simplifies alternative splicing control and ensures that splicing outcomes are robust to the precise location and nature of *cis*-regulatory elements in the pre-mRNA sequence. Therefore, the seemingly more complex
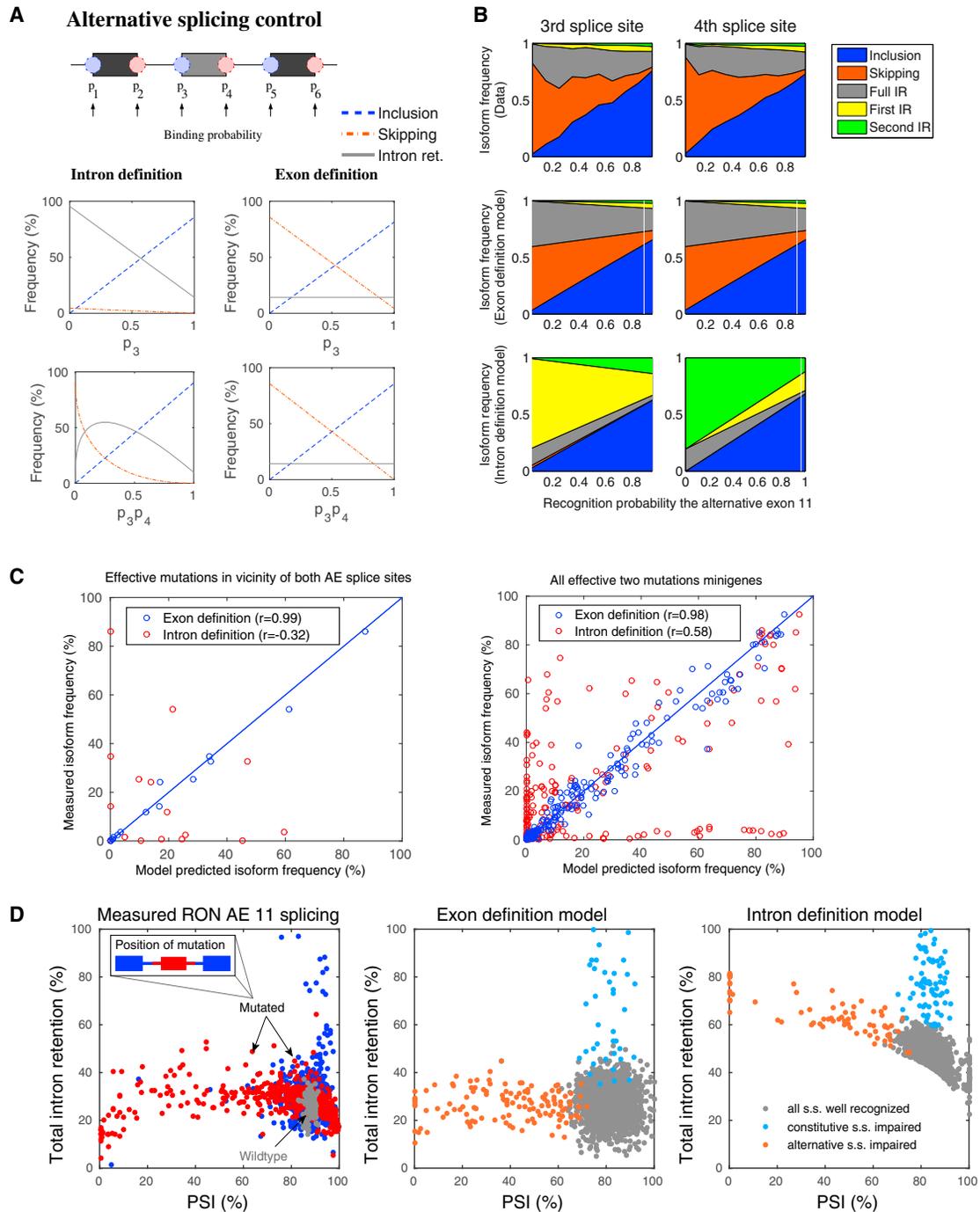
FIGURE 4 Exon definition allows for modular control of alternative splicing and prevents accumulation of IR products. (A) Simulated splice product frequency of inclusion, skipping, and total IR (sum of first, second, and full IR isoforms) in response to varying recognition of the splice sites flanking the alternative exon. Simulations of the intron and exon definition models are shown in the left and right columns, respectively. The upper plots show the splicing probabilities obtained when only the binding probability of the 3′ splice site (p_3) is varied (similar plots are obtained for variation of p_4; data not shown). The bottom plot displays the effects of concerted variation of the two recognition probabilities (p_3 and p_4, x axis: product $p_3 p_4$). In the intron definition scenario, skipping is possible only if p_3 and p_4 are simultaneously regulated and is accompanied by enhanced IR. For the exon definition model, separate or joint changes in p_3 and/or p_4 lead to a switch from skipping to inclusion, without accumulation of IR isoforms. (B) Mutagenesis data confirm the modular control of exon 11 splicing found in the exon definition scenario. Point mutations at positions in a ± 30 nt window around the 5′ (left column) or 3′ (right column) splice sites of exon 11 were selected and sorted according to their effect on the AE recognition probability in the best-fit model (adjusted exon definition model). The measured changes in the splice isoform fractions with varying mutation strength (first row) are similar for both splice sites and agree with simulations of the exon definition model in which p_{34} is systematically varied (second row) but disagree with the intron definition model (third row). See also main text and Supporting Materials and Methods, Section S3. (C) An exon definition model trained on single point mutation data accurately predicts the abundance of five splice isoforms for combined mutations. Measured isoform frequencies in minigenes containing two mutations are plotted against values predicted by an exon definition model fitted only to

(legend continued on next page)

exon definition mechanism in fact simplifies alternative splicing control.

Exon definition further seems beneficial because it prevents the accumulation of potentially toxic intron retention products during splicing regulation; using simulations and analytical calculations, we find that the sum of all intron retention products remains constant in the exon definition model if splicing is regulated by the AE recognition parameter p_{34} (Fig. 4 *A*, *red lines* and Supporting Materials and Methods, Section S5). In these simulations, the degree of intron retention is solely determined by the recognition probabilities of the outer constitutive exons (p_{12} and p_{56}). On the contrary, the intron definition mechanism inevitably leads to a strong accumulation of retention products during alternative splicing regulation, especially if the splice-site-recognition probabilities p_3 or p_4 are regulated separately (Fig. 4 *A*, *left* and Supporting Materials and Methods, Section S5). In fact, in the intron definition model, pronounced switching from inclusion to skipping isoforms is only possible if p_3 and p_4 are concurrently regulated. However, even in this scenario, intron retention species account for $\geq 50\%$ of the splice products during the splicing transition (Supporting Materials and Methods, Section S5).

Using analytical calculations, we confirm that exon modularity and suppression of intron retention also occur for pre-mRNAs containing four exons (see Supporting Materials and Methods, Section S6 and Discussion). This suggests that exon definition is generally beneficial from a regulatory point of view.

Exon definition modularizes splicing regulation

Our simulations show that exon definition modularizes splicing control and prevents the accumulation of intron retention products. To confirm the predicted modularity of alternative splicing regulation, we compared the effects of point mutations located at 3′ and 5′ splice sites of the alternative exon. Because the exon functions as a module in the exon definition model, we expect that these mutations should have very similar effects on the abundance of splice products. We considered all mutations within a ± 30 nt window around the 3′ and 5′ splice sites of exon 11. To account for mutation strength, we sorted mutations according to their effect on the AE recognition probability (p_{34}) in the best-fit model. Then, we plotted the experimentally

measured splice isoform abundances as a function of the assigned mutation strength (Fig. 4 *B*). As found in the simulations of the exon definition model, the observed mutation-strength-dependent isoform changes are almost identical for 3′- and 5′-associated mutations. Furthermore, the measured isoform patterns quantitatively agree with simulations of an exon definition model, in which the AE recognition parameter p_{34} is systematically varied at otherwise constant recognition probabilities (Fig. 4 *B*, *second row*). In contrast, corresponding simulations of the intron definition model completely fail to match the data (Fig. 4 *B*, *third row*). In further support for the exon definition model, we observe highly similar flanking mutation effects not only around the alternative exon but also for the constitutive exon 12 (Fig. S5). In contrast, the intron definition model would predict congruence of mutation effects flanking a common intron, but this behavior is not supported by the experimental data (Figs. 4 *B* and S5). These observations confirm that exon definition allows exons to function as dominant regulatory modules in alternative splicing control.

To further support that modular exons integrate regulation at the 3′ and 5′ splice site into a joint splicing outcome, we turned to the analysis of combined mutation effects. Therefore, we fitted the adjusted exon definition model to the subset of minigenes harboring only a single mutation and predicted splicing outcomes of minigenes with a combination of two mutations. The exon definition model accurately captures how two simultaneous mutations in the vicinity of the 3′ and 5′ splice site of exon 11 (each having a strong effect on splicing) jointly affect splicing outcomes (Fig. 4 *C*, *left panel*). More generally, the exon definition model accurately predicts the combined outcome of any two mutations throughout the minigene (Fig. 4 *C*, *right panel*). In contrast, a similarly trained intron definition model fails to correctly predict combined mutation effects (Fig. 4 *C*, *red dots*).

Taken together, we find that integration of splice-regulatory input signals in *RON* follows an exon definition scenario, which has profound impact on the controllability of alternative splicing.

Exon definition prevents the accumulation of undesired intron retention products

An important observation in our splicing simulations of the exon definition model is that intron retention products

---

single point mutation measurements. The left panel shows three combinations of mutations in a ± 30 nt window around the 3′ and 5′ splice sites of the alternative exon, and the right panel shows all 45 present combinations of two arbitrary mutations throughout the minigene. Only single mutations that induce strong changes were considered (sum of absolute changes in all five isoforms >20%). See Supporting Materials and Methods, Section S4 for details. (*D*) Alternative splicing occurs at low levels of IR in the mutagenesis data (*left panel*). Shown is the sum of all retention products as a function of the PSI metric (PSI = AE inclusion/(AE inclusion + AE skipping)), which measures alternative splicing of exon 11. The distribution of wt minigenes is shown by gray dots, and each colored dot represents a single point mutation. Mutations located to the outer constitutive (and adjacent intron halves) are highlighted in blue, whereas the red dots show corresponding mutation effects in or around the alternative exon (see legend). The middle and right panels show 2000 simulations of the exon and intron definition models, respectively. In these simulations, the splice-site-recognition parameters ($p_1, \ldots, p_6$) were randomly perturbed, one randomly chosen parameter being more affected than the others to mimic the experimentally measured PSI and IR values (see Supporting Materials and Methods, Section S5 for details). Only exon definition allows for alternative splicing at low IR levels.

remain constant if splicing is regulated at the AE (by the AE recognition parameter p_{34}, Fig. 4 A). In contrast, intron retention products inevitably accumulate during alternative splicing regulation in the intron definition model (Fig. 4 A). To intuitively understand why intron and exon definition differentially affect retention products, consider discrete spliceosome binding configurations (Fig. 3 B). If all six splice sites in the three-exon pre-mRNA are occupied by U1 and U2 snRNPs, the splicing outcome is exon inclusion for both mechanisms (Fig. 3 B, I). In the next step, alternative splicing can be induced by reducing the recognition of one or both splice sites of the alternative exon. In exon definition, such regulation yields only exon skipping because the middle exon is always incompletely recognized, and this impairs splicing of both introns (Fig. 3 B, II–IV). In contrast, retention products accumulate in intron definition because one of the introns remains defined and is therefore spliced (Fig. 3 B, II–IV). Our model translates these qualitative arguments into continuous and quantitative predictions of splicing outcomes for five isoforms. For instance, it predicts that in intron definition, retention products strongly accumulate even if the recognition probability of both splice sites is reduced jointly, e.g., to 50% ($p_3 = p_4 = 0.5$). This is because combinatorial spliceosome binding to the 3′ and 5′ splice sites results in an equally distributed mixture of four binding configurations, two of which result in retention products (Fig. 3 A, V). Hence, exon definition seems superior when compared to intron definition because it prevents the accumulation of potentially deleterious intron retention products.

To verify that alternative splicing of *RON* exon 11 is controlled without intron retention, we compared the predictions of our exon definition model to the experimental data. To this end, splicing of the alternative exon was quantified for each point mutation using the PSI metric (percent spliced in; PSI = AE inclusion/(AE inclusion + AE skipping)) and then plotted against the corresponding total intron retention level, i.e., the sum of the full, first, and second intron retention isoforms (Fig. 4 D, left panel). In line with the exon definition model, we observed that the majority of point mutations (*red* and *blue dots*) induce shifts in alternative splicing (PSI) at almost constant intron retention levels when compared with the wild-type (*gray dots*). Only a minority (<2%) of mutations show strong effects on intron retention, but these have in turn only minor effects on the PSI.

These orthogonal changes in either exon inclusion or intron retention could be explained by simulations of the exon definition model, in which we randomly perturbed one of the splice-site-recognition probabilities while sampling the others close to their reference value (Fig. 4 D, middle panel). The model traces changes in PSI at constant retention levels back to altered splice-site recognition of alternative exon 11 (*red dots*), whereas intron retention enhancement at constant PSI involves reduced recognition of the outer constitutive exons (*blue dots*, Supporting Mate-

rials and Methods, Section S5). Consistently, we find in the experimental data that mutations with strong effect on intron retention map to the constitutive exons (Fig. 4 D, left; *blue dots*), whereas mutations affecting PSI are located within or close to the AE (Fig. 4 D, left; *red dots*). Simulations of the intron definition model fail to reconcile the data because the PSI cannot be modulated without accumulation of retention products (Fig. 4 D, right panel; Supporting Materials and Methods, Section S5). In conclusion, modeling and comprehensive mutagenesis data suggest that alternative splicing by an exon definition mechanism prevents mis-splicing over a wide range of exon inclusion levels. This is likely to be important for RON protein function because all intron retention events in this splicing decision give rise to premature stop codons in the mature mRNA.

DISCUSSION

Regulatory networks need to produce a certain outcome in a highly precise and controllable fashion. Mathematical models are valuable tools to understand the design principles of cellular networks that ensure robustness and precision (32–34). To date, only a handful of mechanistic modeling studies on alternative splicing have been published. These mainly focused on the quantification of mutation effects (16,19,35), studied the impact of cotranscriptional splicing (17,36), and analyzed the cell-to-cell variability of the process (22,37). Here, we approach splicing regulation from a different angle and mechanistically describe how splice-site recognition by the spliceosome shapes the splicing outcome. We systematically compare intron and exon definition mechanisms and find that exon definition ensures robust yet simple regulation of *RON* alternative splicing. Thereby, we gain general insights into the efficiency and controllability of splicing.

Using data-based modeling, we identified exon definition as the mechanism of *RON* exon 11 splicing. The prevalence of exon definition is surprising, given that the flanking introns are very short. Previous work showed that vertebrate exons flanked by short introns can switch to an intron definition mechanism if cross-exon spliceosome complexes are inhibited, e.g., by artificially lengthening the exon (12) or by the lack of exonic splicing enhancer elements (38). Our data indicate that a short intron length is not sufficient to switch to intron definition in a natural human exon and that exon definition is more efficient than intron definition in human cells (to further exclude splicing by an intron definition mechanism, we also considered mixed intron and exon definition models in which only a subset of the three exons acts as a functional unit, whereas the remainder affect splicing already when partially defined. Interestingly, only the full exon definition model was consistent with the mutagenesis data, further suggesting that none of the two *RON* introns are spliced by a direct cross-intron spliceosome complex (data not shown)).

Accordingly, we find that exon definition leads to a modularization of splicing regulation. Hence, regulation at one splice site of an exon is transferred to the other splice site such that exons act as functional units. This has important consequences for the robustness and control of alternative splicing: our simulations highlight that for pure intron definition, splicing outcomes would be very distinct if splice-regulatory inputs affect the 3′ or the 5′ splice site of the alternative exon (Fig. 4). Furthermore, exon skipping may be difficult to achieve with intron definition unless both splice sites are jointly regulated (Fig. 4). Accordingly, a global survey of *D. melanogaster* alternative splicing indicated that exons with short flanking introns (likely spliced by an intron definition mechanism) show a strong trend against exon skipping (38). In contrast, in the modular exon definition, inputs at the 3′ and 5′ splice site (or combinations thereof) produce the same splicing outcome. Such signal integration by exon definition is likely to be physiologically relevant because RBPs frequently control alternative exons by binding near only one of the flanking splice sites (39). Arguably, a given RBP can repress or activate splicing depending on its binding position relative to an alternative exon (39). Our model does not exclude such a scenario but predicts that the net effect of the RBP is integrated in a simple way with signals from other RBPs. In conclusion, exon definition allows for reliable splicing regulation, even though alternative exons are typically influenced by a whole battery of distinct *cis*-regulatory elements (10,11,40,41).

Exon definition further prevents the accumulation of potentially nonfunctional intron retention products and thereby improves the fidelity and efficiency of alternative splicing. In line with our observation that intron retention is difficult to achieve in the exon definition scenario, human splice-site mutations most often cause exon skipping and rarely result in intron retention (12). If retention occurs, the mutations are typically located in short introns or affect the first or terminal intron of a pre-mRNA, both of which may be more prone to splicing by an intron definition mechanism (12). Intron retention can also serve as a means of active cellular regulation of gene expression. For instance, during granulocyte differentiation, intron retention is enhanced for dozens of genes. Interestingly, this involves a switch from exon to intron definition because splice factors that favor intron definition complexes are upregulated, which promotes the retention of short introns with weak splice sites (42,43). Our finding that alternative splicing is coupled to intron retention in the intron definition scenario may explain why exon definition is the dominant splicing mechanism in human cells. In contrast, in simpler organisms like *S. cerevisiae*, intron definition may be more prevalent because alternative splicing is largely restricted to the regulated retention of a small number of short introns (43).

In this work, we analyzed a prototypical splicing unit consisting of three exons. Most human genes contain at least four exons, raising the question whether the described regulatory principles also apply for these more complex scenarios. In the Supporting Materials and Methods, we analyze an extended exon definition model containing four exons and show that the inclusion frequency (PSI) of each internal exon is solely determined by its own recognition probably (Supporting Materials and Methods, Section S6). Thus, the inclusion of an exon is regulated independently of the neighboring exons. Importantly, this modularity not only involves reliable signal integration on an exon but also ensures insulation of this exon from other alternative splicing events. In analogy to the three-exon scenario, total intron retention is solely determined by the recognition probabilities of the flanking exons and uncoupled from exon inclusion, i.e., alternative splicing regulation occurs without the accumulation of retention products. Taken together, this suggests that the regulatory benefits of exon definition described in this work continue to hold for more complex pre-mRNAs containing multiple exons.

Genome-wide sequencing indicates that 80% of human exons are spliced co-transcriptionally while RNA polymerase II is elongating the transcript (13). In this work, we assumed that splicing occurs with a delay after nascent RNA synthesis. In the Methods, we show that our model continues to hold true if spliceosome assembly (exon definition) occurs co-transcriptionally, i.e., just after exon synthesis. However, for the model to be valid, the subsequent splicing reactions must only take place after spliceosome binding to the three exons of the considered splicing decision is complete and has reached a steady state. Hence, we assumed that the timescales of nascent RNA synthesis and spliceosome binding are fast compared to that of splicing. Notably, this assumption does not exclude that splicing occurs while the transcript is still attached to elongating RNA polymerase II. Evidence from the literature supports that splicing of human introns occurs with a delay after nascent RNA synthesis (44) and begins only several kilobases after an intron-exon junction leaves the RNA polymerase II complex, with the lag being especially pronounced for alternatively spliced exons (45). Given the median length of human exons and introns (145 and 1964 bp, respectively (1)), the splicing machinery thus likely generates splicing decisions based on sequence stretches containing multiple exons, allowing for neighboring human introns to be spliced concurrently (45,46) or even in inverse order relative to transcription (39,45,46). In simpler organisms, splicing is tightly coupled to the exit from the RNA polymerase II (45,47). Thus, the kinetics of splicing may have coevolved with mechanisms of splice decision making, with slower kinetics being beneficial for exon definition and thus for precise alternative splicing.

CONCLUSION

Our modeling framework integrates the effect of sequence mutations and knockdowns of *trans*-acting RBPs on

spliceosome recruitment and splicing outcomes (Figs. 3 and S4). Thus, it constitutes a first step toward a comprehensive network model of splicing that mechanistically describes the integration of multiple splice-regulatory inputs into a net splicing outcome. In fact, we can successfully predict how multiple point mutations jointly control splicing outcomes (Fig. 4 C), and the same type of prediction is possible for combined RBP knockdowns and a combination of RBP knockdown and sequence mutations. Conceptually, the modeling framework resembles thermodynamic models of transcriptional gene regulation (48–50). However, for the case of splicing, regulation is more complex compared to transcription because both the regulators (RBPs) and the effectors (spliceosomes) show combinatorial binding to multiple sequence elements. Owing to this high level of complexity at multiple levels of splicing regulation, we believe that mechanistic splicing models such as the one presented here will be essential to fully disentangle the intricate networks of splicing regulation.

The sequencing data generated in this study are available from ArrayExpress: E-MTAB-8816.

SUPPORTING MATERIAL

Supporting Material can be found online at https://doi.org/10.1016/j.bpj.2020.02.022.

AUTHOR CONTRIBUTIONS

ACKNOWLEDGMENTS

REFERENCES

1. Lee, Y., and D. C. Rio. 2015. Mechanisms and regulation of alternative pre-mRNA splicing. *Annu. Rev. Biochem.* 84:291–323.

2. Xiong, H. Y., B. Alipanahi, …, B. J. Frey. 2015. RNA splicing. The human splicing code reveals new insights into the genetic determinants of disease. *Science.* 347:1254806.

3. Black, A. J., J. R. Gamarra, and J. Giudice. 2019. More than a messenger: alternative splicing as a therapeutic target. *Biochim. Biophys. Acta. Gene Regul. Mech.* 1862:194395.

4. Coltri, P. P., M. G. P. Dos Santos, and G. H. G. da Silva. 2019. Splicing and cancer: challenges and opportunities. *Wiley Interdiscip. Rev. RNA.* 10:e1527.

5. Yang, Q., J. Zhao, …, Y. Wang. 2019. Aberrant alternative splicing in breast cancer. *J. Mol. Cell Biol.* 11:920–929.

6. Frankiw, L., D. Baltimore, and G. Li. 2019. Alternative mRNA splicing in cancer immunotherapy. *Nat. Rev. Immunol.* 19:675–687.

7. Montes, M., B. L. Sanford, …, D. S. Chandler. 2019. RNA splicing and disease: animal models to therapies. *Trends Genet.* 35:68–87.

8. Siegfried, Z., and R. Karni. 2018. The role of alternative splicing in cancer drug resistance. *Curr. Opin. Genet. Dev.* 48:16–21.

9. Wang, Z., and C. B. Burge. 2008. Splicing regulation: from a parts list of regulatory elements to an integrated splicing code. *RNA.* 14:802–813.

10. Sutandy, F. X. R., S. Ebersberger, …, J. König. 2018. In vitro iCLIP-based modeling uncovers how the splicing factor U2AF2 relies on regulation by cofactors. *Genome Res.* 28:699–713.

11. Hertel, K. J. 2008. Combinatorial control of exon recognition. *J. Biol. Chem.* 283:1211–1215.

12. Berget, S. M. 1995. Exon recognition in vertebrate splicing. *J. Biol. Chem.* 270:2411–2414.

13. De Conti, L., M. Baralle, and E. Buratti. 2013. Exon and intron definition in pre-mRNA splicing. *Wiley Interdiscip. Rev. RNA.* 4:49–60.

14. Ke, S., and L. A. Chasin. 2011. Context-dependent splicing regulation: exon definition, co-occurring motif pairs and tissue specificity. *RNA Biol.* 8:384–388.

15. Chen, S.-Y., C. Li, …, S.-J. Lai. 2019. Sequence and evolutionary features for the alternatively spliced exons of eukaryotic genes. *Int. J. Mol. Sci.* 20:E3834.

16. Arias, M. A., A. Lubkin, and L. A. Chasin. 2015. Splicing of designer exons informs a biophysical model for exon definition. *RNA.* 21:213–229.

17. Davis-Turak, J., T. L. Johnson, and A. Hoffmann. 2018. Mathematical modeling identifies potential gene structure determinants of co-transcriptional control of alternative pre-mRNA splicing. *Nucleic Acids Res.* 46:10598–10607.

18. Carazo, F., J. P. Romero, and A. Rubio. 2019. Upstream analysis of alternative splicing: a review of computational approaches to predict context-dependent splicing factors. *Brief. Bioinform.* 20:1358–1375.

19. Braun, S., M. Enculescu, …, K. Zarnack. 2018. Decoding a cancer-relevant splicing decision in the RON proto-oncogene using high-throughput mutagenesis. *Nat. Commun.* 9:3315.

20. David, C. J., A. R. Boyne, …, J. L. Manley. 2011. The RNA polymerase II C-terminal domain promotes splicing activation through recruitment of a U2AF65-Prp19 complex. *Genes Dev.* 25:972–983.

21. wa Maina, C., A. Honkela, …, M. Rattray. 2014. Inference of RNA polymerase II transcription dynamics from chromatin immunoprecipitation time course data. *PLoS Cumput. Biol.* 10:e1003598.

22. Schmidt, U., E. Basyuk, …, E. Bertrand. 2011. Real-time imaging of cotranscriptional splicing reveals a kinetic model that reduces noise: implications for alternative splicing regulation. *J. Cell Biol.* 193:819–829.

23. Braun, J. E., L. J. Friedman, …, M. J. Moore. 2018. Synergistic assembly of human pre-spliceosomes across introns and exons. *eLife.* 7:e37751.

24. Yeo, G., and C. B. Burge. 2004. Maximum entropy modeling of short sequence motifs with applications to RNA splicing signals. *J. Comput. Biol.* 11:377–394.

25. Di Liddo, A., C. de Oliveira Freitas Machado, …, K. Zarnack. 2019. A combined computational pipeline to detect circular RNAs in human cancer cells under hypoxic stress. *J. Mol. Cell Biol.* 11:829–844.

26. Lykke-Andersen, S., and T. H. Jensen. 2015. Nonsense-mediated mRNA decay: an intricate machinery that shapes transcriptomes. *Nat. Rev. Mol. Cell Biol.* 16:665–677.

27. Desmet, F.-O., D. Hamroun, …, C. Béroud. 2009. Human Splicing Finder: an online bioinformatics tool to predict splicing signals. *Nucleic Acids Res.* 37:e67.

28. Papasaikas, P., J. R. Tejedor, …, J. Valcárcel. 2015. Functional splicing network reveals extensive regulatory potential of the core spliceosomal machinery. *Mol. Cell.* 57:7–22.

29. Adler, A. S., M. L. McCleland, …, R. Firestein. 2014. An integrative analysis of colon cancer identifies an essential function for PRPF6 in tumor growth. *Genes Dev.* 28:1068–1084.

30. Wegener, M., and M. Müller-McNicoll. 2019. View from an mRNP: the roles of SR proteins in assembly, maturation and turnover. *Adv. Exp. Med. Biol.* 1203:83–112.

31. Keiper, S., P. Papasaikas, …, R. Lührmann. 2019. Smu1 and RED are required for activation of spliceosomal B complexes assembled on short introns. *Nat. Commun.* 10:3639.

32. Blüthgen, N., and S. Legewie. 2013. Robustness of signal transduction pathways. *Cell. Mol. Life Sci.* 70:2259–2269.

33. Kamenz, J., T. Mihaljev, …, S. Hauf. 2015. Robust ordering of anaphase events by adaptive thresholds and competing degradation pathways. *Mol. Cell.* 60:446–459.

34. Enculescu, M., C. Metzendorf, …, S. Legewie. 2017. Modelling systemic iron regulation during dietary iron overload and acute inflammation: role of hepcidin-independent mechanisms. *PLoS Comput. Biol.* 13:e1005322.

35. Baeza-Centurion, P., B. Miñana, …, B. Lehner. 2019. Combinatorial genetics reveals a scaling law for the effects of mutations on splicing. *Cell.* 176:549–563.e23.

36. Davis-Turak, J. C., K. Allison, …, A. Hoffmann. 2015. Considering the kinetics of mRNA synthesis in the analysis of the genome and epigenome reveals determinants of co-transcriptional splicing. *Nucleic Acids Res.* 43:699–707.

37. Waks, Z., A. M. Klein, and P. A. Silver. 2011. Cell-to-cell variability of alternative RNA splicing. *Mol. Syst. Biol.* 7:506.

38. Fox-Walsh, K. L., Y. Dou, …, K. J. Hertel. 2005. The architecture of pre-mRNAs affects mechanisms of splice-site pairing. *Proc. Natl. Acad. Sci. USA.* 102:16176–16181.

39. Witten, J. T., and J. Ule. 2011. Understanding splicing regulation through RNA splicing maps. *Trends Genet.* 27:89–97.

40. Shenasa, H., and K. J. Hertel. 2019. Combinatorial regulation of alternative splicing. *Biochim. Biophys. Acta. Gene Regul. Mech.* 1862:194392.

41. Ule, J., and B. J. Blencowe. 2019. Alternative splicing regulatory networks: functions, mechanisms, and evolution. *Mol. Cell.* 76:329–345.

42. Wong, J. J., W. Ritchie, …, J. E. Rasko. 2013. Orchestrated intron retention regulates normal granulocyte differentiation. *Cell.* 154:583–595.

43. Jacob, A. G., and C. W. J. Smith. 2017. Intron retention as a component of regulated gene expression programs. *Hum. Genet.* 136:1043–1057.

44. Nojima, T., T. Gomes, …, N. J. Proudfoot. 2016. Mammalian NET-seq analysis defines nascent RNA profiles and associated RNA processing genome-wide. *Nat. Protoc.* 11:413–428.

45. Drexler, H. L., K. Choquet, and L. S. Churchman. 2019. Human co-transcriptional splicing kinetics and coordination revealed by direct nascent RNA sequencing. *bioRxiv* https://doi.org/10.1101/611020 https://www.biorxiv.org/content/10.1101/611020v2.

46. Kim, S. W., A. J. Taggart, …, W. G. Fairbrother. 2017. Widespread intra-dependencies in the removal of introns from human transcripts. *Nucleic Acids Res.* 45:9503–9513.

47. Oesterreich, F. C., L. Herzel, …, K. M. Neugebauer. 2016. Splicing of nascent RNA Coincides with intron exit from RNA polymerase II. *Cell.* 165:372–381.

48. Bintu, L., N. E. Buchler, …, R. Phillips. 2005. Transcriptional regulation by the numbers: models. *Curr. Opin. Genet. Dev.* 15:116–124.

49. Casanovas, G., A. Banerji, …, S. Legewie. 2014. A multi-scale model of hepcidin promoter regulation reveals factors controlling systemic iron homeostasis. *PLoS Comput. Biol.* 10:e1003421.

50. Schulthess, P., A. Löffler, …, N. Blüthgen. 2015. Signal integration by the CYP1A1 promoter–a quantitative study. *Nucleic Acids Res.* 43:5318–5330.

Supplemental Information

Exon Definition Facilitates Reliable Control of Alternative Splicing in the *RON* Proto-Oncogene

Mihaela Enculescu, Simon Braun, Samarth Thonta Setty, Anke Busch, Kathi Zarnack, Julian König, and Stefan Legewie

1 Splice site mutation effects

Mutations in splice site consensus sequences impair the recognition of the splice sites by the spliceosome. Thus, they specifically lower one of the binding probabilities $p_i, i = 1, \dots, 6$, suggesting that measurements of splicing outcomes for these mutations are valuable to test our models.

1.1 Effects of splice site mutations in the intron and exon definition models

Interestingly, the binding probabilities modulate the splicing outcome differently in the intron and exon definition models, as found by comparing Eqs. (9) and (10): For example, the recognition probability of the last splice site p_6 has an effect on all splice isoforms in the exon definition model, but does not affect splicing in the intron definition model.

Fig. S2 compares the experimentally measured effects of splice site mutations in our mutagenesis screen to the effects predicted by the intron and exon definition models (and Fig. 3D shows a subset of this analysis). Plotted are changes in the frequency of each isoform with respect to wildtype for splice site mutations at the 2nd to 6th splice sites. Mutations affecting the first splice site were not present in our minigene library and were therefore excluded from this analysis. The experimentally measured changes are plotted as a median of the isoform changes among all mutations affecting the first two or last two positions of an intron (GT and AG splice site consensus sequences, respectively). For both models, qualitative simulations were performed (middle panels) and the parameters were set to $p_1 = 1$ and $p_i = 0.9, i = 2, \dots, 6$ in wildtype. The effect of a splice site mutation is qualitatively simulated by reducing the corresponding probability from 0.9 to 0.1. The rightmost panel in Fig. S2 shows the quantitative fit of the final adjusted exon definition model to the data (same data as in Fig. 3C, right). In general, the exon definition model (and in particular its best-fit version) agrees much better with the data than the intron definition model.

In fact, using analytical calculations (Section 1.2), one can show that the directionality of isoform changes upon splice site mutations, shown in the middle panels of Fig. S2, holds true for arbitrary values of the recognition parameters $p_i, i = 2, \dots, 6$. Hence, the qualitative effects of splice site mutations on splice isoforms provide a unique footprint that distinguishes intron and exon definition models. The data (left panel) in Fig. S2 supports exon definition in contrast to intron definition in several points:

1. Mutations of the 6th splice site affect all isoforms (dark blue bars).

2. Mutations of the 3rd and 4th splice sites (red bars) induce comparable changes for each of the isoforms, supporting that the AE acts as module, as predicted by the exon definition model. In contrast, the intron definition model predicts that the recognition parameters p_3 and p_4 induce opposite changes in first and second intron retention.

3. Mutation effects on inclusion and skipping correspond also quantitatively to the exon definition model, while the intron definition model leads to a much smaller amplitude of changes in skipping for all splice site mutations.

4. Directionality of changes agrees to the exon definition model for 23 out of 25 effects, with exception of the changes in full intron retention at mutated AE splice sites (3rd and 4th splice sites, red bars). As shown below, a full match between exon definition model and data for all 25 effects can be achieved by additional model extensions (Sections 1.3 and 1.4).

Our data therefore strongly indicate that an exon definition mechanism controls *RON* AE 11 splicing.

1.2 Directionality of splice site mutations effects in the intron and exon definition models

Using the models in Eqs. (9) and (13) as well as Eq. (11) we can uniquely determine the directionality of changes in the splice isoform frequencies upon splice site mutations. If we denote by $\nabla p_{isoform}^{ID}$ the derivatives of the isoform frequencies in the intron definition model w.r.t. the model parameters (p_2, p_3, p_4, p_5), we get from Eqs. (9) and (11)

$$\nabla p_{inclusion}^{ID} = [p_3 p_4 p_5, p_2 p_4 p_5, p_2 p_3 p_5, p_2 p_3 p_4],$$
$$\nabla p_{skipping}^{ID} = [(1-p_3)(1-p_4)p_5, -p_2(1-p_4)p_5, -p_2(1-p_3)p_5, p_2(1-p_3)(1-p_4)],$$
$$\nabla p_{firstIR}^{ID} = [-p_3 p_4 p_5, -p_2 p_4 p_5, (1-p_2 p_3)p_5, (1-p_2 p_3)p_4], \qquad (14)$$
$$\nabla p_{secondIR}^{ID} = [p_3(1-p_4 p_5), p_2(1-p_4 p_5), -p_2 p_3 p_5, -p_2 p_3 p_4],$$
$$\nabla p_{fullIR}^{ID} = [-p_3(1-p_5)-p_5(1-p_4), -p_2(1-p_5), -p_5(1-p_2), -p_2(1-p_3)-p_4(1-p_2)].$$

Since the splice site recognition probabilities are bounded between 0 and 1, the sign of the all derivatives with respect to the model parameters is fixed, e.g.

$$\frac{dp_{first}^{ID}}{dp_3} = -p_2 p_4 p_5 < 0, \text{for all } 0 < p_i < 1, i = 2,4,5. \qquad (15)$$

Similarly, for the exon definition model we can denote by $\nabla p_{isoform}^{ED}$ the derivatives of the single isoform frequencies w.r.t. to the exon definition probabilities (p_{12}, p_{34}, p_{56}). Using Eqs. (11) and (13) we find

$$\nabla p_{inclusion}^{ED} = [p_{34} p_{56}, p_{12} p_{56}, p_{12} p_{34}],$$
$$\nabla p_{skipping}^{ED} = [(1-p_{34})p_{56}, -p_{12} p_{56}, p_{12}(1-p_{34})],$$
$$\nabla p_{firstIR}^{ED} = [-p_{34} p_{56}, (1-p_{12})p_{56}, (1-p_{12})p_{34}], \qquad (16)$$
$$\nabla p_{secondIR}^{ED} = [p_{34}(1-p_{56}), p_{12}(1-p_{56}), -p_{12} p_{34}],$$
$$\nabla p_{fullIR}^{ED} = -[p_{34}(1-p_{56})+p_{56}(1-p_{34}), p_{12}(1-p_{56})+p_{56}(1-p_{12}), p_{12}(1-p_{34})+p_{34}(1-p_{12})].$$

Also for the exon definition model, all derivatives have fixed sign, e.g.

$$\frac{dp_{first}^{ED}}{dp_{34}} = (1-p_{12})p_{56} > 0, \text{for all } 0 < p_i < 1, i = 12,56. \qquad (17)$$

By comparing the signs of the single terms in Eqs. (14) and (16) we can find differences in the directionality of predicted changes for splice site mutations in the two models, and thereby discriminate both models based on experimental data (see Section 1.3). For instance, a mutation in the 3rd splice site decreases the recognition probabilities p_3 and p_{34} in the intron and exon definition models, respectively p_{34}. By comparing Eqs. (15) and (17) we find that for such a mutation, first intron retention is predicted to increase in the intron definition model, but to decrease in the exon definition model. The latter is observed experimentally (Fig. S2), which supports the exon definition model.

The analytically calculated directionalities of isoform changes in response to splice site mutations for intron and exon definition mechanisms are indicated by '+' and '-' signs in the bottom of Fig. 3D.

1.3 Adjusted exon definition model with isoform-specific degradation rates

The exon definition model reproduces almost completely the directionality of splice isoform changes upon splice site mutations (see Fig. S2, first and third columns). However, it fails to reproduce the measured changes in full IR, overestimates mutation effects on first and second intron retention, and slightly underestimates the effects on skipping. As detailed below, these quantitative differences between model and data can be counterbalanced by assuming that different splice products degrade at different rates (see Fig. S2, right panel).

In the adjusted exon definition model, the measured splice isoforms are assumed to be produced at a rate proportional to the individual splice isoform probabilities derived in Eqs. (13), but are degraded at individual rates. This leads to the following kinetic model

$$\frac{d}{dt}inclusion = s\,p_{inclusion}^{ED}\,premRNA - d_1\,inclusion,$$

$$\frac{d}{dt}skipping = s\,p_{skipping}^{ED}\,premRNA - d_2\,skipping,$$

$$\frac{d}{dt}fullIRtot = \frac{d}{dt}premRNA + \frac{d}{dt}fullIR = trans - (s + d_0)premRNA$$

$$+ s\left(1 - p_{inclusion}^{ED} - p_{skipping}^{ED} - p_{firstIR}^{ED} - p_{secondIR}^{ED}\right)premRNA - d_3\left(fullIRtot - premRNA\right),$$

$$\frac{d}{dt}first = s\,p_{firstIR}^{ED}\,premRNA - d_4\,firstIR,$$

$$\frac{d}{dt}secondIR = s\,p_{secondIR}^{ED}\,premRNA - d_5\,secondIR.$$

$$(18)$$

Here, *fullIRtot* is the sum of the two unspliced species, nascent pre-mRNA and mature unspliced mRNA (*fullIR*), which cannot be distinguished experimentally. The nascent pre-mRNA is produced by transcription at a rate *trans*, spliced at total rate s and degraded at rate d_0.

The steady state found by inserting Eqs. (13) in (18) is given by

$$premRNA = \frac{trans}{s + d_0}, inclusion = premRNA\,\frac{s}{d_1}\,p_{12}\,p_{34}\,p_{56},$$

$$skipping = premRNA\,\frac{s}{d_2}\,p_{12}\left(1 - p_{34}\right)p_{56},$$

$$fullIRtot = premRNA\left[1 + \frac{s}{d_3}\left(1 - p_{12}p_{34} - p_{12}p_{56} - p_{34}p_{56} + 2\,p_{12}p_{34}p_{56}\right)\right],$$

$$firstIR = premRNA\,\frac{s}{d_4}\left(1 - p_{12}\right)p_{34}\,p_{56}, secondIR = premRNA\,\frac{s}{d_5}\,p_{12}\,p_{34}\left(1 - p_{56}\right).$$

$$(19)$$

In these steady state equations, synthesis and degradation terms always occur as ratios (e.g., s and d_1 for inclusion). This implies that the model also accommodates that each isoform may be generated with its own splicing rate s_i from the pre-mRNA precursor, as this would ultimately lead to an isoform-specific value for the ratio (s_i/d_i), much like an isoform-specific degradation rate. Likewise, length biases in RNA sequencing – which may disfavor the detection of long isoforms such as full intron retention – are expected to scale this ratio and are therefore effectively considered in the model. Hence, the exon definition model with isoform-specific degradation takes into account various technical and biological effects leading to isoform biases and thereby allows

for a more realistic description of splicing decisions.

Finally, we can connect the steady state to the measured isoform *frequencies* by normalizing Eqs. (19) with the total number of measured RNA transcripts:

$$total = inclusion + skipping + fullIRtot + firstIR + secondIR, \quad (20)$$

and find

$$p_{inclusion} = \frac{s\, p_{12}\, p_{34}\, p_{56}}{d_1 R}, \; p_{skipping} = \frac{s\, p_{12}(1 - p_{34})\, p_{56}}{d_2 R},$$

$$p_{fullIR} = \frac{\left[d_3 + s\left(1 - p_{12} p_{34} - p_{12} p_{56} - p_{34} p_{56} + 2 p_{12} p_{34} p_{56}\right)\right]}{d_3 R}, \quad (21)$$

$$p_{firstIR} = \frac{s\left(1 - p_{12}\right) p_{34}\, p_{56}}{d_4 R}, \; p_{secondIR} = \frac{s\, p_{12}\, p_{34}\left(1 - p_{56}\right)}{d_5 R}.$$

Here, the factor R in Eqs. (21) equals the total quantified RNA to pre-mRNA ratio

$$R = \frac{total}{premRNA} = \frac{mRNA + premRNA}{premRNA} \quad (22)$$

and is equal to $\left(1 + s/d\right)$ if all degradation rates are the same ($d_i = d, i = 1, ..., 5$). In this case, the simple model given in Eqs. (13) is recovered. For variable degradation rates, R reads

$$R = 1 + \frac{s\, p_{12}\, p_{34}\, p_{56}}{d_1} + \frac{s\, p_{12}(1 - p_{34})\, p_{56}}{d_2} + \frac{s\left(1 - p_{12} p_{34} - p_{12} p_{56} - p_{34} p_{56} + 2 p_{12} p_{34} p_{56}\right)}{d_3}$$
$$+ \frac{s\left(1 - p_{12}\right) p_{34}\, p_{56}}{d_4} + \frac{s\, p_{12}\, p_{34}\left(1 - p_{56}\right)}{d_5}. \quad (23)$$

1.4 Effect of variable degradation rates on the directionality of changes upon splice site mutations

The inclusion of isoform-specific degradation rates leads to a better quantitative model fit of the exon definition to the mutagenesis data (Fig. 3C). Furthermore, on a qualitative level, this model extension can fix the disagreement between the exon definition model and the experimental data with respect to the directionality of splice site mutation effects on the full IR isoform (Fig. S2). In fact, this will be proven below by showing that the consideration of variable degradation rates does not switch the directionality of splice isoform changes compared to a model with common degradation rates, except for the isoform full IR.

The proof of this claim can be done by looking at the structure of the adjusted model derived in Eqs. (21). When computing the derivative of the splice isoforms inclusion, skipping, first or second IR with respect to a certain exon definition probability p_i we find either

$$\frac{\partial p_{isoform}}{\partial p_i} = \frac{p_{isoform}}{p_i R}\left(R - p_i \frac{\partial R}{\partial p_i}\right), \quad (24)$$

if the particular isoform $p_{isoform}$ increases with p_i ($p_{isoform} \sim p_i$) in the basic exon definition model

derived in Eqs. (13), or

$$\frac{\partial p_{isoform}}{\partial p_i} = -\frac{p_{isoform}}{(1-p_i)R}\left(R + (1-p_i)\frac{\partial R}{\partial p_i}\right), \quad (25)$$

if the particular isoform decreases with p_i ($p_{isoform} \sim (1-p_i)$) in the unadjusted model of Eqs. (13). For example, for the skipping isoform $p_{skipping} = \frac{p_{12}(1-p_{34})p_{56}}{d_2 R}$ we get:

$$\frac{\partial p_{skipping}}{\partial p_{12}} = \frac{p_{skipping}}{p_{12}R}\left(R - p_{12}\frac{\partial R}{\partial p_{12}}\right),$$

$$\frac{\partial p_{skipping}}{\partial p_{34}} = -\frac{p_{skipping}}{(1-p_{34})R}\left(R + (1-p_{34})\frac{\partial R}{\partial p_{34}}\right), \quad (26)$$

$$\frac{\partial p_{skipping}}{\partial p_{56}} = \frac{p_{skipping}}{p_{56}R}\left(R - p_{56}\frac{\partial R}{\partial p_{56}}\right).$$

The normalization factor R depends on the exon definition probabilities $p_i, i = 12, 34, 56$ like a first order polynomial, as given in Eq. (23). We thus have

$$R - p_{12}\frac{\partial R}{\partial p_{12}} = 1 + \frac{s}{d_3}(1 - p_{34}p_{56}) + \frac{p_{34}p_{56}}{d_4} > 1,$$

$$R - p_{34}\frac{\partial R}{\partial p_{34}} = 1 + \frac{s}{d_3}(1 - p_{12}p_{56}) + \frac{p_{12}p_{56}}{d_2} > 1, \quad (27)$$

$$R - p_{56}\frac{\partial R}{\partial p_{56}} = 1 + \frac{s}{d_3}(1 - p_{12}p_{34}) + \frac{p_{12}p_{34}}{d_5} > 1.$$

Furthermore, from Eq. (23) we can calculate

$$R + (1-p_{12})\frac{\partial R}{\partial p_{12}} = 1 + \frac{s\,p_{34}p_{56}}{d_1} + \frac{s(1-p_{34})p_{56}}{d_2} + \frac{s(1-p_{34})(1-p_{56})}{d_3} + \frac{s\,p_{34}(1-p_{56})}{d_5} > 1,$$

$$R + (1-p_{34})\frac{\partial R}{\partial p_{34}} = 1 + \frac{s\,p_{12}p_{56}}{d_1} + \frac{s(1-p_{12})(1-p_{56})}{d_3} + \frac{s(1-p_{12})p_{56}}{d_4} + \frac{s\,p_{12}(1-p_{56})}{d_5} > 1, \quad (28)$$

$$R + (1-p_{56})\frac{\partial R}{\partial p_{56}} = 1 + \frac{s\,p_{12}p_{34}}{d_1} + \frac{s\,p_{12}(1-p_{34})}{d_2} + \frac{s(1-p_{12})(1-p_{34})}{d_3} + \frac{s(1-p_{12})p_{34}}{d_4} > 1.$$

Note that we have used the fact that all probabilities $p_i, i = 12, 34, 56$ are positive numbers smaller than 1. By combining Eqs. (24) and (27) we thus find

$$\frac{\partial p_{isoform}}{\partial p_i} = \frac{p_{isoform}}{p_i R}\left(R - p_i\frac{\partial R}{\partial p_i}\right) > 0, \quad (28)$$

for all isoforms $p_{isoform}$ that increase with p_i in the basic exon definition model derived in Eqs. (13). By combining Eqs. (25) and (28) we further find

$$\frac{\partial p_{isoform}}{\partial p_i} = -\frac{p_{isoform}}{(1-p_i)R}\left(R + (1-p_i)\frac{\partial R}{\partial p_i}\right) < 0, \quad (30)$$

for all isoforms $p_{isoform}$ that decrease with p_i in the unadjusted exon definition model derived in Eqs.

(13). Therefore, the introduction of individual degradation rates cannot induce a switch in the directionality of changes with respect to the exon definition probabilities, but can adjust only the amplitude of changes for inclusion, skipping, first and second intron retention.

In contrast, numeric simulations show that variable degradation rates can induce a switch of the directionality in the changes of full intron retention, and thus correct the difference between the basic exon definition model and data (see Fig. S2).

2 Quantitative estimation of mutations effects on splice site definition

Both intron and exon definition models as well as the adjusted exon definition model were fitted to the single mutation effects on the isoforms frequencies inferred from our RNA-seq data (see Methods). Since our microscopic model does not handle non-standard isoforms (e.g., those using cryptic splice sites or those including insertion/deletion mutations), mutations that have a significant effect on the measured non-standard isoforms ('others') were filtered out from the dataset. More precisely, we keep mutations with $p_{others} < 2\, p_{others}^{wt}$, where p_{others} denotes the frequency of non-standard isoforms in the mutated gene and p_{others}^{wt} denotes the corresponding mean frequency in the wildtype minigenes. Furthermore, the frequencies of the five canonical isoforms (inclusion, skipping, full IR, first IR and second IR) were re-normalized, such that their total summed up frequency is one, like expected in the model.

In total, 1854 single point mutation effects and the wildtype values of five canonical splice isoforms were fitted. We assume that each mutation may affect spliceosome binding to splice sites, and thus allowed all recognition probabilities to be fitted independently for each mutation and the wildtype. For the intron definition model in Eqs. (9), we have four unknown parameters per mutation, namely the recognition probabilities of the 3' and 5' ends of each intron p_2, p_3, p_4, p_5. The recognition probability p_6 does not affect splicing outcomes in this model. For the exon definition model in Eqs. (13), there are only three parameters per mutation, that correspond to the joint recognition probabilities of the three exons p_{12}, p_{34}, p_{56}. The adjusted definition model in Eqs. (21) includes five additional parameters, i.e., the ratios of the degradation to splicing rates of the five splice products $d_1/s, \ldots, d_5/s$. These five parameters are assumed to have the same values for all mutations and the wildtype (i.e., mutations effects on degradation rates are neglected), and were thus fitted globally to all mutation and wildtype measurements.

The total number of parameters was therefore 7420, 5565 and 5570 for the intron, exon and adjusted exon definition models, respectively. Fitting was done by minimizing the squared norm of the difference vector between model (Eqs. (9), (13) and (21), respectively) and measured values using Matlab subroutine lsqnonlin. Starting parameter values were sampled using latin hypercube sampling. Minimization was repeated for 100 sets of starting parameters, which led to stable results for the optimal parameter values.

Optimization was done while restricting parameter values to [0,1] for all recognition probabilities. For the adjusted exon definition model, the degradation rates d_1, d_2, d_4, d_5 of the isoforms inclusion, skipping, first and second intron retention were constrained to be between 0.3 and 3.33 times the degradation rate d_3 of the full intron retention isoform. The ratio d_3/s was at its turn constrained between 0 and 3.33. The best-fit values of the global parameters were

$d_1/s=0.059, d_2/s=0.079, d_3/s=0.197, d_4/s=0.562, d_5/s=0.648$. Thus, inclusion and skipping isoforms were more stable compared to retention isoforms as expected based on the literature (*26*). The best-fit values of the recognition probabilities were $p_{12}^{wt}=0.60, p_{34}^{wt}=0.79, p_{56}^{wt}=0.73$ for the wildtype. The corresponding values for all single mutation effects are summarized in Table S1.

3 Analysis of alternative exon modularity

In the exon definition model, exons function as modules as the recognition parameters corresponding to the surrounding splice sites enter the overall exon recognition parameter in a multiplicative fashion (Eqs. (12)). Hence, mutations should have identical effects on splice isoforms, irrespective of whether they target the 3' and 5' splice sites of the exon, which would not be the case for the intron definition model in Eqs. (9). To confirm the predicted modularity, we analyzed mutations nearby splice sites, sorted them according to mutation strength and compared their effects on splice isoforms (Fig. 4B and Fig. S5). In line with the exon definition hypothesis, we found that 3' and 5' mutations in the alternative exon have almost identical effects on splicing outcomes.

For the plots in Fig. 4B, mutations in a +/- 30-nt window around the 5' and 3' splice sites of the AE 11 were selected (164 mutations at positions 266-325 and 157 mutations at positions 415-474, respectively). The best-fit parameters of the adjusted exon definition model in Eqs. (21) were used to sort these mutations according to their effect on the recognition probability of the alternative exon p_{34} (reflecting the mutation strength), and classified the mutations into 10 uniform bins between $p_{34}=0$ and $p_{34}=1$ (e.g. the 5th bin contains mutations that lead to an exon recognition probability p_{34} between 0.4 and 0.5). The top plots in Fig. 4B show the experimentally measured splice isoform frequencies as the mean in each bin vs. bin center value of p_{34}. Mutations in the vicinity of the left and right AE splice sites induce similar effects, supporting the concept that the alternative exon is recognized as a module. The plots below show simulations of the adjusted exon definition model (middle) as well as intron definition model (bottom). For the exon definition model, the degradation to splice rates $d_1/s, ..., d_5/s$ are fixed to the best-fit values. For both models, the recognition probabilities p_{12}, p_{56} and p_2, p_5 respectively, take the best-fit values obtained for the wildtype minigenes. To mimic 5' regulation of the alternative exon, the parameter p_3 is varied from 0 to 1 in the left plots, while keeping $p_4=0.9$. In the right column, 3' regulation is simulated by varying p_4 from 0 to 1 while keeping $p_3=0.9$.

Similar plots for mutations within a +/- 30-nt window around the 2nd, 5th and 6th splice sites are shown in Fig. S5. For these plots, 168 mutations within positions 180-240 (left column), 132 mutations within positions 490-550 (middle column) and 127 mutations within positions 660-720 (right column) were selected. The best-fit parameters of the adjusted exon definition model in Eqs. (21) were used to sort these mutations according to their effect on the recognition probability of the constitutive exons (p_{12} in the left column and p_{56} in the middle and right columns). For the data plots (top row), mutations were classified as already described in uniform bins according to the values of p_{12} and p_{56}, respectively. For the adjusted exon definition model (middle row) the parameters p_{34}, p_{56} (left column) or p_{12}, p_{34} (middle and right columns) were fixed at their best-fit values. For the intron definition model (bottom row) the parameters p_3, p_4, p_5 (left column) or p_2, p_3, p_4 (middle and right columns) were fixed at their best fit values. To mimic the regulation of

the constitutive exon 10, the parameter p_2 is varied between 0 and 1 in the left column. To mimic the regulation of the constitutive exon 12, p_5 (middle column) or p_6 (right column) are varied between 0 and 1, while keeping $p_6 = 0.9$ or $p_5 = 0.9$, respectively. The available data shows similar isoform distribution for mutations on both sites of the constitutive exon 12 (top, middle and right), supporting again the modular character of splicing reflected by the exon definition model in contrast to the intron definition model. Note that data on mutated 5th splice site is partially missing (top, middle), since these mutations lead to the activation of a cryptic splice site and formation of non-canonical isoforms, that are not currently described by the model.

4 Prediction of combined mutation effects

To further support modular exon regulation, we assessed whether the adjusted exon definition model trained on single mutation effects (Fig. 3B, right) could successfully predict combined mutation effects. For the plots in Fig. 4C, we focused on predicting a subset of 908 minigenes in our mutagenesis data that contained only two point mutations. However, most of these individual mutations do not have a strong effect on *RON* splicing, so that the prediction of their combined effect would be trivial. We therefore further filtered for those single point mutations that induce more than 20% change with respect to wildtype taken as a sum of all absolute isoform changes

($\sum \left| p_i - p_i^{wt} \right| > 0.2$) and ended up with 45 double mutation minigenes that could be used to test the exon definition model.

The combined effect of two mutations was calculated based on the assumption that mutations multiplicatively affect the k^{on}/k^{off} ratio of the spliceosome binding to the single exons. Thus, in similarity to Eqs. (3), we assume for each exon recognition probability in a double mutation minigene:

$$p_{combined} = \frac{k^{on}_{combined}/k^{off}_{combined}}{1 + k^{on}_{combined}/k^{off}_{combined}}, \quad (31)$$

with

$$\frac{k^{on}_{combined}}{k^{off}_{combined}} = \left(\frac{k^{on}_{wt}}{k^{off}_{wt}} \right)^{-1} \frac{k^{on}_1}{k^{off}_1} \cdot \frac{k^{on}_2}{k^{off}_2} \quad (32)$$

and

$$\frac{k^{on}_i}{k^{off}_i} = \frac{p_i}{1 - p_i}, i = wt, 1, 2. \quad (33)$$

In (32) and (33) $p_{wt}, k^{on}_{wt}, k^{off}_{wt}$ are the exon definition probabilities and binding/unbinding rates fitted to the wildtype and $p_i, k^{on}_i, k^{off}_i, i = 1, 2$ are the corresponding values associated with the single mutation effects. Thus, Eqs. (31-33) allow us to calculate the exon recognition probabilities in the double mutation minigene from the estimated exon recognition probabilities in the single mutation minigenes. Finally, predictions of the five isoform frequencies in minigenes containing two mutations are made using the models in Eqs. (9) and (21). These predictions (in total 225 isoform values for each model) are compared to the experimental measurements in Fig. 4C (right panel).

For the left panel in Fig. 4, the analysis was further restricted based on the positions of mutations: specifically, only mutations in a +/- 30 nt window around the 3' and 5' sites of the AE were considered (positions 275-330 and 415-475). This leads to a subset of 3 double mutation minigenes (in total 15 isoform value predictions for each model).

5 Simulation of mutation effects on PSI and total intron retention

We used the model to investigate how alternative splicing regulation relates to intron retention. For simplicity, we did not distinguish intron retention isoforms but considered only total intron retention, i.e., the sum of all retention products. Considering that all isoform frequencies sum up to 1, we derive an analytical expression for *totalIR* from Eqs. (13)

$$totalIR = 1 - p_{inclusion} - p_{skipping} = 1 - p_{12} p_{56}, \quad (34)$$

For the PSI of the middle exon as a measure of alternative splicing, we obtain

$$PSI = \frac{p_{inclusion}}{p_{inclusion} + p_{skipping}} = p_{34}. \quad (35)$$

Hence, alternative splicing and the degree of intron retention are controlled independently in the exon definition model (if all splice isoforms are degraded turned over with the same rates), and alternative splicing regulation occurs without the accumulation of retention products.

For the intron definition model *totalIR* and *PSI* cannot be uncoupled in the same way. Specifically, we obtain from Eq. (11):

$$totalIR = 1 - 2 p_2 p_3 p_4 p_5 - p_2 p_5 + p_2 p_3 p_5 + p_2 p_4 p_5,$$
$$PSI = \frac{p_3 p_4}{2 p_3 p_4 + 1 - p_3 - p_4}. \quad (36)$$

If both splice sites flanking the alternative exon are jointly recognized ($p_3 = p_4 = 0$), or jointly not recognized ($p_3 = p_4 = 1$), we have

$$totalIR = 1 - p_2 p_5, \quad (37)$$

which resembles Eq. (34). In contrast to the exon definition model, *totalIR* approaches 1 if only one of the splice sites is recognized ($(p_3 = 1 \wedge p_4 = 0) \vee (p_3 = 0 \wedge p_4 = 1)$). Hence, both splice sites need to be regulated jointly to prevent retention in the intron definition model.

However, even in this scenario of joint regulation ($p_3 = \alpha p_4$), intron retention isoforms accumulate at intermediate *PSI* values, i.e., during the switch from exon skipping to inclusion. Plugging $p_3 = \alpha p_4$ into Eqs. (36) yields

$$totalIR = 1 - \frac{2\alpha}{(1+\alpha)^2} \quad (38)$$

for $PSI = 0.5$ and $p_2 = p_5 = 1$. Hence, even if the splice sites of the outer exons are perfectly recognized ($p_2 = p_5 = 1$) *totalIR* will accumulate to at least 50% of all splice products at intermediate inclusion levels (PSI=0.5). Less complete recognition of the outer exons results in even higher

retention (not shown), implying alternative splicing regulation in the intron definition model inevitably results in the accumulation of retention products.

To visualize the distinct accumulation of retention products in the intron and exon definition models, Monte-Carlo simulations mimicking point mutation effects were performed (Fig. 4D, middle and right). To this end, 2000 sets of binding probabilities $(p_1, \ldots, p_6)$ were used. In all runs, five of the six binding probabilities $(p_2 - p_6)$ are drawn from a Gauss distribution (standard deviation 5%). In 45 of the runs, one of the constitutive exons splice sites (2,5,6) is randomly chosen and its binding probability additionally perturbed (standard deviation 50%). In other 300 of the runs, one of the alternative exons splice sites (3 or 4) is randomly chosen and the corresponding binding probability is additionally perturbed (standard deviation 50%). The distributions for $p_2 - p_6$ are centered around (0.95,0.7,0.7,0.95,0.95) and (0.9, 0.9, 0.9, 0.9, 0.9) for the intron and exon definition models, respectively. These values were chosen to mimic the experimentally measured wildtype PSI and intron retention values. The value of p_1 is set to 1 in both models since the minigene used in the experiment does not include the 1st splice site.

6 Analysis of splicing for a pre-mRNA containing four exons

In this section, we theoretically analyze splicing of a four-exon gene to show that the same principles we derived above also hold for longer sequences and more complex splicing scenarios.

Consider a gene with four exons in which the recognition is denoted in a binary fashion, e.g., (1111) and (0000) for the fully bound (all exons or recognized) and empty states (no exon recognized), respectively. We define the sum of the states (1111), (1011), (1101) and (1001) as the *productive states,* as only for these cases no intron will be retained after splicing (following the same splicing rules as in Section 1).

With p_i being the individual recognition probability of each exon, we obtain for the frequency of total intron retention, i.e., the sum of all retention isoforms

$$totalIR = 1 - productive\,states = 1 - p_1 p_4 \quad (39)$$

and

$$productive\,states = p_1 p_4. \quad (40)$$

This expression resembles Eq. (34) and shows that *totalIR* solely depends on the recognition of the outer exons.

The percent spliced-in (*PSI*) for the second and third (i.e., the inner) exons is given by

$$PSI_2 = \frac{p_{1111} + p_{1101}}{productive\,states} = p_2,$$
$$PSI_3 = \frac{p_{1111} + p_{1011}}{productive\,states} = p_3. \quad (41)$$

Thus, as for the three-exon case (Eq. (35)), alternative splicing is controlled independently of *totalIR*. Furthermore, alternative splicing regulation is modularized in two ways: (i) By assigning a

total recognition probability to each exon (p_i), we implicitly assumed that splice signals acting on the two splice sites of this exon are integrated into a net outcome (within-exon modularity); (ii) According to Eqs. (41), the inclusion level of exon is controlled only by its own recognition probability independent of its neighboring exons. This gives rise to an additional cross-exon modularity that was not present in the three-exon case (Section 1).

Similar conclusions also hold for more complex scenarios involving more than four exons (as long as we assume that exon skipping can also occur across long sequences comprising multiple introns and exons). Taken together, these calculations support that exon definition is generally beneficial for the alternative splicing regulation, also for long pre-mRNAs with complex exon structure.

7 Analysis of the *HNRNPH* knockdown response and synergistic effects

In order to analyze how *HNRNPH* affects *RON* splicing, we quantitatively analyzed *HNRNP* knockdown data in HEK293T cells using our model. The distribution of the exon recognition probabilities in wildtype minigenes and the mutation effects on these probabilities were calculated by fitting the adjusted exon definition model to the *HNRNPH* knockdown data as described in Section 2. Here, the global parameters $d_1/s,\dots,d_5/s$ were kept at the values determined for control conditions.

The distribution of the exon recognition probabilities p_{12}, p_{34}, p_{56} for the wildtype minigenes is shown in Fig. S4C. The knockdown mainly increases the recognition probability of the alternative exon p_{34}, while the recognition probabilities of the constitutive exons p_{12}, p_{56} are comparable to control values.

In order to identify which sites are most relevant for HNRNPH-dependent regulation, we inferred the splicing response of single point mutation variants upon *HNRNPH* knockdown using our model. We hypothesized that mutations that either weaken or reinforce an HNRNPH binding site would display positive or negative synergy with the *HNRNPH* knockdown. For instance, a reduced knockdown response compared to the wildtype minigene would be expected if an important HNRNPH binding site is compromised by a mutation (negative synergy). For the exon recognition probabilities $p_i, i=12,34,56$ in mutated minigenes, a z-score was calculated based on the mean and standard deviation in wildtype minigenes:

$$z_i = \frac{\log\left(p_i^{KD}/p_i^{control}\right) - wtmean}{wtstd}, \quad (42)$$

where *wtmean* and *wtstd* are the mean and standard deviation of $\log\left(p_i^{KD}/p_i^{control}\right)$ in wildtype minigenes. Mutations with $|z_i|>5$ indicate a highly distinct knockdown response in wildtype and mutant background and were considered as a synergistic interaction which hints to the presence of a cis-regulated element targeted by HNRNPH. The density of such interactions in a 5-nt sliding window is plotted in Fig. S4D. The most reliable synergistic interactions are found for the recognition probability p_{34} of the alternative exon with corresponding mutations located in the alternative exon or flanking introns. For a similar analysis in MCF7

cells see also Fig. 5 in (*19*).
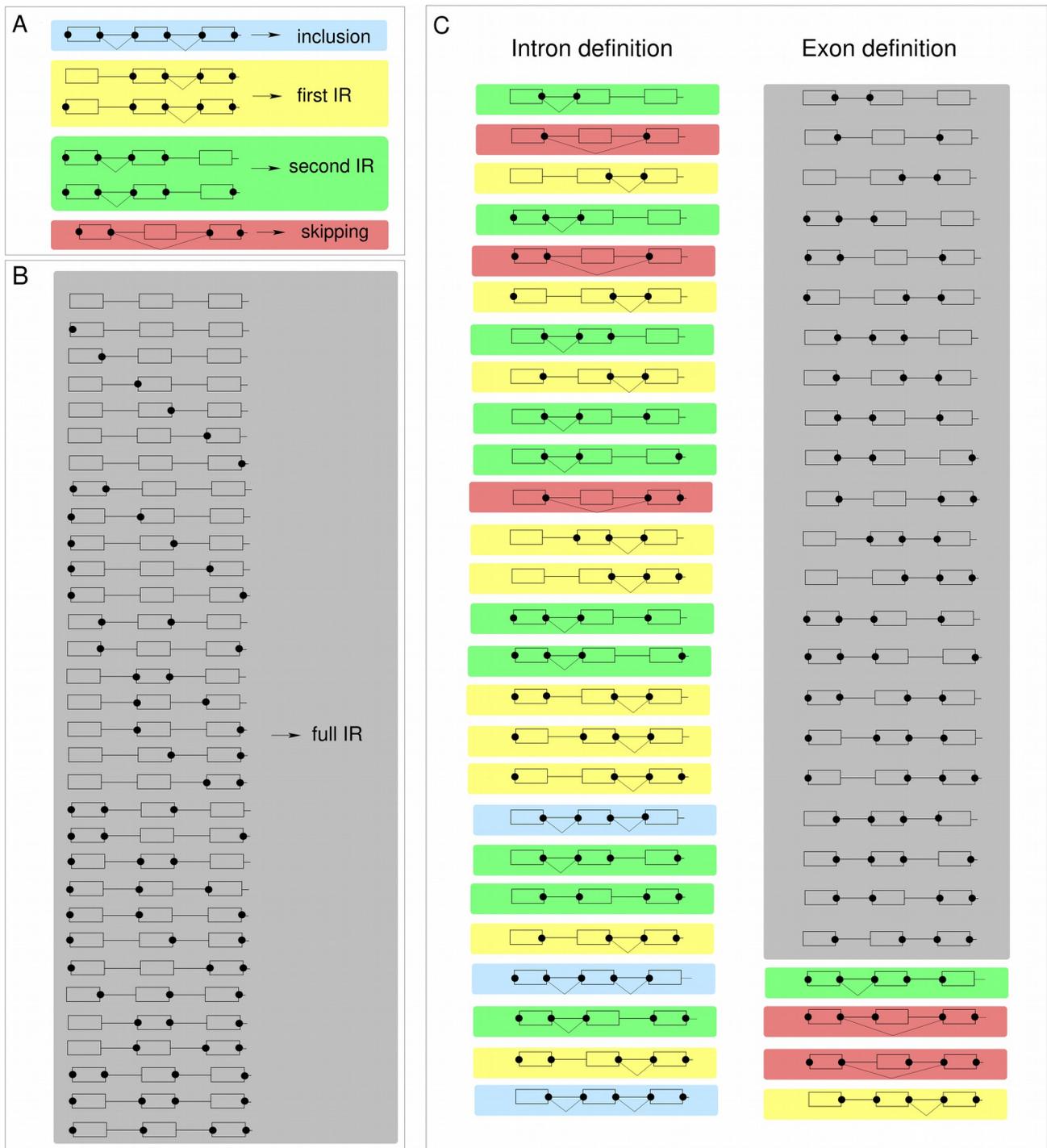
Fig. S1. Common and distinct splicing decisions in intron vs. exon definition models. A Spliceosomal binding states leading to identical splicing outcomes in both models. **B** Binding states with no matching 3' and 5' splice sites across introns. Since no splicing reaction can take place, these binding states lead to the full intron retention isoform in both models. **C** Binding states that lead to different splice outcomes in the intron (left column) and exon definition (right column) model. Black dots indicate U1 and U2 binding to splice sites. Splicing reactions are indicated by triangular black lines. The background color reflects the splice outcome (blue: inclusion, red: skipping, yellow: first IR, green: second IR, gray: full IR).
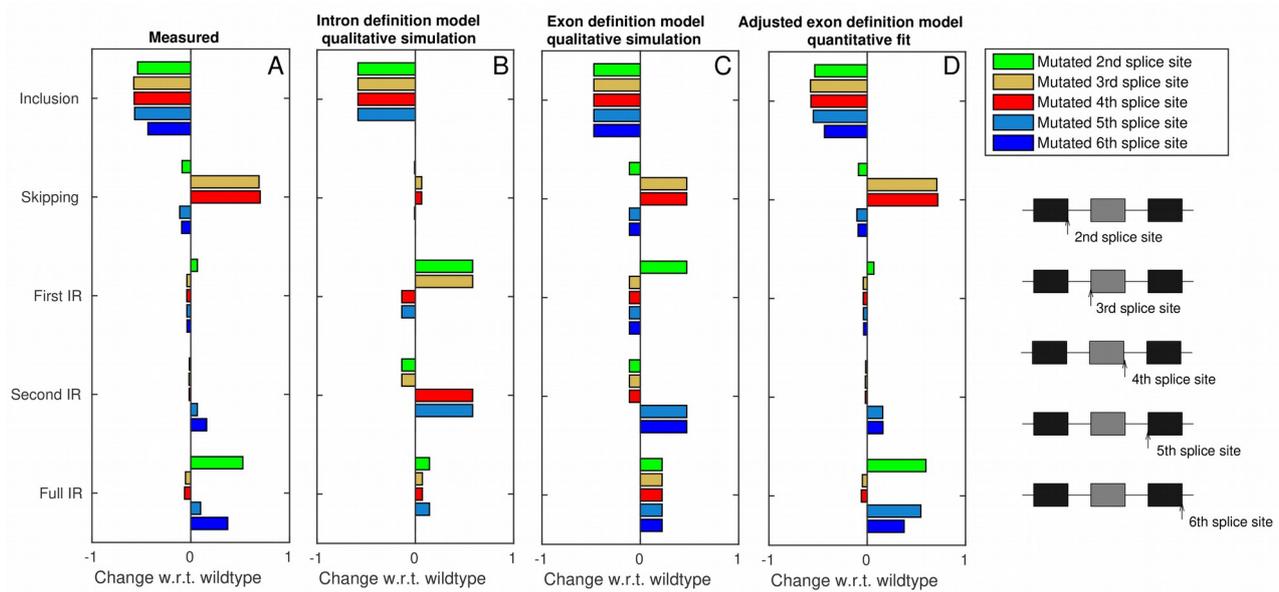
Fig. S2. Splice site mutation effects on splice isoforms support the exon definition model. A Bar plots showing the median isoform differences w.r.t. wildtype for directly measured minigenes containing single point mutations at different splice sites. Splice sites are defined as the first and last two positions within an intron (sites 211-212,296-297,445-446,523-524,691-692). Mutations at these positions have the strongest effect on splicing outcomes within the library. A subset of this data is shown in Fig. 3D. **B,C** Predictions of splice site mutation effects based on qualitative simulations of the intron and exon definition models, respectively. Importantly, the directionality of the simulated isoform changes hold true for arbitrary sets of splice recognition parameters (see Sections 1.1 and 1.2 for details). The exon definition (but not the intron definition) model reproduces 23 out of 25 splice mutation effects, and only fails to describe AE splice site effects on full IR. **D** The adjusted exon definition model with isoform-specific degradation and fitted parameters (Fig. 3B, right) qualitatively and quantitatively reproduces all measured splice site effects.
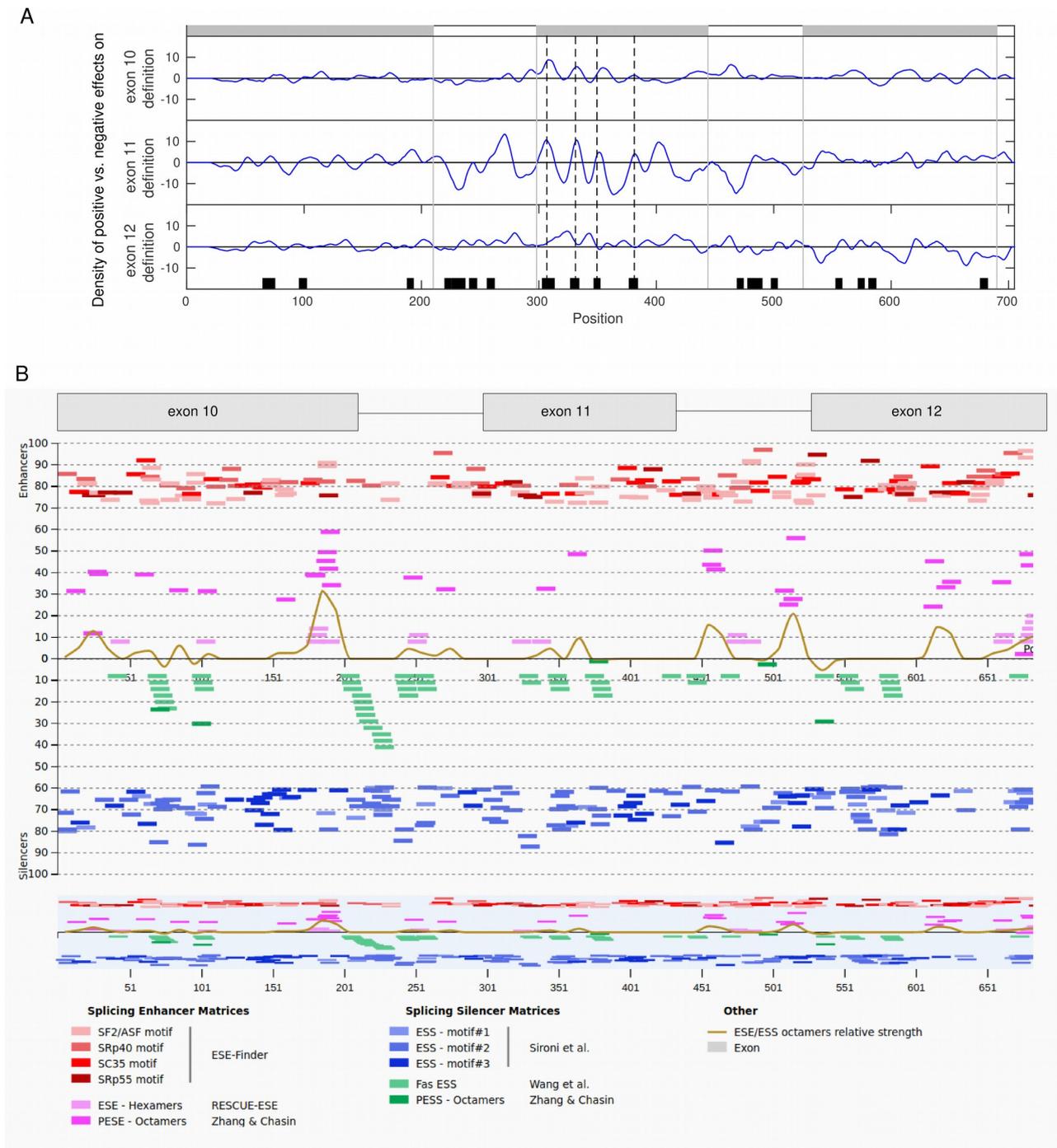
Fig. S3 Strong point mutation effects partially overlap with known RBP motifs. A Maps showing the densities of positive vs. negative point mutation effects on the recognition probabilities of the three exons. The difference in the number of positive effects (z-score >2) and the number of negative effects (z-score < -2) on each exon recognition probability was calculated for adjacent 8-nt windows along the minigene. The mean value of this difference over a sliding 8-nt window is plotted. Effects within 2-nt distance from the splice sites were excluded. Exons and splice sites are marked by grey boxes and grey vertical lines, respectively. HNRNPH splice-regulatory binding sites (SRBS) predicted in (*19*) are shown as black boxes. Four of the positions with enhanced positive effects on exon 11 recognition correspond to HNRNPH SRBS within the alternative exon (dashed vertical lines). **B** Summary of exonic splicing enhancers (ESE) and exonic splicing silencers (ESS) predicted for the wildtype minigene sequence. The plot was generated with the Human Splicing Finder, Version 3.1. Results are also summarized in Table S2.
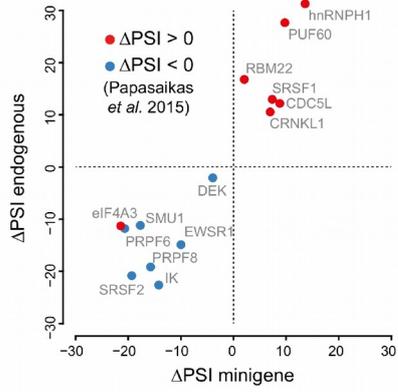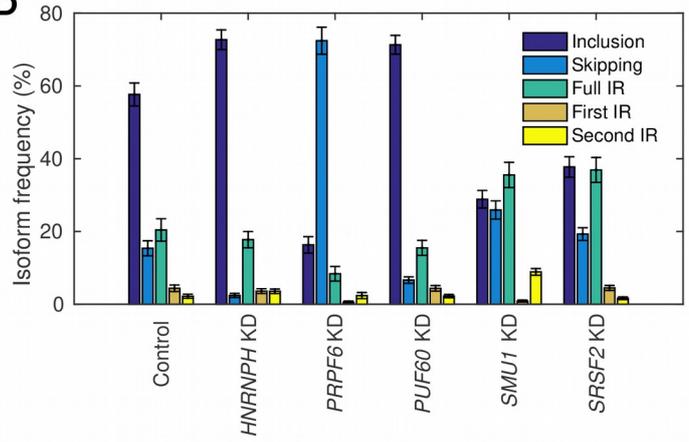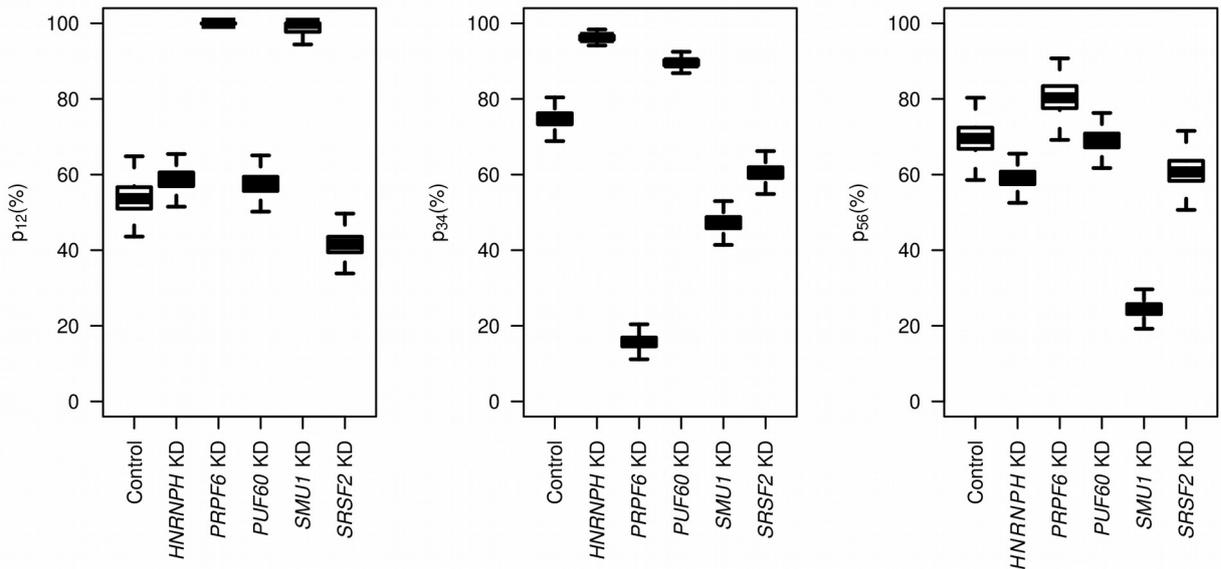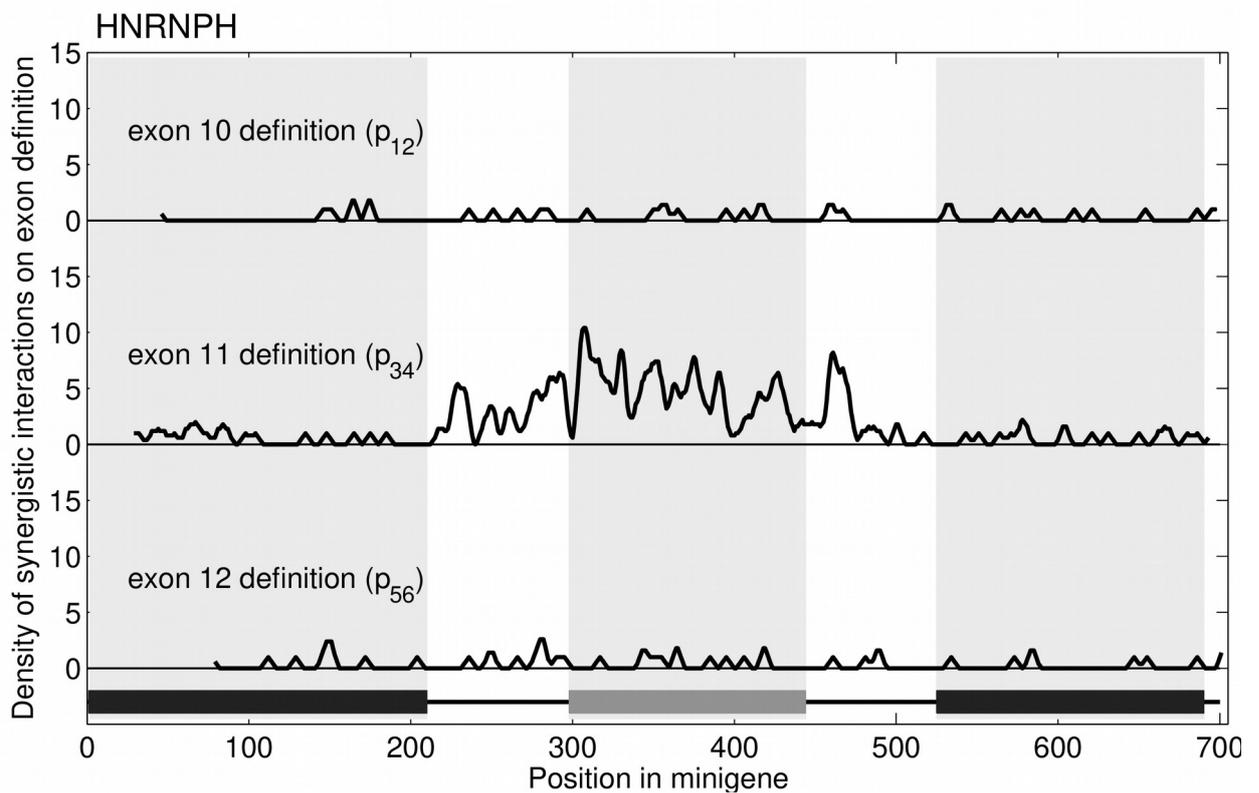
Fig. S4. Knockdowns of RNA-binding proteins most prominently affect the recognition probability of the alternative exon. A The change in the percent spliced-in metric relative to scrambled control (ΔPSI) upon RBP knockdown for the minigene construct (x-axis) and for the endogeneous exon 11 (y-axis). Semi-quantitative RT-PCR of exon 11 splicing in the minigene and the endogeneous *RON* gene was performed as described in (*19)*. Data points are coloured based on their regulation in a previous study (*28*). **B** Measured isoform frequencies for wildtype minigenes in control and *HNRNPH, PRPF6, PUF60, SMU1* or *SRSF2* knockdown conditions. Error bars indicate the standard deviation of all 586 wildtype plasmids in the mutagenesis library. Targeted RNA sequencing and data analysis was performed as described in (*19*). **C** Model-based quantification of knockdown effects. Boxplots show the distribution of the best-fit recognition probabilities p_{12}, p_{34}, p_{56} of the three exons in wildtype minigenes under control and knockdown conditions. The fit was generated using the adjusted exon definition model by separately fitting all wildtype minigenes (see Section 7 for details). **D** HNRNPH may target cis-regulatory elements in the alternative exon, as evidenced by a synergistic interaction of *HNRNPH* knockdown with point mutations in this region. Maps show the density of synergistic mutation-knockdown effects on the three exon recognition probabilities. Single mutation effects on the exon recognition were determined separately for control and *HNRNPH* knockdown conditions. The difference (in logarithmic space) between control and *HNRNPH* knockdown values for single point mutations was compared to the knockdown response of wildtype minigenes and expressed as a z-score relative to the within-wildtype-variation (see Section 7 and (*19*)). Large z-scores indicate a synergistic interaction with the *HNRNPH* knockdown. The density of mutations with a | z-score | >5 in a 5-nt sliding window is plotted.
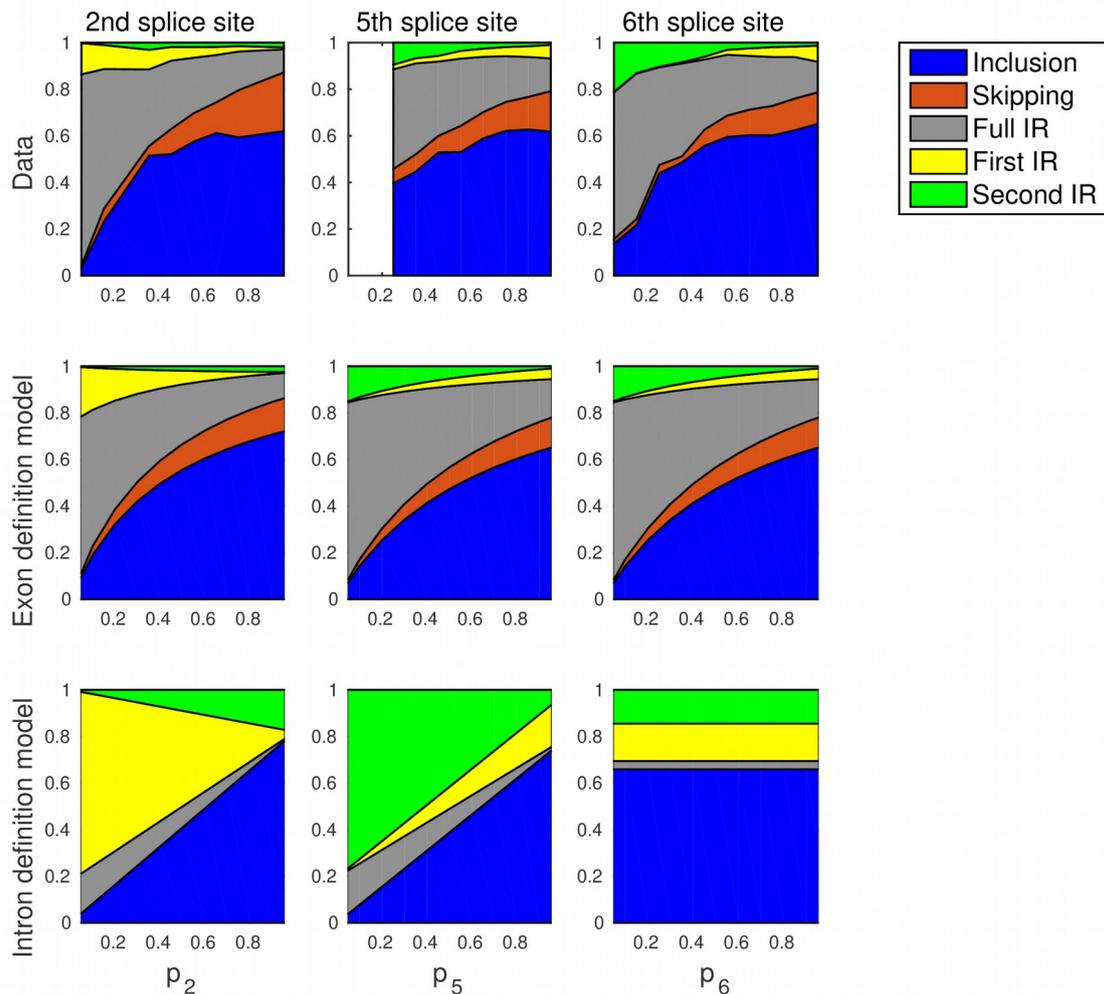
Fig. S5. Position-dependent mutation effects on splice isoforms support the exon definition model (related to Fig. 4B). Plots show a similar analysis as in Fig. 4B for the other splice sites. Mutations at positions in a +/- 30-nt window around the 2nd, 5th and 6th splice sites were selected. The mutations were sorted according to their effect on the recognition probability p_{12}(left) or p_{56} (middle and right) in the best-fit model (adjusted exon definition model; Fig. 3B, right). The measured changes in the splice isoform fractions with varying mutation strength (1st row) are similar for the 5th and 6th splice splice sites, and agree with simulations of the exon definition model in which p_{56} is systematically varied (2nd row), but disagree with the intron definition model (3rd row). Furthermore, mutations at the 2nd splice site induce similar changes as mutations at the 5th and 6th splice sites for the inclusion, skipping and full intron retention isoforms, as reflected by the exon definition model in contrast to the intron definition model. The vertical white line is located at the best-fit parameter values corresponding to wildtype minigenes.

Best Fit Values of Model Parameters

	Exon Definition Model			Intron Definition Model			
	p_{12}	p_{34}	p_{56}	p_2	p_3	p_4	p_5
wildtype	0.60	0.79	0.73	0.80	1.00	0.97	0.85
A26T	0.58	0.79	0.71	0.80	0.99	1.00	0.81
A26G	0.58	0.79	0.61	0.77	0.99	0.99	0.78
G27T	0.67	0.71	0.77	0.95	0.84	0.88	0.92
G27C	0.69	0.76	0.66	0.82	0.99	0.99	0.82
G27A	0.53	0.78	0.67	0.76	0.99	0.99	0.77
C28T	0.58	0.82	0.70	0.81	1.00	1.00	0.82
C28G	0.40	0.64	0.97	0.85	0.79	0.82	0.88
C28A	0.66	0.75	0.63	0.80	1.00	0.99	0.80
T29G	0.61	0.76	0.75	0.83	0.97	0.98	0.83
T29C	0.63	0.79	0.70	0.81	0.99	0.99	0.83
T29A	0.54	0.78	0.66	0.76	0.99	1.00	0.78
G30A	0.56	0.79	0.73	0.80	0.99	1.00	0.81
T31G	0.61	0.79	0.73	0.81	1.00	0.99	0.83
T31C	0.61	0.81	0.71	0.81	1.00	0.99	0.83
T31A	0.61	0.79	0.67	0.81	0.98	1.00	0.81
G32T	0.60	0.80	0.68	0.80	1.00	0.99	0.81
G32C	0.44	0.61	0.75	0.71	0.80	0.80	0.73
G32A	0.60	0.76	0.67	0.78	0.99	0.99	0.79
C33T	0.62	0.78	0.77	0.83	0.99	0.98	0.85
C33G	0.78	0.65	0.60	0.90	0.86	0.84	0.90
C33A	0.68	0.88	0.78	0.87	1.00	0.99	0.89
C34T	0.56	0.78	0.63	0.76	0.99	0.99	0.77
C34A	0.51	0.85	0.73	0.79	1.00	0.96	0.86
G35T	0.49	0.80	0.73	0.76	0.99	1.00	0.79
G35A	0.57	0.81	0.71	0.81	0.99	1.00	0.82
C36T	0.61	0.84	0.77	0.84	1.00	1.00	0.86
C36G	0.54	0.73	0.69	0.74	0.99	0.98	0.77
C36A	0.66	0.77	0.79	0.89	0.93	0.97	0.87
C37T	0.61	0.79	0.71	0.82	0.98	0.99	0.83
C37A	0.53	0.79	0.71	0.77	1.00	0.98	0.81
CT38C	0.54	0.79	0.79	0.80	0.99	0.98	0.83
T38G	0.65	0.73	0.71	0.79	1.00	0.99	0.81
T38C	0.57	0.79	0.70	0.79	0.99	0.99	0.81
T38A	0.62	0.80	0.74	0.82	1.00	0.99	0.84
T39C	0.59	0.78	0.72	0.80	0.99	0.98	0.83
T39A	0.64	0.73	0.70	0.81	0.97	0.98	0.82
TC40T	0.59	0.75	0.72	0.78	1.00	0.96	0.82
C40T	0.49	0.74	0.64	0.71	0.97	0.98	0.72
C40A	0.58	0.56	0.81	0.90	0.72	0.71	0.94
C41T	0.55	0.77	0.79	0.80	0.99	0.99	0.82
C41G	0.69	0.77	0.68	0.84	0.98	1.00	0.82
C41A	0.59	0.79	0.72	0.80	0.99	0.99	0.81
T42G	0.65	0.81	0.68	0.82	1.00	0.97	0.85
T42C	0.64	0.82	0.67	0.82	1.00	0.98	0.84
T42A	0.57	0.82	0.77	0.82	1.00	0.99	0.85
G43T	0.55	0.76	0.46	0.70	0.79	0.98	0.56
G43C	0.55	0.78	0.72	0.77	1.00	0.99	0.80
G43A	0.57	0.78	0.73	0.79	0.99	0.98	0.82
A44T	0.47	0.80	0.71	0.80	0.92	1.00	0.77
A44G	0.53	0.77	0.74	0.77	0.99	0.98	0.80

A44C	0.51	0.73	0.68	0.72	1.00	0.98	0.76
A45T	0.59	0.82	0.72	0.83	0.98	1.00	0.83
A45G	0.60	0.82	0.66	0.81	1.00	0.99	0.82
T46G	0.68	0.76	0.82	0.95	0.88	0.90	0.94
T46C	0.62	0.76	0.68	0.82	0.95	1.00	0.79
T46A	0.58	0.80	0.77	0.82	0.99	0.99	0.84
A47T	0.56	0.71	0.79	0.83	0.92	0.96	0.82
A47G	0.54	0.74	0.82	0.80	0.97	0.96	0.84
T48G	0.62	0.97	0.82	0.91	0.98	1.00	0.92
T48C	0.59	0.75	0.78	0.82	0.97	0.97	0.83
T48A	0.61	0.78	0.61	0.78	0.99	1.00	0.78
G49C	0.73	0.88	0.76	0.89	1.00	1.00	0.90
G49A	0.68	0.82	0.76	0.86	0.99	0.99	0.88
T50G	0.57	0.87	0.65	0.82	1.00	1.00	0.83
T50C	0.60	0.79	0.75	0.81	0.99	0.99	0.83
T50A	0.59	0.80	0.79	0.82	1.00	0.99	0.85
TG51T	0.56	0.80	0.60	0.75	1.00	0.99	0.77
G51T	0.52	0.85	0.74	0.80	1.00	1.00	0.83
G51A	0.63	0.83	0.68	0.83	1.00	1.00	0.84
G52T	0.58	0.82	0.77	0.82	1.00	1.00	0.84
G52C	0.62	0.78	0.71	0.81	0.99	1.00	0.82
G52A	0.65	0.75	0.74	0.82	0.99	0.98	0.84
T53G	0.49	0.82	0.74	0.77	0.99	1.00	0.81
T53C	0.58	0.79	0.73	0.81	0.99	0.98	0.84
T53A	0.58	0.81	0.83	0.83	0.99	0.99	0.85
C54T	0.59	0.80	0.73	0.81	0.99	0.99	0.83
C54G	0.63	0.64	0.87	0.98	0.78	0.79	0.99
C54A	0.51	0.86	0.68	0.79	1.00	1.00	0.81
C55T	0.55	0.79	0.74	0.78	1.00	0.98	0.82
C55G	0.54	0.82	0.84	0.83	0.98	1.00	0.85
C55A	0.52	0.81	0.72	0.78	0.99	0.99	0.80
G56T	0.54	0.66	0.96	0.97	0.78	0.80	0.98
G56C	0.36	0.79	0.91	0.73	0.99	1.00	0.78
G56A	0.60	0.78	0.70	0.80	0.99	0.99	0.81
GA57G	0.65	0.78	0.80	0.83	1.00	0.95	0.89
A57T	0.56	0.81	0.81	0.82	1.00	0.97	0.86
A57G	0.55	0.87	0.70	0.81	1.00	1.00	0.83
G58T	0.52	0.68	0.80	0.81	0.89	0.88	0.85
G58A	0.61	0.76	0.68	0.78	1.00	0.99	0.80
A59T	0.67	0.75	0.60	0.79	0.99	1.00	0.78
A59G	0.64	0.80	0.70	0.82	1.00	0.99	0.84
AC60A	0.54	0.73	0.70	0.77	0.96	0.98	0.77
C60T	0.71	0.83	0.65	0.85	1.00	1.00	0.85
C60A	0.57	0.75	0.68	0.76	1.00	0.98	0.79
C61T	0.59	0.78	0.76	0.82	0.98	1.00	0.83
C61G	0.61	0.94	0.77	0.87	1.00	1.00	0.89
C61A	0.62	0.74	0.80	0.86	0.94	0.93	0.88
C62T	0.68	0.77	0.77	0.89	0.94	0.99	0.85
C62A	0.61	0.80	0.68	0.80	1.00	0.99	0.82
C63T	0.64	0.78	0.71	0.82	0.99	0.99	0.83
C63G	0.45	0.73	1.00	0.97	0.76	0.83	0.98
C63A	0.62	0.86	0.62	0.82	1.00	1.00	0.82
C63CT	0.55	0.83	0.73	0.83	0.96	1.00	0.83

Best Fit Values of Model Parameters

C64T	0.48	0.79	0.88	0.79	1.00	0.99	0.84
C64A	0.58	0.82	0.69	0.80	1.00	0.99	0.82
C64CA	0.66	0.74	0.78	0.90	0.90	0.91	0.91
CA65C	0.50	0.67	0.89	0.88	0.84	0.87	0.88
A65T	0.61	0.79	0.75	0.82	0.99	0.99	0.83
A65G	0.61	0.84	0.73	0.84	0.98	1.00	0.84
A65C	0.58	0.81	0.73	0.81	1.00	0.99	0.83
AG66A	0.57	0.77	0.67	0.77	0.99	0.99	0.77
G66T	0.68	0.75	0.78	0.92	0.90	0.93	0.90
G66A	0.63	0.79	0.73	0.82	1.00	0.98	0.84
G67T	0.67	0.77	0.79	0.90	0.92	0.97	0.87
G67C	0.82	0.61	0.79	1.00	0.78	0.78	1.00
G67A	0.69	0.79	0.76	0.86	0.98	0.97	0.87
G68A	0.70	0.81	0.78	0.86	0.99	0.98	0.88
A69T	0.59	0.85	0.70	0.82	1.00	1.00	0.84
A69G	0.57	0.82	0.67	0.80	0.99	1.00	0.81
A69C	0.68	0.89	0.77	0.88	1.00	0.99	0.90
A69AT	0.47	0.80	0.87	0.81	0.97	1.00	0.82
T70G	0.69	0.86	0.74	0.87	1.00	1.00	0.87
T70C	0.60	0.81	0.73	0.82	0.99	0.99	0.84
T70A	0.57	0.86	0.68	0.81	1.00	1.00	0.82
TG71T	0.62	0.83	0.75	0.84	1.00	0.99	0.86
G71C	0.68	0.81	0.90	0.95	0.91	0.93	0.96
G71A	0.58	0.81	0.74	0.81	1.00	0.99	0.84
G72T	0.67	0.78	0.67	0.82	0.99	0.99	0.82
G72C	0.71	0.81	0.73	0.86	0.99	0.99	0.86
G72A	0.63	0.79	0.69	0.81	0.99	0.99	0.82
G73T	0.70	0.78	0.81	0.91	0.93	0.93	0.92
G73C	0.67	0.89	0.80	0.89	0.99	1.00	0.89
G73A	0.70	0.78	0.80	0.93	0.91	0.91	0.93
T74G	0.43	0.70	0.99	0.85	0.87	0.83	0.96
T74C	0.63	0.77	0.72	0.82	0.99	0.97	0.83
T74A	0.61	0.79	0.68	0.81	0.98	0.99	0.82
T74TG	0.66	0.76	0.73	0.82	0.99	0.98	0.84
G75T	0.55	0.81	0.79	0.81	1.00	1.00	0.84
G75A	0.63	0.79	0.75	0.89	0.92	1.00	0.84
G76T	0.64	0.78	0.68	0.80	1.00	0.96	0.84
G76C	0.66	0.80	0.72	0.83	1.00	0.98	0.85
G76A	0.66	0.77	0.76	0.83	0.99	0.98	0.86
C77T	0.60	0.83	0.66	0.81	1.00	1.00	0.82
C77G	0.56	0.89	0.44	0.74	0.97	0.99	0.71
C77A	0.62	0.83	0.70	0.83	1.00	0.99	0.84
CA78C	0.56	0.76	0.76	0.78	1.00	0.98	0.81
A78T	0.58	0.81	0.75	0.81	1.00	0.99	0.83
A78G	0.59	0.80	0.73	0.81	0.99	1.00	0.83
A78C	0.65	0.68	0.75	0.91	0.84	0.86	0.90
AG79A	0.72	0.82	0.72	0.85	1.00	0.97	0.88
G79T	0.69	0.77	0.75	0.85	0.97	0.97	0.86
G79C	0.53	0.76	0.67	0.74	0.99	1.00	0.76
G79A	0.70	0.79	0.71	0.84	0.99	0.99	0.85
G80T	0.70	0.79	0.78	0.87	0.97	0.97	0.88
G80C	0.60	0.71	0.84	0.92	0.86	0.86	0.93
G80A	0.71	0.81	0.74	0.86	0.99	0.97	0.88

Best Fit Values of Model Parameters

G81T	0.64	0.72	0.63	0.77	1.00	0.99	0.78
G81A	0.66	0.79	0.78	0.86	0.97	0.98	0.86
A82T	0.56	0.80	0.75	0.80	1.00	0.99	0.82
A82G	0.64	0.80	0.71	0.82	1.00	0.99	0.84
A82C	0.58	0.80	0.74	0.80	1.00	0.99	0.83
A83T	0.56	0.79	0.81	0.81	0.99	0.99	0.84
A83G	0.61	0.79	0.75	0.82	0.99	0.99	0.84
T84G	0.69	0.83	0.71	0.85	1.00	1.00	0.86
T84C	0.63	0.80	0.72	0.82	0.99	0.99	0.83
T84A	0.69	0.78	0.70	0.83	1.00	0.99	0.84
C85T	0.59	0.67	0.69	0.82	0.88	0.91	0.80
C85A	0.48	0.75	0.79	0.78	0.95	0.99	0.78
T86G	0.72	0.70	0.52	0.79	0.94	0.96	0.76
T86C	0.56	0.72	0.73	0.78	0.97	0.97	0.79
T86A	0.52	0.71	0.75	0.75	0.98	0.93	0.81
G87T	0.54	0.72	0.70	0.75	0.97	0.97	0.77
G87A	0.58	0.79	0.73	0.81	0.98	0.99	0.82
A88T	0.51	0.72	0.77	0.76	0.98	0.97	0.79
A88G	0.50	0.76	0.76	0.75	0.99	1.00	0.78
A88C	0.64	0.75	1.00	1.00	0.83	0.86	1.00
G89T	0.61	0.73	0.74	0.80	0.97	0.93	0.85
G89A	0.62	0.83	0.66	0.82	1.00	1.00	0.83
T90G	0.48	0.76	0.71	0.73	0.99	0.99	0.76
T90C	0.60	0.76	0.79	0.89	0.90	1.00	0.83
T90A	0.58	0.77	0.77	0.81	0.99	0.99	0.83
G91C	0.50	0.76	0.86	0.80	0.97	0.99	0.82
G91A	0.58	0.79	0.70	0.80	0.99	0.99	0.81
GC92G	0.69	0.77	0.74	0.86	0.96	0.97	0.86
C92T	0.61	0.77	0.68	0.79	0.99	1.00	0.80
C92A	0.72	0.81	0.75	0.86	1.00	0.97	0.89
C93T	0.58	0.78	0.71	0.79	0.99	0.99	0.81
C93A	0.48	0.80	0.83	0.80	0.98	1.00	0.83
C94T	0.59	0.78	0.73	0.80	0.99	0.97	0.83
C94G	0.52	0.75	0.82	0.79	0.97	0.97	0.82
C94A	0.68	0.84	0.73	0.86	1.00	1.00	0.87
G95T	0.60	0.81	0.71	0.82	1.00	1.00	0.83
G95C	0.85	0.84	0.76	0.93	0.96	0.98	0.91
G95A	0.58	0.81	0.69	0.80	1.00	1.00	0.82
G95GA	0.55	0.81	0.75	0.81	0.99	1.00	0.83
GA96G	0.44	0.66	0.83	0.71	0.95	0.90	0.78
A96T	0.60	0.75	0.68	0.78	0.99	0.98	0.80
A96G	0.58	0.81	0.72	0.81	1.00	1.00	0.82
A96C	0.64	0.82	0.69	0.83	1.00	1.00	0.84
AG97A	0.64	0.81	0.70	0.82	1.00	0.99	0.84
G97T	0.66	0.78	0.73	0.83	0.99	0.99	0.84
G97C	0.63	0.70	0.75	0.83	0.93	0.87	0.91
G97A	0.61	0.80	0.74	0.82	1.00	1.00	0.84
G98T	0.66	0.77	0.76	0.85	0.97	0.96	0.87
G98C	0.77	0.89	0.92	0.91	1.00	0.98	0.95
G98A	0.64	0.80	0.77	0.85	0.97	1.00	0.85
G99T	0.62	0.82	0.78	0.83	1.00	0.98	0.86
G99C	0.57	0.79	0.79	0.81	0.99	0.98	0.84
G99A	0.64	0.77	0.78	0.86	0.95	0.96	0.86

Best Fit Values of Model Parameters

G100T	0.56	0.81	0.70	0.79	1.00	1.00	0.81
G100C	0.61	0.78	0.71	0.80	1.00	0.99	0.82
G100A	0.66	0.82	0.68	0.83	1.00	1.00	0.84
A101T	0.59	0.77	0.78	0.81	0.99	0.98	0.84
A101G	0.59	0.78	0.73	0.80	0.99	0.99	0.82
T102C	0.57	0.81	0.77	0.81	1.00	0.99	0.84
T102A	0.55	0.79	0.78	0.81	0.99	0.99	0.83
TG103T	0.68	0.85	0.77	0.87	0.99	1.00	0.88
G103T	0.67	0.77	0.59	0.79	0.99	1.00	0.78
G103A	0.58	0.84	0.66	0.80	1.00	0.99	0.82
G104A	0.59	0.80	0.73	0.84	0.96	1.00	0.83
GA105G	0.58	0.85	0.67	0.81	0.99	1.00	0.82
A105T	0.63	0.81	0.71	0.83	0.99	0.99	0.84
A105G	0.57	0.82	0.69	0.80	1.00	0.99	0.82
A105C	0.61	0.76	0.53	0.73	1.00	0.97	0.75
G106T	0.65	0.78	0.77	0.83	1.00	0.98	0.86
G106C	0.53	0.73	0.97	0.98	0.82	0.88	0.95
G106A	0.59	0.79	0.73	0.80	1.00	0.98	0.84
C107T	0.64	0.79	0.65	0.81	0.99	1.00	0.81
C107G	0.51	0.83	0.81	0.80	1.00	0.97	0.86
C107A	0.60	0.78	0.74	0.80	1.00	1.00	0.82
T108G	0.67	0.83	0.71	0.84	1.00	1.00	0.85
T108C	0.62	0.84	0.74	0.84	1.00	0.99	0.86
T108A	0.62	0.79	0.69	0.82	0.98	0.99	0.82
G109T	0.55	0.74	0.67	0.75	0.99	1.00	0.77
G109C	0.64	0.77	0.74	0.83	0.98	0.97	0.85
G109A	0.56	0.77	0.78	0.81	0.98	0.99	0.82
C110T	0.62	0.87	0.76	0.91	0.93	1.00	0.87
C110A	0.59	0.84	0.66	0.81	0.99	1.00	0.82
T111G	0.59	0.79	0.81	0.82	0.99	0.98	0.85
T111C	0.57	0.81	0.73	0.81	1.00	0.99	0.83
T111A	0.60	0.82	0.75	0.82	0.99	1.00	0.84
TG112T	0.61	0.78	0.77	0.83	0.97	1.00	0.83
G112T	0.65	0.79	0.65	0.80	1.00	0.99	0.82
G112C	0.71	0.85	0.80	0.88	1.00	0.99	0.89
G112A	0.55	0.76	0.86	0.82	0.98	0.95	0.87
G113T	0.65	0.75	0.76	0.84	0.96	0.94	0.87
G113C	0.78	0.78	0.75	0.94	0.91	0.90	0.95
G113A	0.62	0.80	0.79	0.83	0.99	0.99	0.86
C114T	0.68	0.81	0.70	0.86	0.97	1.00	0.84
C114G	0.61	0.79	0.81	0.83	0.99	0.98	0.86
C114A	0.73	0.77	0.79	0.97	0.87	0.88	0.96
CT115C	0.66	0.83	0.68	0.83	1.00	0.99	0.85
T115G	0.75	0.63	0.63	0.92	0.81	0.83	0.89
T115C	0.62	0.82	0.78	0.84	1.00	0.99	0.86
T115A	0.57	0.80	0.75	0.81	0.99	1.00	0.82
T116C	0.58	0.82	0.74	0.82	0.99	1.00	0.83
T116A	0.64	0.81	0.71	0.83	1.00	1.00	0.84
T117C	0.64	0.77	0.76	0.85	0.96	1.00	0.83
T117A	0.59	0.72	0.75	0.79	0.98	1.00	0.79
TA118T	0.57	0.84	0.76	0.83	0.98	1.00	0.85
A118T	0.51	0.79	0.81	0.79	0.99	0.99	0.82
A118G	0.65	0.82	0.73	0.84	1.00	0.99	0.85

A118C	0.66	0.74	0.74	0.86	0.93	0.95	0.86
C119T	0.60	0.82	0.70	0.81	1.00	0.96	0.86
C119G	0.52	0.75	0.84	0.81	0.96	0.98	0.82
C119A	0.56	0.81	0.54	0.74	0.99	1.00	0.73
A120T	0.59	0.80	0.70	0.80	0.99	0.99	0.82
A120G	0.57	0.81	0.72	0.81	0.99	1.00	0.82
A120C	0.52	0.81	0.89	0.85	0.96	1.00	0.86
C121T	0.56	0.78	0.74	0.79	0.99	0.99	0.82
C121G	0.48	0.81	0.87	0.80	0.99	1.00	0.83
C121A	0.56	0.79	0.71	0.79	0.99	0.98	0.81
T122G	0.62	0.82	0.77	0.84	1.00	0.99	0.86
T122C	0.62	0.77	0.80	0.83	0.98	0.97	0.86
T122A	0.64	0.78	0.71	0.82	0.99	0.98	0.85
G123T	0.62	0.81	0.77	0.84	0.99	0.99	0.86
G123C	0.58	0.83	0.71	0.81	1.00	1.00	0.82
G123A	0.58	0.82	0.69	0.80	1.00	1.00	0.82
C124T	0.60	0.83	0.78	0.87	0.95	1.00	0.85
C124G	0.53	0.75	0.81	0.80	0.97	0.99	0.81
C124A	0.64	0.79	0.69	0.82	0.99	0.99	0.83
C125T	0.59	0.77	0.79	0.82	0.99	0.98	0.84
C125A	0.62	0.82	0.70	0.83	0.99	1.00	0.83
T126G	0.83	0.75	0.56	0.85	0.94	0.92	0.85
T126C	0.62	0.76	0.70	0.80	0.99	0.99	0.81
T126A	0.46	0.80	0.75	0.75	0.99	0.99	0.79
G127T	0.57	0.78	0.70	0.79	0.99	0.99	0.81
G127A	0.59	0.88	0.86	0.88	0.97	1.00	0.89
G128T	0.62	0.87	0.68	0.87	0.97	1.00	0.85
G128C	0.67	0.81	0.78	0.86	0.98	1.00	0.87
G128A	0.65	0.84	0.71	0.84	1.00	0.99	0.86
C129T	0.59	0.82	0.76	0.82	0.99	0.99	0.84
C129G	0.64	0.74	0.82	0.91	0.89	0.92	0.91
C129A	0.63	0.76	0.77	0.83	0.98	0.97	0.85
CT130C	0.69	0.90	0.81	0.89	1.00	0.98	0.92
T130G	0.65	0.75	0.77	0.89	0.91	0.99	0.83
T130C	0.64	0.75	0.81	0.89	0.91	0.93	0.89
T130A	0.56	0.80	0.72	0.79	1.00	1.00	0.82
T131G	0.44	0.79	0.82	0.76	0.99	0.99	0.79
T131C	0.59	0.77	0.67	0.78	0.99	0.99	0.79
T131A	0.61	0.75	0.72	0.78	1.00	0.94	0.85
T132C	0.62	0.79	0.74	0.82	1.00	0.99	0.84
T132A	0.58	0.84	0.67	0.80	0.99	1.00	0.81
TC133T	0.75	0.89	0.65	0.88	1.00	1.00	0.87
C133T	0.58	0.79	0.69	0.79	0.99	1.00	0.80
C133G	0.67	0.65	0.97	1.00	0.79	0.81	1.00
C133A	0.64	0.74	0.85	0.96	0.85	0.88	0.95
G134T	0.66	0.86	0.68	0.85	1.00	1.00	0.86
G134C	0.64	0.82	0.69	0.83	0.99	1.00	0.83
G134A	0.59	0.80	0.72	0.80	1.00	0.99	0.83
C135T	0.59	0.72	0.71	0.78	0.98	0.94	0.82
C135G	0.36	0.43	1.00	0.82	0.20	0.32	0.72
C135A	0.52	0.92	0.95	0.86	0.99	0.99	0.92
T136C	0.59	0.78	0.80	0.81	1.00	0.98	0.85
T136A	0.55	0.78	0.72	0.78	1.00	0.99	0.80

Best Fit Values of Model Parameters

T137G	0.62	0.78	0.76	0.81	1.00	0.97	0.85
T137C	0.60	0.80	0.70	0.80	1.00	1.00	0.82
T137A	0.58	0.82	0.75	0.82	1.00	0.99	0.84
TC138T	0.63	0.78	0.68	0.81	0.98	0.99	0.81
C138T	0.58	0.77	0.69	0.78	1.00	0.93	0.85
C139T	0.56	0.78	0.70	0.78	0.99	1.00	0.80
C139A	0.58	0.79	0.72	0.80	0.99	0.98	0.83
T140C	0.60	0.78	0.73	0.81	0.99	1.00	0.82
T140A	0.59	0.78	0.74	0.80	0.99	0.99	0.82
A141T	0.56	0.80	0.74	0.80	0.99	1.00	0.82
A141G	0.61	0.79	0.77	0.82	0.99	0.98	0.85
A141C	0.60	0.73	0.79	0.82	0.96	0.93	0.87
A141AC	0.56	0.81	0.73	0.80	1.00	0.99	0.83
AC142A	0.65	0.81	0.70	0.83	1.00	1.00	0.84
C142T	0.60	0.80	0.73	0.82	0.99	1.00	0.82
C142G	0.57	0.77	0.78	0.79	1.00	0.98	0.83
C142A	0.64	0.67	0.77	0.90	0.85	0.84	0.93
C143T	0.62	0.73	0.64	0.77	0.99	0.99	0.78
C143G	0.55	0.76	0.76	0.79	0.98	0.98	0.81
C143A	0.65	0.77	0.74	0.83	0.98	1.00	0.83
C144T	0.61	0.74	0.78	0.80	0.99	0.97	0.84
C144G	0.81	0.82	0.61	0.86	0.99	1.00	0.84
C144A	0.70	0.82	0.80	0.87	0.98	0.99	0.87
C145T	0.63	0.80	0.68	0.81	1.00	0.99	0.83
C145G	0.62	0.77	0.75	0.82	0.98	0.98	0.83
C145A	0.67	0.77	0.62	0.80	1.00	0.99	0.80
C146T	0.62	0.82	0.72	0.82	1.00	1.00	0.84
C146A	0.60	0.84	0.75	0.83	1.00	0.99	0.86
CA147C	0.62	0.62	0.66	0.79	0.89	0.85	0.84
A147T	0.60	0.81	0.73	0.82	0.99	1.00	0.83
A147G	0.59	0.80	0.76	0.82	0.99	0.99	0.84
A147C	0.62	0.80	0.74	0.82	1.00	0.98	0.85
A147AC	0.58	0.83	0.77	0.82	1.00	0.99	0.85
AC148A	0.64	0.80	0.75	0.83	1.00	1.00	0.84
C148T	0.66	0.79	0.74	0.84	0.98	0.99	0.85
C148G	0.62	0.82	0.74	0.83	0.99	0.99	0.85
C148A	0.73	0.88	0.70	0.89	1.00	1.00	0.89
C149T	0.62	0.79	0.76	0.82	1.00	0.99	0.84
C149G	0.49	0.79	0.80	0.77	1.00	0.99	0.81
C149A	0.58	0.76	0.71	0.79	0.99	0.98	0.81
C150T	0.60	0.74	0.79	0.89	0.89	0.98	0.83
C150G	0.78	0.79	0.61	0.85	0.98	0.99	0.83
C150A	0.65	0.78	0.73	0.88	0.93	1.00	0.83
C151T	0.55	0.74	0.77	0.78	0.98	0.98	0.80
C151CT	0.58	0.87	0.64	0.81	1.00	0.96	0.86
A152T	0.59	0.77	0.73	0.80	0.99	0.99	0.82
A152G	0.58	0.78	0.76	0.80	1.00	0.99	0.83
A152C	0.68	0.81	0.81	0.86	0.99	0.99	0.88
AT153A	0.68	0.86	0.76	0.86	1.00	0.99	0.88
T153C	0.61	0.77	0.70	0.80	0.99	0.99	0.81
T153A	0.61	0.75	0.78	0.81	0.99	0.99	0.83
C154T	0.58	0.83	0.70	0.81	0.99	1.00	0.83
C154G	0.59	0.75	0.68	0.78	0.98	0.98	0.79

Best Fit Values of Model Parameters

C154A	0.56	0.81	0.72	0.80	1.00	0.99	0.82
C155T	0.57	0.81	0.72	0.81	0.99	0.99	0.83
C155G	0.62	0.82	0.75	0.83	1.00	0.99	0.85
C155A	0.61	0.76	0.73	0.80	0.99	0.98	0.83
CA156C	0.60	0.86	0.67	0.82	1.00	1.00	0.84
A156T	0.60	0.82	0.70	0.81	1.00	0.99	0.83
A156G	0.58	0.78	0.73	0.79	1.00	0.99	0.82
A156C	0.69	0.81	0.78	0.87	0.98	0.98	0.88
AC157A	0.60	0.81	0.71	0.81	1.00	0.99	0.83
C157T	0.65	0.82	0.73	0.85	0.98	1.00	0.85
C157G	0.62	0.81	0.67	0.81	1.00	0.99	0.82
C157A	0.62	0.73	0.56	0.71	1.00	0.90	0.79
C158T	0.57	0.79	0.72	0.80	1.00	1.00	0.81
C158G	0.56	0.76	0.71	0.77	0.99	0.98	0.79
C158A	0.62	0.77	0.71	0.82	0.97	0.99	0.82
C159T	0.61	0.80	0.64	0.80	0.99	1.00	0.80
C159G	0.67	0.81	0.57	0.80	1.00	0.99	0.80
C159A	0.72	0.92	0.76	0.89	1.00	1.00	0.91
CA160C	0.61	0.86	0.77	0.85	1.00	0.99	0.87
A160T	0.67	0.77	0.71	0.85	0.96	1.00	0.82
A160G	0.70	0.75	0.75	0.90	0.92	0.94	0.88
A160C	0.60	0.84	0.71	0.83	1.00	0.99	0.85
G161T	0.56	0.83	0.72	0.81	1.00	0.98	0.84
G161C	0.50	0.75	0.84	0.79	0.97	0.98	0.81
G161A	0.54	0.79	0.77	0.79	0.99	0.99	0.82
T162G	0.60	0.84	0.66	0.82	0.99	1.00	0.82
T162C	0.64	0.80	0.73	0.82	1.00	0.99	0.84
T162A	0.60	0.79	0.73	0.82	0.98	0.99	0.83
G163T	0.52	0.84	0.67	0.78	1.00	1.00	0.80
G163C	0.60	0.69	0.67	0.77	0.95	0.97	0.77
G163A	0.59	0.80	0.75	0.81	1.00	1.00	0.84
C164T	0.60	0.79	0.73	0.82	0.98	1.00	0.82
C164G	0.55	0.92	0.73	0.84	1.00	1.00	0.86
C164A	0.78	0.78	0.71	0.89	0.96	0.94	0.90
C165T	0.54	0.76	0.73	0.77	0.99	1.00	0.79
C165G	0.77	0.88	0.57	0.87	1.00	1.00	0.85
C165A	0.66	0.77	0.92	0.99	0.85	0.87	0.99
CA166C	0.47	0.76	1.00	0.90	0.87	0.91	0.93
A166T	0.66	0.80	0.68	0.83	0.99	1.00	0.83
A166G	0.64	0.79	0.74	0.83	0.99	0.99	0.84
A166C	0.58	0.82	0.70	0.80	1.00	0.99	0.82
A167T	0.59	0.75	0.78	0.83	0.95	0.99	0.81
A167G	0.58	0.83	0.65	0.80	1.00	1.00	0.81
AC168A	0.46	0.72	0.76	0.72	0.98	0.98	0.75
C168T	0.63	0.82	0.66	0.82	1.00	1.00	0.83
C168G	0.65	0.82	0.68	0.83	1.00	1.00	0.83
C168A	0.61	0.85	0.69	0.90	0.93	1.00	0.85
C169T	0.62	0.82	0.69	0.82	1.00	1.00	0.83
C169G	0.55	0.72	0.83	0.79	0.98	0.93	0.86
C169A	0.64	0.80	0.76	0.84	0.99	1.00	0.85
T170G	0.71	0.79	0.79	0.91	0.93	0.98	0.88
T170C	0.61	0.77	0.73	0.82	0.97	0.99	0.82
T170A	0.61	0.79	0.71	0.81	1.00	0.97	0.84

Best Fit Values of Model Parameters

A171T	0.65	0.78	0.74	0.82	1.00	0.99	0.84
A171G	0.60	0.76	0.84	0.85	0.96	0.95	0.88
A171C	0.71	0.64	0.77	0.99	0.77	0.78	0.98
G172T	0.59	0.78	0.93	0.95	0.87	0.92	0.94
G172A	0.61	0.77	0.75	0.83	0.97	0.98	0.83
GT173G	0.90	0.94	0.93	0.97	0.98	1.00	0.96
T173G	0.61	0.82	0.71	0.82	1.00	0.99	0.84
T173C	0.62	0.80	0.71	0.81	1.00	0.99	0.83
T173A	0.60	0.79	0.79	0.82	0.99	0.99	0.85
T174G	0.57	0.67	0.52	0.63	0.78	0.69	0.71
T174C	0.55	0.77	0.70	0.76	1.00	0.94	0.83
T174A	0.65	0.82	0.75	0.84	1.00	0.99	0.86
C175T	0.60	0.82	0.63	0.79	1.00	1.00	0.80
C175G	0.52	0.75	0.87	0.82	0.95	0.95	0.86
C175A	0.69	0.97	0.72	0.90	1.00	1.00	0.91
C176T	0.69	0.79	0.70	0.84	0.99	0.97	0.86
C176A	0.67	0.80	0.63	0.81	1.00	0.99	0.82
A177T	0.55	0.81	0.64	0.77	0.99	1.00	0.79
A177G	0.65	0.80	0.63	0.81	0.99	1.00	0.81
A177C	0.62	0.63	0.73	0.89	0.82	0.83	0.88
C178T	0.71	0.78	0.74	0.86	0.98	0.98	0.87
C178G	0.73	0.82	0.82	0.88	0.99	0.97	0.91
C178A	0.58	0.83	0.70	0.81	1.00	0.99	0.84
T179G	0.62	0.74	0.77	0.81	0.99	0.96	0.85
T179C	0.60	0.80	0.77	0.82	1.00	0.94	0.89
T179A	0.57	0.83	0.73	0.81	1.00	1.00	0.83
G180T	0.48	0.82	0.68	0.74	1.00	0.99	0.78
G180A	0.48	0.75	0.69	0.73	0.98	1.00	0.73
A181T	0.55	0.79	0.65	0.76	1.00	0.96	0.81
A181G	0.68	0.79	0.68	0.83	0.99	0.99	0.84
A181C	0.53	0.77	1.00	0.96	0.85	0.89	0.96
A182T	0.45	0.78	0.92	0.79	0.99	0.99	0.84
A182G	0.59	0.84	0.67	0.81	0.99	0.99	0.83
A182C	0.57	0.84	0.52	0.75	0.99	0.98	0.75
G183T	0.53	0.85	0.89	0.84	0.99	0.99	0.87
G183C	0.48	0.88	0.63	0.75	1.00	0.99	0.78
G183A	0.58	0.77	0.72	0.80	0.98	1.00	0.80
C184T	0.67	0.80	0.88	0.96	0.89	0.95	0.92
C184A	0.94	0.70	0.70	1.00	0.85	0.83	1.00
C185T	0.77	0.77	0.79	0.95	0.91	0.89	0.97
C185A	0.70	0.72	0.66	0.82	0.98	0.97	0.82
T186G	0.35	0.96	0.84	0.77	1.00	1.00	0.82
T186C	0.62	0.78	0.73	0.82	0.99	0.99	0.83
T186A	0.63	0.80	0.71	0.82	0.99	0.98	0.84
G187T	0.69	0.85	0.58	0.84	1.00	0.99	0.84
G187A	0.50	0.72	0.84	0.78	0.97	0.95	0.82
A188T	0.55	0.80	0.72	0.83	0.94	1.00	0.81
A188G	0.59	0.81	0.66	0.80	1.00	1.00	0.82
A188C	0.62	0.80	0.72	0.83	0.98	1.00	0.83
AG189A	0.58	0.82	0.62	0.79	1.00	1.00	0.80
G189T	0.56	0.85	0.66	0.80	1.00	1.00	0.82
G189C	0.60	0.80	0.67	0.80	0.99	1.00	0.81
G189A	0.55	0.78	0.80	0.80	0.99	0.99	0.83

Best Fit Values of Model Parameters

G190T	0.53	0.86	0.65	0.78	1.00	0.97	0.83
G190A	0.64	0.84	0.80	0.85	1.00	0.99	0.88
A191T	0.52	0.80	0.71	0.78	0.99	0.99	0.80
A191G	0.56	0.84	0.65	0.79	0.99	0.99	0.81
A191C	0.57	0.87	0.65	0.81	1.00	1.00	0.82
G192T	0.66	0.84	0.75	0.85	1.00	0.99	0.87
G192C	0.62	0.79	0.65	0.80	1.00	1.00	0.80
G192A	0.59	0.76	0.75	0.80	0.99	0.99	0.81
C193T	0.66	0.81	0.71	0.84	0.99	1.00	0.84
C193G	0.58	0.83	0.73	0.82	0.99	1.00	0.84
C193A	0.65	0.82	0.64	0.85	0.96	1.00	0.82
A194T	0.59	0.77	0.69	0.78	1.00	0.97	0.81
A194G	0.60	0.81	0.73	0.82	0.99	0.99	0.83
T195G	0.61	0.81	0.68	0.81	1.00	1.00	0.83
T195C	0.59	0.79	0.75	0.82	0.99	0.99	0.83
T195A	0.65	0.78	0.77	0.83	0.99	1.00	0.84
G196T	0.61	0.79	0.76	0.84	0.97	1.00	0.84
G196C	0.63	0.84	0.69	0.83	0.99	1.00	0.84
G196A	0.63	0.82	0.74	0.83	1.00	0.98	0.86
C197T	0.52	0.79	0.80	0.79	0.99	0.99	0.82
C197G	0.45	0.82	0.80	0.77	0.99	1.00	0.80
C197A	0.63	0.79	0.69	0.82	0.98	0.99	0.83
C198T	0.56	0.78	0.70	0.78	0.99	1.00	0.80
C198G	0.75	0.80	0.84	0.98	0.89	0.93	0.95
C198A	0.54	0.73	0.73	0.77	0.97	0.98	0.79
A199T	0.61	0.83	0.72	0.82	1.00	1.00	0.84
A199G	0.65	0.81	0.66	0.82	1.00	1.00	0.82
A199C	0.61	0.83	0.75	0.83	0.99	1.00	0.85
AT200A	0.41	0.87	0.97	0.81	0.99	0.99	0.87
T200C	0.65	0.81	0.74	0.83	1.00	0.99	0.85
T200A	0.63	0.79	0.71	0.82	0.99	0.99	0.83
T201G	0.68	0.72	0.85	0.99	0.83	0.84	0.99
T201C	0.53	0.78	0.88	0.82	0.98	0.97	0.86
T201A	0.63	0.79	0.79	0.83	0.99	0.98	0.86
A202T	0.65	0.79	0.74	0.83	0.99	1.00	0.84
A202G	0.60	0.77	0.74	0.81	0.98	0.98	0.83
A202C	0.63	0.74	0.72	0.83	0.96	0.99	0.82
A203T	0.54	0.78	0.83	0.82	0.97	0.98	0.84
A203G	0.57	0.78	0.63	0.76	1.00	0.99	0.78
G204T	0.55	0.93	0.64	0.83	1.00	1.00	0.85
G204C	0.52	0.82	0.81	0.80	1.00	1.00	0.83
G204A	0.62	0.77	0.93	0.98	0.85	0.89	0.96
T205G	0.68	0.76	0.86	0.97	0.87	0.88	0.98
T205C	0.62	0.82	0.79	0.84	0.99	0.98	0.87
T205A	0.66	0.80	0.68	0.83	1.00	0.99	0.84
T206G	0.57	0.80	0.65	0.78	1.00	1.00	0.79
T206C	0.61	0.77	0.77	0.82	0.99	0.99	0.83
T206A	0.57	0.80	0.73	0.80	0.99	1.00	0.82
T207G	0.57	0.79	0.73	0.80	1.00	1.00	0.81
T207C	0.63	0.84	0.77	0.84	1.00	0.99	0.87
T207A	0.64	0.85	0.67	0.84	1.00	0.99	0.86
G208T	0.57	0.75	0.72	0.79	0.99	0.99	0.81
G208A	0.65	0.79	0.75	0.83	1.00	0.93	0.90

Best Fit Values of Model Parameters

A209T	0.61	0.79	0.68	0.82	0.97	1.00	0.81
A209G	0.53	0.81	0.63	0.76	1.00	0.99	0.78
A209C	0.65	0.85	0.69	0.85	1.00	1.00	0.86
G210T	0.47	0.82	0.51	0.64	0.95	0.95	0.65
G210C	0.60	0.84	0.63	0.81	1.00	1.00	0.83
G210A	0.49	0.79	0.64	0.73	0.98	0.99	0.75
G211T	0.03	0.73	0.49	0.07	0.23	0.37	0.35
T212C	0.19	0.76	0.56	0.37	0.34	0.37	0.52
T212A	0.02	0.66	0.63	0.07	0.26	0.31	0.51
A213T	0.40	0.82	0.49	0.53	0.65	0.79	0.46
A213G	0.58	0.79	0.66	0.78	1.00	0.99	0.80
A214T	0.53	0.85	0.67	0.79	1.00	1.00	0.81
A214G	0.53	0.79	0.64	0.75	0.99	1.00	0.77
A214C	0.57	0.90	0.72	0.84	1.00	1.00	0.87
G215C	0.41	0.82	0.54	0.56	0.99	0.93	0.62
G215A	0.46	0.85	0.51	0.93	0.69	1.00	0.66
T216G	0.48	0.89	0.48	0.71	0.95	0.98	0.69
T216C	0.59	0.80	0.66	0.83	0.96	1.00	0.81
T216A	0.53	0.79	0.64	0.75	0.99	0.99	0.77
G217T	0.60	0.72	0.68	0.78	0.97	0.96	0.79
G217C	0.59	0.75	0.87	0.92	0.87	0.88	0.93
G217A	0.63	0.84	0.68	0.83	1.00	1.00	0.84
GT218G	1.00	0.59	0.92	1.00	0.81	0.80	1.00
T218G	0.52	0.93	0.74	0.83	1.00	1.00	0.88
T218C	0.54	0.80	0.73	0.78	1.00	0.99	0.81
T218A	0.65	0.78	0.70	0.82	1.00	0.99	0.83
TA219T	0.64	0.77	0.64	0.80	0.98	0.99	0.80
A219T	0.60	0.80	0.66	0.81	0.99	1.00	0.81
A219G	0.65	0.84	0.72	0.84	1.00	1.00	0.85
A220T	0.62	0.68	0.83	0.95	0.82	0.83	0.95
A220G	0.55	0.81	0.74	0.81	0.98	1.00	0.82
A220C	0.69	0.80	0.77	0.87	0.97	1.00	0.85
AG221A	0.63	0.66	0.69	0.81	0.92	0.85	0.89
G221T	0.62	0.73	0.70	0.78	0.99	0.99	0.79
G221A	0.57	0.79	0.60	0.76	1.00	0.97	0.79
G222T	0.57	0.83	0.67	0.80	1.00	0.99	0.81
G222A	0.50	0.83	0.64	0.76	1.00	1.00	0.78
G223T	0.71	0.77	0.81	0.94	0.90	0.91	0.94
G223A	0.56	0.76	0.70	0.77	1.00	0.98	0.80
A224T	0.59	0.73	0.74	0.79	0.98	0.97	0.82
A224G	0.57	0.73	0.86	0.88	0.89	0.90	0.90
T225C	0.65	0.77	0.80	0.84	0.98	0.95	0.89
TA226T	0.76	0.50	0.83	1.00	0.64	0.65	1.00
A226T	0.51	0.73	0.81	0.78	0.97	0.96	0.81
A226G	0.65	0.77	0.82	0.90	0.92	0.93	0.90
A226C	0.73	0.59	0.65	0.94	0.76	0.78	0.91
A226AT	0.47	0.85	0.74	0.77	1.00	1.00	0.81
A226AG	0.59	0.85	0.72	0.82	1.00	1.00	0.85
AG227A	0.59	0.79	0.50	0.73	0.98	0.99	0.72
G227T	0.52	0.78	0.80	0.78	1.00	0.99	0.81
G227C	0.50	0.34	0.51	0.64	0.16	0.16	0.65
G227A	0.47	0.73	0.81	0.75	0.98	0.98	0.78
G228T	0.65	0.59	0.53	0.68	0.45	0.39	0.78

Best Fit Values of Model Parameters

G228A	0.49	0.62	0.74	0.75	0.80	0.74	0.84
G228GT	0.68	0.72	0.66	0.82	0.96	0.97	0.81
G229T	0.60	0.62	0.67	0.83	0.82	0.90	0.77
G229A	0.47	0.63	0.71	0.85	0.58	0.75	0.68
G230T	0.55	0.61	0.79	0.88	0.77	0.80	0.87
G230C	0.51	0.68	0.67	0.73	0.91	0.95	0.72
G230A	0.57	0.71	0.70	0.77	0.96	0.95	0.79
C231T	0.55	0.80	0.74	0.79	1.00	1.00	0.82
C231A	0.58	0.81	0.82	0.86	0.96	1.00	0.84
CA232C	0.54	0.83	0.96	0.86	0.98	0.98	0.89
A232T	0.59	0.77	0.79	0.83	0.97	0.99	0.83
A232G	0.59	0.83	0.74	0.82	0.99	1.00	0.84
A232C	0.62	0.71	0.77	0.88	0.89	0.90	0.88
AG233A	0.64	0.70	0.68	0.78	0.98	0.99	0.78
G233T	0.49	0.65	0.88	0.91	0.79	0.84	0.88
G233C	0.58	0.69	0.70	0.78	0.94	0.94	0.79
G233A	0.58	0.64	0.85	0.96	0.77	0.82	0.92
G234T	0.62	0.58	0.81	0.97	0.73	0.76	0.94
G234C	0.67	0.69	0.79	0.96	0.83	0.87	0.93
G234A	0.56	0.58	0.85	0.91	0.76	0.72	0.98
G235T	0.64	0.65	0.73	0.86	0.87	0.83	0.92
G235A	0.58	0.70	0.75	0.81	0.93	0.97	0.80
A236T	0.61	0.79	0.81	0.83	0.99	0.97	0.87
A236G	0.57	0.80	0.87	0.83	1.00	0.97	0.87
A236C	0.57	0.73	0.55	0.75	0.90	0.92	0.74
C237T	0.65	0.79	0.70	0.82	0.99	0.99	0.83
C237G	0.55	0.83	0.70	0.79	0.99	1.00	0.81
A238T	0.58	0.80	0.77	0.82	0.98	1.00	0.83
A238G	0.62	0.80	0.77	0.83	0.99	0.97	0.86
A238C	0.50	0.83	0.89	0.84	0.96	1.00	0.84
G239T	0.57	0.70	0.80	0.82	0.93	0.89	0.88
G239C	0.55	0.76	0.75	0.78	0.99	0.99	0.80
G239A	0.61	0.75	0.73	0.81	0.98	0.97	0.83
T240C	0.62	0.76	0.74	0.80	1.00	0.95	0.86
T240A	0.61	0.78	0.70	0.80	0.99	0.99	0.82
T241G	0.67	0.82	0.83	0.87	0.99	0.99	0.88
T241C	0.64	0.82	0.72	0.83	1.00	0.96	0.88
T241A	0.60	0.72	0.74	0.79	0.98	0.98	0.81
TG242T	0.58	0.84	0.77	0.83	1.00	1.00	0.86
G242T	0.49	0.76	0.87	0.81	0.96	0.98	0.83
G242C	0.51	0.84	0.74	0.79	1.00	1.00	0.82
G242A	0.54	0.83	0.59	0.77	0.98	1.00	0.77
G243T	0.57	0.87	0.63	0.80	1.00	1.00	0.82
G243A	0.63	0.84	0.61	0.82	1.00	1.00	0.82
G244T	0.57	0.90	0.70	0.85	0.97	1.00	0.86
G244A	0.58	0.86	0.67	0.82	1.00	1.00	0.84
G245T	0.62	0.83	0.75	0.85	0.98	1.00	0.85
G245C	0.44	0.68	0.78	0.69	0.98	0.91	0.77
G245A	0.60	0.80	0.68	0.80	1.00	1.00	0.81
G245GT	1.00	0.02	1.00	0.99	0.01	0.02	0.99
GA246G	0.61	0.56	0.73	0.80	0.62	0.55	0.91
A246T	0.63	0.77	0.73	0.82	0.98	0.98	0.84
A246G	0.56	0.48	0.89	0.84	0.32	0.35	0.81

Best Fit Values of Model Parameters

T247G	0.62	0.77	0.71	0.80	1.00	0.98	0.83
T247C	0.52	0.74	0.89	0.81	0.96	0.97	0.84
T247A	0.53	0.81	0.76	0.80	1.00	1.00	0.82
C248T	0.58	0.79	0.77	0.82	0.99	0.99	0.83
C248G	0.31	0.68	1.00	0.86	0.68	0.74	0.88
C248A	0.59	0.77	0.84	0.85	0.96	0.96	0.87
T249G	0.56	0.73	0.81	0.83	0.94	0.97	0.83
T249C	0.59	0.73	0.73	0.79	0.98	0.97	0.81
T249A	0.59	0.76	0.75	0.80	0.99	0.99	0.81
G250T	0.52	0.81	0.73	0.78	0.99	0.99	0.81
G250C	0.57	0.81	0.71	0.80	1.00	1.00	0.82
G250A	0.57	0.80	0.74	0.80	1.00	0.99	0.82
GA251G	0.60	0.69	0.64	0.76	0.95	0.96	0.76
A251T	0.57	0.78	0.69	0.78	0.99	0.99	0.80
A251G	0.59	0.76	0.72	0.80	0.97	1.00	0.80
A251C	0.54	0.78	0.66	0.76	1.00	0.99	0.79
A252T	0.56	0.72	0.74	0.82	0.92	1.00	0.78
A252G	0.56	0.62	0.88	0.94	0.77	0.78	0.96
A252C	0.42	0.83	0.82	0.76	1.00	1.00	0.81
A253T	0.60	0.80	0.72	0.81	1.00	0.99	0.83
A253G	0.61	0.73	0.72	0.81	0.96	0.98	0.81
A253C	0.71	0.78	0.78	0.88	0.95	0.91	0.93
G254T	0.55	0.68	0.57	0.75	0.85	0.97	0.66
G254C	0.61	0.77	0.64	0.79	0.99	0.99	0.80
G254A	0.60	0.84	0.64	0.81	1.00	1.00	0.82
T255G	0.49	0.61	0.85	0.91	0.73	0.81	0.84
T255C	0.57	0.85	0.73	0.82	1.00	1.00	0.84
T255A	0.67	0.85	0.68	0.86	0.99	1.00	0.85
A256T	0.61	0.83	0.75	0.83	1.00	0.99	0.86
A256G	0.57	0.87	0.78	0.84	1.00	1.00	0.87
AG257A	0.53	0.81	0.72	0.78	1.00	1.00	0.81
G257T	0.69	0.83	0.77	0.86	0.99	1.00	0.87
G257A	0.61	0.84	0.68	0.82	1.00	1.00	0.83
G258T	0.53	0.82	0.79	0.80	1.00	0.99	0.84
G258A	0.58	0.70	0.76	0.79	0.96	0.94	0.83
G259T	0.60	0.94	0.75	0.87	1.00	1.00	0.88
G259C	0.40	0.90	0.99	0.82	0.98	0.99	0.89
G259A	0.65	0.81	0.68	0.83	0.99	1.00	0.83
G260C	0.73	0.72	0.63	0.83	0.96	0.97	0.82
G260A	0.63	0.73	0.72	0.81	0.97	0.97	0.82
GC261G	0.43	0.84	0.82	0.77	1.00	0.99	0.82
C261T	0.59	0.78	0.73	0.80	0.99	0.99	0.81
C261G	0.54	0.73	0.77	0.82	0.93	0.99	0.79
C261A	0.79	0.10	0.94	0.83	0.04	0.07	0.96
C262T	0.59	0.83	0.77	0.83	1.00	0.99	0.85
C262G	0.72	0.84	1.00	1.00	0.88	0.91	1.00
C262A	0.63	0.76	0.70	0.80	1.00	0.99	0.82
A263T	0.64	0.82	0.72	0.83	1.00	0.94	0.89
A263G	0.64	0.78	0.69	0.81	0.99	1.00	0.81
A263C	0.64	0.88	0.86	0.87	1.00	0.99	0.89
G264T	0.69	0.91	0.77	0.89	1.00	1.00	0.90
G264C	0.61	0.94	0.76	0.87	1.00	1.00	0.89
G264A	0.65	0.87	0.71	0.85	1.00	1.00	0.86

Best Fit Values of Model Parameters

C265T	0.53	0.81	0.78	0.80	1.00	0.99	0.83
C265G	0.45	0.92	0.77	0.80	1.00	1.00	0.84
C265A	0.64	0.82	0.74	0.84	0.98	1.00	0.84
C266T	0.70	0.94	0.75	0.90	1.00	1.00	0.91
C266G	0.23	0.63	1.00	0.97	0.34	0.67	0.68
C266A	0.36	0.81	0.81	0.71	0.99	0.99	0.76
T267C	0.51	0.84	0.85	0.81	1.00	0.95	0.89
T267A	0.71	0.93	0.67	0.89	1.00	1.00	0.89
TA268T	0.47	0.91	0.80	0.81	1.00	1.00	0.86
A268T	0.54	0.90	0.84	0.85	1.00	1.00	0.89
A268G	0.47	0.87	0.82	0.80	1.00	1.00	0.84
A268C	0.82	0.74	0.83	1.00	0.86	0.86	1.00
C269T	0.55	0.88	0.73	0.82	1.00	1.00	0.85
C269G	0.50	0.78	0.83	0.79	0.98	1.00	0.81
C269A	0.87	0.96	0.64	0.93	1.00	1.00	0.90
T270G	0.56	0.89	0.71	0.82	1.00	1.00	0.85
T270C	0.61	0.81	0.67	0.81	0.99	0.99	0.83
T270A	0.70	0.87	0.75	0.87	1.00	0.99	0.89
TG271T	0.40	0.84	0.81	0.75	0.99	1.00	0.79
G271T	0.59	0.93	0.77	0.86	1.00	1.00	0.89
G271C	0.65	0.87	0.64	0.87	0.96	1.00	0.84
G271A	0.75	0.93	0.72	0.90	1.00	0.99	0.91
G272T	0.63	0.94	0.80	0.88	1.00	1.00	0.90
G272C	0.50	0.73	1.00	0.97	0.81	0.85	0.99
G272A	0.77	0.96	0.68	0.90	1.00	1.00	0.90
C273T	0.64	0.84	0.67	0.83	1.00	1.00	0.83
C273G	0.57	0.73	0.77	0.80	0.97	0.96	0.82
C273A	0.74	0.92	0.69	0.89	1.00	1.00	0.89
T274G	0.79	0.94	0.57	0.90	1.00	1.00	0.87
T274C	0.64	0.83	0.72	0.85	0.98	1.00	0.85
T274A	0.63	0.80	0.71	0.82	1.00	0.98	0.85
TG275T	0.41	0.64	0.86	0.69	0.93	0.78	0.88
G275T	0.62	0.84	0.72	0.84	0.99	1.00	0.84
G275C	0.71	0.90	0.65	0.88	1.00	1.00	0.87
G275A	0.61	0.81	0.83	0.84	1.00	0.98	0.88
G276T	0.56	0.85	0.80	0.83	1.00	0.99	0.86
G276C	0.54	0.76	0.65	0.75	0.98	0.99	0.76
G276A	0.64	0.94	0.84	0.89	1.00	0.99	0.91
T277C	0.46	0.72	0.88	0.77	0.96	0.98	0.79
T277A	0.53	0.72	0.76	0.77	0.96	0.97	0.79
C278T	0.53	0.85	0.84	0.82	1.00	0.99	0.86
C278G	0.51	0.58	0.97	0.96	0.72	0.75	0.96
C278A	0.53	0.76	0.84	0.83	0.94	1.00	0.82
C279T	0.63	0.67	0.69	0.80	0.93	0.88	0.86
C279A	0.59	0.77	0.72	0.79	0.99	0.99	0.80
CT280C	0.47	0.12	0.96	0.85	0.03	0.14	0.74
T280G	0.77	0.03	0.69	0.91	0.01	0.03	0.74
T280C	0.40	0.21	0.95	0.80	0.07	0.12	0.69
T280A	0.52	0.19	0.96	0.76	0.07	0.09	0.84
C281T	0.53	0.75	0.81	0.79	0.98	0.99	0.81
C281A	0.53	0.83	0.82	0.85	0.96	1.00	0.84
A282T	0.57	0.46	0.68	0.63	0.24	0.19	0.86
A282G	0.62	0.10	0.75	0.91	0.03	0.05	0.67

Best Fit Values of Model Parameters

A282C	0.38	0.27	0.78	0.91	0.06	0.16	0.51
T283C	0.45	0.75	0.79	0.75	0.97	0.99	0.77
T283A	0.73	0.06	0.71	0.89	0.02	0.04	0.74
G284T	0.78	0.94	0.79	0.92	1.00	0.99	0.93
G284A	0.59	0.87	0.72	0.83	1.00	1.00	0.85
A285T	0.51	0.82	0.80	0.80	1.00	1.00	0.83
A285G	0.63	0.52	0.82	0.93	0.68	0.65	0.99
AC286A	0.43	0.68	0.54	0.61	0.39	0.41	0.62
C286T	0.63	0.55	0.73	0.88	0.68	0.67	0.91
C286G	0.59	0.46	0.70	0.75	0.22	0.23	0.75
C286A	0.60	0.80	0.67	0.80	1.00	0.99	0.81
C287T	0.59	0.97	0.86	0.89	1.00	1.00	0.92
C287G	0.64	0.76	0.77	0.89	0.92	0.99	0.84
C287A	0.56	0.87	0.74	0.82	1.00	0.99	0.85
C288T	0.63	0.91	0.75	0.86	1.00	1.00	0.88
C288A	0.59	0.65	0.68	0.81	0.86	0.84	0.84
T289C	0.66	0.15	0.91	0.76	0.06	0.06	0.93
T289A	0.60	0.22	0.79	0.76	0.08	0.09	0.80
C290T	0.72	0.80	0.63	0.83	0.99	0.99	0.83
C290A	0.62	0.37	0.83	0.76	0.19	0.18	0.86
T291C	0.62	0.18	0.82	0.94	0.06	0.10	0.69
T291A	0.80	0.06	0.77	0.98	0.02	0.03	0.73
C292T	0.76	0.93	0.65	0.89	1.00	1.00	0.88
C292G	0.71	0.11	0.75	0.81	0.04	0.04	0.81
C292A	0.68	0.10	0.81	0.82	0.03	0.04	0.82
T293G	0.98	0.03	1.00	0.95	0.01	0.04	0.98
T293C	0.61	0.87	0.73	0.84	1.00	1.00	0.86
G294T	0.59	0.49	0.80	0.81	0.30	0.32	0.79
G294C	0.67	0.64	0.65	0.87	0.84	0.89	0.82
G294A	0.65	0.86	0.80	0.87	1.00	1.00	0.88
C295T	0.63	0.41	0.92	0.94	0.20	0.27	0.75
C295G	0.92	0.01	0.96	0.90	0.01	0.00	0.97
C295A	0.90	0.01	0.93	0.92	0.01	0.01	0.92
CA296C	0.95	0.01	0.90	0.91	0.01	0.00	0.95
A296T	0.96	0.01	0.94	0.92	0.00	0.00	0.96
A296G	0.95	0.01	0.94	1.00	0.00	0.01	0.88
A296C	0.96	0.01	0.89	0.92	0.00	0.00	0.93
G297T	0.95	0.01	0.99	0.95	0.01	0.00	0.94
G297C	0.95	0.01	0.96	0.99	0.00	0.01	0.90
G297A	0.92	0.01	0.96	0.93	0.01	0.00	0.94
G298T	0.92	0.03	0.79	0.89	0.01	0.01	0.88
G298C	0.88	0.05	0.75	0.80	0.02	0.02	0.93
G298A	0.73	0.12	0.79	0.79	0.05	0.05	0.88
A299T	0.66	0.87	0.68	0.84	1.00	1.00	0.85
A299G	0.90	0.07	0.84	0.86	0.03	0.03	0.93
T300C	0.82	0.89	0.80	0.91	1.00	0.99	0.92
T300A	0.59	0.90	0.63	0.83	1.00	1.00	0.84
A301T	0.69	0.81	0.70	0.84	0.99	1.00	0.85
A301G	0.57	0.77	0.70	0.79	0.98	0.99	0.80
T302C	0.60	0.87	0.75	0.84	1.00	1.00	0.86
T302A	0.59	0.75	0.81	0.82	0.97	0.96	0.85
T303C	0.71	0.95	0.78	0.91	0.99	1.00	0.91
T303A	0.65	0.90	0.70	0.86	0.99	1.00	0.86

Best Fit Values of Model Parameters

TG304T	0.62	0.91	0.75	0.86	1.00	1.00	0.87
G304T	0.69	0.97	0.88	0.92	1.00	1.00	0.94
G304A	0.66	0.94	0.68	0.88	1.00	1.00	0.88
G305T	0.73	0.97	0.71	0.91	0.99	1.00	0.90
G305C	0.55	0.97	0.80	0.86	1.00	1.00	0.88
G305A	0.72	0.98	0.74	0.91	1.00	1.00	0.92
G306T	0.76	0.97	0.80	0.92	1.00	1.00	0.93
G306C	0.75	0.98	0.79	0.92	1.00	1.00	0.93
G306A	0.71	0.98	0.78	0.91	1.00	1.00	0.92
C307T	0.56	0.26	0.95	0.91	0.09	0.14	0.73
C307G	0.96	0.04	0.74	0.88	0.01	0.01	0.89
C307A	0.57	0.64	0.76	0.89	0.81	0.90	0.82
T308G	0.58	0.56	0.80	0.90	0.73	0.72	0.94
T308C	0.70	0.95	0.76	0.91	0.99	1.00	0.90
T308A	0.58	0.82	0.69	0.80	0.99	1.00	0.82
TG309T	0.58	0.93	0.74	0.88	0.97	1.00	0.87
G309T	0.71	0.97	0.51	0.87	1.00	1.00	0.84
G309C	0.79	0.99	0.78	0.94	1.00	1.00	0.94
G309A	0.59	0.89	0.64	0.82	1.00	1.00	0.83
G310T	0.74	0.97	0.73	0.91	1.00	0.96	0.95
G310A	0.70	0.97	0.83	0.91	1.00	0.98	0.94
G311T	0.83	0.92	0.96	0.94	0.99	0.99	0.96
G311A	0.83	0.98	0.74	0.93	1.00	1.00	0.92
C312T	0.53	0.45	0.94	0.81	0.28	0.29	0.82
C312A	0.59	0.79	0.72	0.80	1.00	0.99	0.82
G313T	0.60	0.37	0.85	0.89	0.15	0.20	0.73
G313C	0.49	0.83	0.85	0.80	1.00	0.99	0.84
G313A	0.55	0.46	0.85	0.84	0.24	0.29	0.75
C314A	0.54	0.63	0.80	0.83	0.84	0.77	0.93
T315G	0.57	0.58	0.78	0.88	0.76	0.74	0.92
T315C	0.65	0.89	0.75	0.86	1.00	1.00	0.88
T315A	0.55	0.65	0.78	0.85	0.85	0.87	0.84
G316T	0.62	0.56	0.80	0.97	0.69	0.75	0.92
G316C	0.84	0.52	0.69	0.98	0.66	0.66	0.97
G316A	0.67	0.64	0.66	0.84	0.87	0.85	0.87
T317C	0.62	0.93	0.79	0.87	1.00	0.92	0.96
T317A	0.51	0.72	0.73	0.72	1.00	0.96	0.77
G318T	0.63	0.90	0.66	0.85	1.00	1.00	0.86
G318C	0.69	0.93	0.69	0.89	0.99	1.00	0.89
G318A	0.65	0.68	0.67	0.78	0.97	0.92	0.83
G319T	0.60	0.69	0.73	0.81	0.94	0.93	0.83
G319C	0.42	0.76	0.91	0.77	0.98	0.98	0.81
G319A	0.69	0.85	0.74	0.86	1.00	0.99	0.87
C320T	0.59	0.36	0.91	0.78	0.19	0.19	0.86
C320G	0.88	0.03	0.95	0.92	0.01	0.02	0.92
C320A	0.50	0.69	0.72	0.73	0.96	0.98	0.73
T321G	0.53	0.75	0.76	0.77	0.98	0.99	0.79
T321C	0.63	0.89	0.75	0.86	1.00	1.00	0.87
T321A	0.53	0.62	0.82	0.85	0.81	0.77	0.92
G322T	0.51	0.36	0.99	0.85	0.17	0.23	0.78
G322C	0.54	0.63	0.79	0.97	0.72	0.89	0.80
G322A	0.53	0.37	0.99	0.88	0.17	0.22	0.76
A323T	0.58	0.70	0.80	0.85	0.90	0.90	0.88

A323G	0.61	0.48	0.84	0.79	0.34	0.32	0.87
A323C	0.66	0.82	0.73	0.84	1.00	0.98	0.87
C324T	0.60	0.55	0.82	0.93	0.71	0.71	0.95
C324A	0.62	0.60	0.94	1.00	0.75	0.76	1.00
T325G	0.30	0.98	1.00	0.78	0.97	1.00	0.91
T325C	0.70	0.94	0.86	0.91	1.00	0.99	0.94
T325A	0.58	0.63	0.73	0.81	0.87	0.82	0.87
TG326T	0.54	0.72	0.89	0.89	0.88	0.89	0.92
G326T	0.52	0.74	0.80	0.79	0.97	0.98	0.81
G326C	0.61	0.86	0.69	0.84	1.00	1.00	0.85
G326A	0.60	0.70	0.75	0.82	0.93	0.93	0.84
T327C	0.72	0.96	0.74	0.91	1.00	1.00	0.91
T327A	0.59	0.85	0.73	0.83	0.99	1.00	0.84
G328T	0.66	0.85	0.67	0.86	0.99	1.00	0.85
G328C	0.77	0.92	0.71	0.90	1.00	1.00	0.90
G328A	0.65	0.78	0.74	0.83	0.99	0.99	0.84
T329G	0.53	0.52	0.92	0.81	0.56	0.49	0.96
T329C	0.69	0.96	0.77	0.90	1.00	1.00	0.91
T329A	0.66	0.92	0.74	0.88	1.00	1.00	0.89
TG330T	0.65	0.96	0.86	0.90	1.00	1.00	0.92
G330T	0.77	0.97	0.65	0.92	0.99	1.00	0.90
G330C	0.86	0.97	0.63	0.94	0.97	1.00	0.90
G330A	0.52	0.86	0.57	0.75	1.00	0.99	0.77
G331T	0.66	0.96	0.78	0.89	1.00	1.00	0.91
G331C	0.76	0.97	0.75	0.92	1.00	1.00	0.91
G331A	0.71	0.97	0.60	0.88	1.00	1.00	0.88
G332C	0.58	0.93	0.86	0.87	1.00	1.00	0.90
G332A	0.78	0.98	0.80	0.93	0.99	1.00	0.93
T333C	0.67	0.94	0.73	0.88	1.00	0.99	0.90
T333A	0.68	0.93	0.72	0.88	1.00	1.00	0.89
A334T	0.56	0.79	0.66	0.77	0.99	0.99	0.79
A334G	0.58	0.82	0.79	0.83	1.00	0.99	0.86
T335C	0.60	0.83	0.77	0.83	1.00	1.00	0.85
T335A	0.56	0.69	0.72	0.74	0.99	0.96	0.78
C336T	0.68	0.19	0.91	0.83	0.07	0.09	0.86
C336A	0.89	0.83	0.64	0.90	0.97	0.97	0.89
A337T	0.58	0.74	0.80	0.82	0.97	0.97	0.84
A337G	0.64	0.90	0.72	0.86	1.00	1.00	0.88
A337C	0.59	0.75	0.67	0.79	0.97	1.00	0.78
A338T	0.57	0.79	0.72	0.80	0.99	0.99	0.81
A338G	0.61	0.67	0.73	0.85	0.88	0.89	0.85
A338C	0.59	0.79	0.78	0.82	1.00	0.99	0.84
C339T	0.61	0.20	0.94	0.84	0.08	0.09	0.82
C339A	0.70	0.17	0.83	0.79	0.07	0.07	0.88
G340T	0.44	0.64	1.00	0.93	0.76	0.80	0.94
G340C	0.60	0.62	0.64	0.76	0.73	0.68	0.82
G340A	0.55	0.58	0.81	0.90	0.72	0.76	0.88
T341G	0.74	0.12	0.87	0.83	0.05	0.05	0.88
T341C	0.63	0.89	0.74	0.86	1.00	1.00	0.88
T341A	0.65	0.77	0.75	0.83	0.98	0.98	0.85
G342T	0.63	0.71	0.72	0.79	0.98	0.98	0.81
G342A	0.49	0.48	0.95	0.78	0.33	0.33	0.85
A343T	0.57	0.60	0.81	0.92	0.76	0.78	0.92

Best Fit Values of Model Parameters

A343G	0.56	0.71	0.85	0.91	0.86	0.90	0.89
A343C	0.48	0.60	0.98	0.96	0.72	0.77	0.95
AC344A	0.47	0.91	0.88	0.84	0.99	1.00	0.88
C344T	0.60	0.74	0.70	0.79	0.98	0.99	0.80
C344A	0.64	0.18	0.90	0.91	0.06	0.09	0.76
C345T	0.57	0.53	0.74	0.74	0.55	0.46	0.90
C345G	0.69	0.53	0.83	0.99	0.69	0.70	0.99
C345A	0.58	0.48	0.83	0.85	0.27	0.32	0.76
G346T	0.60	0.83	0.80	0.84	1.00	0.98	0.87
G346C	0.63	0.73	0.80	0.88	0.91	0.88	0.92
G346A	0.65	0.88	0.69	0.86	1.00	1.00	0.86
T347G	0.55	0.48	0.91	0.87	0.33	0.38	0.81
T347C	0.65	0.91	0.75	0.87	1.00	0.99	0.88
T347A	0.69	0.90	0.68	0.87	1.00	1.00	0.87
TG348T	0.66	0.92	0.53	0.84	1.00	1.00	0.82
G348T	0.58	0.91	0.62	0.82	1.00	0.99	0.84
G348C	0.55	0.99	0.99	0.89	1.00	0.99	0.95
G349T	0.58	0.86	0.63	0.80	1.00	1.00	0.81
G349C	0.51	0.53	0.76	0.75	0.31	0.33	0.76
G349A	0.72	0.98	0.74	0.91	0.99	1.00	0.91
G350C	0.49	0.67	0.54	0.55	0.51	0.39	0.75
G350A	0.78	0.99	0.80	0.93	1.00	0.96	0.96
G35G1	0.99	0.91	0.11	0.68	0.96	0.95	0.50
GT351G	0.53	0.93	0.68	0.82	1.00	1.00	0.85
T351C	0.59	0.89	0.67	0.83	1.00	1.00	0.85
T351A	0.72	0.96	0.74	0.90	1.00	0.98	0.92
TG352T	0.59	0.82	0.62	0.79	0.99	1.00	0.79
G352T	0.62	0.89	0.75	0.86	1.00	0.99	0.88
G352C	0.65	0.95	0.83	0.89	1.00	0.99	0.91
G352A	0.58	0.77	0.70	0.79	0.98	0.99	0.81
G353T	0.86	0.95	0.68	0.93	1.00	1.00	0.91
G353C	0.59	0.94	0.68	0.85	1.00	0.97	0.89
G353A	0.62	0.97	0.83	0.89	1.00	1.00	0.91
GT354G	0.95	0.09	0.91	0.90	0.05	0.04	0.95
T354G	0.66	0.76	0.69	0.79	1.00	0.94	0.85
T354C	0.56	0.71	0.67	0.75	0.96	0.97	0.76
T354A	0.66	0.92	0.75	0.88	1.00	1.00	0.89
G355T	0.74	0.26	0.64	0.78	0.10	0.09	0.77
G355C	0.33	0.62	0.99	0.90	0.61	0.78	0.80
G355A	0.62	0.53	0.70	0.85	0.38	0.43	0.75
GA356G	0.53	0.69	0.67	0.70	0.99	0.90	0.79
A356T	0.56	0.69	0.80	0.87	0.86	0.92	0.84
A356G	0.79	0.06	0.97	0.87	0.02	0.03	0.93
G357T	0.58	0.44	0.91	0.72	0.27	0.23	0.94
G357A	0.57	0.74	0.70	0.77	0.98	1.00	0.77
A358T	0.78	0.45	0.58	0.74	0.26	0.22	0.82
A358G	0.89	0.04	0.88	0.91	0.01	0.02	0.90
A358C	0.54	0.70	0.77	0.79	0.94	0.93	0.82
G359T	0.65	0.83	0.72	0.84	1.00	0.96	0.88
G359C	0.64	0.85	0.56	0.81	1.00	1.00	0.80
G359A	0.53	0.75	0.74	0.79	0.96	0.99	0.79
C360T	0.53	0.52	0.87	0.74	0.55	0.42	1.00
C360A	0.60	0.74	0.79	0.85	0.94	0.96	0.85

T361G	0.62	0.87	0.60	0.84	0.99	1.00	0.84
T361C	0.56	0.73	0.77	0.79	0.98	0.93	0.84
T361A	0.60	0.64	0.79	0.90	0.82	0.81	0.93
G362C	0.63	0.28	0.98	0.80	0.14	0.15	0.91
G362A	0.60	0.69	0.77	0.87	0.88	0.90	0.87
GC363G	0.51	0.65	0.83	0.84	0.85	0.86	0.86
C363T	0.61	0.59	0.78	0.90	0.78	0.75	0.95
C363G	0.56	0.57	0.63	0.75	0.38	0.41	0.71
C363A	0.53	0.74	0.80	0.81	0.95	0.99	0.81
C364T	0.66	0.46	0.77	0.77	0.28	0.26	0.85
C364G	0.33	0.64	1.00	0.82	0.70	0.72	0.91
C364A	0.65	0.83	0.62	0.82	0.99	1.00	0.82
A365T	0.56	0.59	0.80	0.91	0.75	0.79	0.90
A365G	0.60	0.83	0.74	0.83	1.00	1.00	0.85
A365C	0.51	0.53	0.63	0.76	0.23	0.30	0.63
G366T	0.60	0.73	0.75	0.81	0.97	0.98	0.82
G366C	0.47	0.48	0.85	0.69	0.29	0.27	0.85
G366A	0.63	0.66	0.76	0.91	0.83	0.83	0.92
C367T	0.63	0.64	0.82	0.96	0.79	0.79	0.97
C367G	0.64	0.71	0.79	0.92	0.86	0.89	0.91
C367A	0.62	0.87	0.79	0.86	0.99	1.00	0.87
C367CA	0.69	0.90	0.65	0.86	1.00	0.99	0.87
A368T	0.58	0.60	0.76	0.87	0.78	0.77	0.89
A368G	0.60	0.83	0.72	0.84	0.97	1.00	0.83
A368C	0.55	0.59	0.86	0.92	0.76	0.75	0.96
C369T	0.62	0.59	0.71	0.89	0.71	0.75	0.86
C369G	0.56	0.79	0.77	0.80	1.00	0.99	0.83
C369A	0.59	0.89	0.71	0.83	1.00	1.00	0.85
G370T	0.64	0.31	0.85	0.83	0.13	0.15	0.80
G370A	0.60	0.71	0.73	0.80	0.96	0.95	0.83
A371T	0.60	0.69	0.70	0.81	0.92	0.95	0.79
A371G	0.49	0.24	0.93	0.94	0.08	0.14	0.65
G372A	0.73	0.68	0.65	0.84	0.93	0.78	0.99
GT373G	0.32	0.64	0.96	0.73	0.80	0.83	0.76
T373C	0.52	0.72	0.78	0.78	0.96	0.97	0.80
T373A	0.66	0.88	0.71	0.86	1.00	1.00	0.87
T374G	0.50	0.78	0.62	0.71	1.00	0.99	0.73
T374C	0.54	0.53	0.81	0.83	0.52	0.54	0.84
T374A	0.61	0.78	0.75	0.81	1.00	0.99	0.83
C375T	0.60	0.63	0.70	0.82	0.84	0.81	0.87
C375G	0.68	0.66	0.67	0.86	0.87	0.85	0.88
C376T	0.55	0.59	0.81	0.88	0.77	0.76	0.92
C376G	0.71	0.46	0.87	0.89	0.31	0.33	0.86
C376A	0.63	0.69	0.68	0.80	0.94	0.94	0.80
C376CG	0.60	0.51	0.80	0.95	0.37	0.49	0.74
CG377C	0.52	0.88	0.75	0.81	1.00	0.99	0.85
G377T	0.61	0.89	0.79	0.86	1.00	1.00	0.88
G377C	0.44	0.82	0.86	0.78	1.00	0.99	0.84
G377A	0.62	0.89	0.63	0.83	1.00	1.00	0.84
G378A	0.63	0.93	0.71	0.87	1.00	1.00	0.88
G379T	0.62	0.94	0.72	0.87	1.00	1.00	0.88
G379A	0.65	0.97	0.83	0.90	1.00	1.00	0.92
G380T	0.51	0.92	0.70	0.81	1.00	1.00	0.84

G380C	0.87	0.92	0.75	0.93	1.00	0.99	0.92
G380A	0.71	0.95	0.74	0.90	1.00	1.00	0.90
G38G4	0.63	0.83	0.71	0.83	1.00	1.00	0.84
G381C	0.56	0.94	0.70	0.84	1.00	1.00	0.87
G381A	0.63	0.95	0.68	0.88	0.99	1.00	0.88
G382A	0.61	0.84	0.62	0.80	1.00	1.00	0.81
A383G	0.59	0.79	0.72	0.80	1.00	0.95	0.86
A383C	0.57	0.82	0.62	0.78	0.99	1.00	0.79
C384T	0.56	0.41	0.93	0.76	0.23	0.21	0.88
C384G	1.00	0.45	0.51	0.80	0.33	0.28	0.87
C384A	0.59	0.45	0.89	0.85	0.26	0.29	0.81
A385T	0.60	0.73	0.65	0.76	0.99	0.98	0.77
A385G	0.59	0.78	0.78	0.82	0.98	0.98	0.85
A385C	0.46	0.76	0.82	0.77	0.97	0.99	0.80
T386G	0.37	0.83	0.95	0.76	0.99	1.00	0.82
T386C	0.64	0.85	0.70	0.84	1.00	1.00	0.85
T386A	0.65	0.80	0.73	0.83	0.99	0.99	0.85
TG387T	0.61	0.81	0.72	0.82	1.00	0.99	0.84
G387T	0.54	0.71	0.78	0.78	0.96	0.93	0.83
G387A	0.58	0.51	0.81	0.77	0.35	0.34	0.84
G388T	0.51	0.78	0.75	0.77	0.99	1.00	0.80
G388C	0.59	0.76	0.74	0.79	0.99	0.99	0.81
GT389G	0.61	0.80	0.68	0.80	1.00	1.00	0.81
T389G	0.56	0.69	0.85	0.92	0.83	0.89	0.89
T389C	0.56	0.92	0.73	0.84	1.00	1.00	0.87
T389A	0.67	0.96	0.76	0.89	1.00	1.00	0.91
T390G	0.59	0.77	0.73	0.80	0.99	1.00	0.81
T390C	0.60	0.94	0.76	0.86	1.00	1.00	0.89
T390A	0.60	0.49	0.81	0.77	0.33	0.31	0.86
G391T	0.61	0.52	0.85	0.96	0.66	0.68	0.95
G391C	0.55	0.63	0.79	0.91	0.77	0.85	0.84
G391A	0.60	0.63	0.82	0.92	0.80	0.79	0.96
T392C	0.63	0.78	0.75	0.84	0.97	0.98	0.84
C393T	0.60	0.49	0.84	0.90	0.31	0.38	0.77
C393G	0.50	0.71	0.79	0.83	0.88	0.99	0.77
C393A	0.70	0.65	0.80	0.99	0.79	0.80	0.98
T394G	0.66	0.82	0.73	0.84	0.99	0.99	0.86
T394C	0.64	0.93	0.68	0.86	1.00	0.97	0.90
T394A	0.57	0.72	0.80	0.82	0.96	0.92	0.87
G395T	0.54	0.81	0.67	0.78	0.99	0.99	0.79
G395C	0.59	0.79	0.77	0.81	1.00	0.99	0.83
G395A	0.62	0.79	0.70	0.81	0.99	0.99	0.83
G395GC	0.61	0.84	0.72	0.83	1.00	1.00	0.85
GC396G	0.57	0.86	0.70	0.82	1.00	1.00	0.84
C396T	0.58	0.85	0.69	0.82	1.00	1.00	0.83
C396G	0.56	0.73	0.86	0.85	0.93	0.92	0.89
C397T	0.55	0.87	0.71	0.82	0.99	1.00	0.84
C397G	0.60	0.93	0.83	0.87	1.00	1.00	0.90
C397A	0.65	0.93	0.77	0.88	1.00	0.99	0.91
C398T	0.64	0.92	0.69	0.87	1.00	1.00	0.88
C398A	0.60	0.90	0.70	0.84	1.00	1.00	0.86
C399T	0.66	0.78	0.75	0.83	0.99	0.99	0.85
C399A	0.60	0.87	0.72	0.83	1.00	1.00	0.85

Best Fit Values of Model Parameters

C400T	0.60	0.80	0.71	0.81	1.00	0.99	0.82
C400G	0.62	0.84	0.68	0.82	1.00	0.99	0.84
C400A	0.60	0.82	0.71	0.82	1.00	0.99	0.84
T401G	0.75	0.84	0.56	0.85	0.99	1.00	0.83
T401C	0.58	0.88	0.71	0.86	0.97	1.00	0.85
T401A	0.58	0.85	0.70	0.82	1.00	1.00	0.84
G402T	0.49	0.70	0.77	0.76	0.94	0.99	0.75
G402C	0.57	0.80	0.74	0.80	1.00	0.97	0.83
G402A	0.54	0.78	0.73	0.78	1.00	0.99	0.80
GC403G	0.59	0.79	0.67	0.79	0.99	1.00	0.80
C403T	0.58	0.85	0.64	0.80	1.00	1.00	0.82
C403G	0.47	0.76	0.93	0.80	0.97	0.98	0.83
C403A	0.54	0.83	0.81	0.81	1.00	0.99	0.85
C404T	0.63	0.77	0.72	0.81	0.99	0.99	0.82
C404A	0.62	0.91	0.70	0.86	0.99	1.00	0.87
C405T	0.61	0.87	0.68	0.84	0.99	1.00	0.85
C405A	0.64	0.89	0.68	0.88	0.97	1.00	0.86
C406T	0.57	0.86	0.72	0.82	1.00	0.95	0.88
C406G	0.35	0.97	1.00	0.82	0.97	1.00	0.91
C406A	0.54	0.88	0.73	0.82	1.00	0.99	0.86
C407T	0.67	0.64	0.71	0.87	0.86	0.79	0.95
C407G	0.65	0.93	0.71	0.87	1.00	1.00	0.89
C407A	0.65	0.65	0.80	0.97	0.78	0.81	0.95
A408T	0.57	0.71	0.72	0.77	0.97	0.94	0.81
A408G	0.61	0.87	0.69	0.84	0.99	1.00	0.85
A408C	0.62	0.74	0.71	0.80	0.98	0.96	0.82
T409G	0.65	0.82	0.76	0.84	1.00	0.99	0.87
T409C	0.62	0.84	0.71	0.83	1.00	1.00	0.85
T409A	0.63	0.85	0.75	0.84	1.00	0.95	0.90
TC410T	0.66	0.71	0.71	0.90	0.88	0.96	0.83
C410T	0.50	0.79	0.78	0.78	0.99	1.00	0.81
C410A	0.56	0.79	0.79	0.81	0.99	0.99	0.84
C411T	0.61	0.92	0.77	0.87	1.00	1.00	0.89
C411A	0.55	0.94	0.71	0.84	1.00	1.00	0.87
C412T	0.48	0.60	0.88	0.88	0.76	0.78	0.89
C412A	0.83	0.75	0.69	0.95	0.89	0.89	0.95
CT413C	0.58	0.84	0.76	0.83	0.99	1.00	0.85
T413G	0.64	0.43	1.00	0.91	0.26	0.30	0.84
T413C	0.65	0.73	0.74	0.84	0.96	0.94	0.86
T413A	0.65	0.73	0.71	0.80	0.99	0.98	0.81
G414T	0.55	0.70	0.84	0.86	0.88	0.89	0.88
G414C	0.61	0.81	0.69	0.80	1.00	1.00	0.81
G414A	0.47	0.62	0.88	0.85	0.80	0.80	0.88
C415T	0.68	0.26	0.91	0.84	0.11	0.12	0.85
C415G	0.67	0.54	0.91	1.00	0.69	0.70	1.00
C415A	0.64	0.87	0.76	0.86	1.00	1.00	0.88
A416T	0.61	0.82	0.68	0.81	1.00	0.99	0.83
A416G	0.63	0.70	0.73	0.86	0.90	0.92	0.85
A416C	0.74	0.37	0.78	0.77	0.19	0.17	0.89
G417T	0.60	0.82	0.78	0.83	0.99	0.99	0.86
G417C	0.54	0.83	0.72	0.79	1.00	1.00	0.82
G417A	0.56	0.80	0.75	0.80	0.99	0.99	0.83
C418T	0.62	0.56	0.80	0.93	0.73	0.72	0.95

Best Fit Values of Model Parameters

C418A	0.44	0.59	0.85	0.93	0.61	0.80	0.75
CT419C	0.42	0.81	0.66	0.69	0.99	0.98	0.74
T419G	0.59	0.77	0.71	0.80	0.98	1.00	0.80
T419C	0.60	0.87	0.76	0.84	1.00	1.00	0.87
T419A	0.62	0.85	0.72	0.84	1.00	1.00	0.85
T420G	0.73	0.65	0.77	0.99	0.79	0.80	0.99
T420C	0.63	0.87	0.69	0.84	1.00	1.00	0.85
T420A	0.78	0.28	0.91	0.85	0.14	0.13	0.90
G421T	0.61	0.68	0.68	0.78	0.96	0.95	0.79
G422T	0.58	0.81	0.82	0.82	1.00	0.97	0.88
G422C	0.49	0.77	0.78	0.76	0.99	0.99	0.80
GC423G	0.69	0.56	0.71	0.91	0.73	0.71	0.94
C423T	0.65	0.61	0.71	0.97	0.74	0.85	0.85
C423G	0.62	0.40	0.80	0.67	0.22	0.17	0.95
C424T	0.65	0.42	0.86	0.76	0.25	0.22	0.91
A425G	0.63	0.43	0.78	0.75	0.23	0.22	0.84
A425C	0.61	0.82	0.73	0.82	1.00	0.97	0.86
G427T	0.67	0.37	0.88	0.80	0.19	0.18	0.87
G427C	0.49	0.60	0.88	0.86	0.79	0.77	0.92
G427A	0.75	0.50	0.62	0.79	0.33	0.32	0.81
GA428G	0.68	0.53	0.80	0.98	0.69	0.69	0.98
A428G	0.73	0.25	0.87	0.88	0.10	0.12	0.82
A428C	0.72	0.36	0.84	0.77	0.21	0.17	0.94
T429C	0.64	0.85	0.71	0.84	1.00	1.00	0.85
T429A	0.64	0.72	0.71	0.82	0.96	0.96	0.82
G430A	0.64	0.46	0.73	0.87	0.23	0.29	0.72
G431T	0.64	0.80	0.70	0.83	0.98	0.99	0.84
G431C	0.66	0.81	0.65	0.82	0.99	1.00	0.82
G431A	0.64	0.91	0.76	0.87	1.00	1.00	0.89
T432G	0.83	0.61	0.72	1.00	0.77	0.77	1.00
T432C	0.62	0.86	0.73	0.84	1.00	0.97	0.88
T432A	0.62	0.93	0.73	0.86	1.00	1.00	0.88
G433C	0.62	0.78	0.66	0.81	0.98	0.99	0.80
G433A	0.62	0.75	0.67	0.79	0.99	0.99	0.79
GC434G	0.62	0.75	0.72	0.82	0.97	0.98	0.82
C434G	0.77	0.48	0.55	0.83	0.25	0.28	0.71
C434A	0.67	0.89	0.76	0.87	1.00	0.99	0.90
C435A	0.53	0.90	0.82	0.86	0.98	1.00	0.87
C436A	0.61	0.87	0.70	0.84	1.00	1.00	0.85
C437T	0.61	0.74	0.75	0.79	1.00	0.92	0.88
C437G	0.58	0.87	0.71	0.83	1.00	1.00	0.84
C437A	0.62	0.79	0.62	0.79	1.00	1.00	0.79
CA438C	0.77	0.31	0.52	0.79	0.13	0.13	0.70
A438T	0.68	0.71	0.71	0.94	0.85	0.97	0.82
A438G	0.61	0.73	0.73	0.81	0.96	0.96	0.83
A438C	0.52	0.63	0.88	0.92	0.77	0.81	0.91
A438AT	0.65	0.67	0.61	0.77	0.94	0.95	0.77
AT439A	0.64	0.70	0.67	0.79	0.97	0.96	0.80
T439C	0.64	0.69	0.76	0.89	0.88	0.85	0.93
T439A	0.67	0.88	0.76	0.87	1.00	1.00	0.88
T440G	0.70	0.77	0.76	0.84	1.00	0.97	0.88
T440C	0.71	0.84	0.72	0.92	0.93	1.00	0.86
T440A	0.64	0.73	0.64	0.78	0.99	0.97	0.79

Best Fit Values of Model Parameters

G441T	0.63	0.80	0.63	0.79	1.00	1.00	0.80
G441C	0.66	0.75	0.64	0.79	0.99	0.99	0.80
G441A	0.63	0.83	0.66	0.82	1.00	0.94	0.88
C442T	0.68	0.18	0.95	0.93	0.07	0.09	0.79
C442G	0.82	0.26	0.88	0.87	0.11	0.11	0.88
C442A	0.67	0.87	0.76	0.87	1.00	1.00	0.88
A443T	0.91	0.05	0.97	0.93	0.02	0.02	0.93
A443G	0.96	0.03	0.96	0.95	0.01	0.01	0.93
A443C	0.99	0.04	0.99	0.98	0.02	0.01	0.92
AG444A	0.99	0.01	0.98	0.92	0.00	0.00	0.99
G444T	0.91	0.01	0.97	0.96	0.01	0.01	0.91
G444C	1.00	0.00	1.00	1.00	0.00	0.00	0.96
G444A	0.95	0.02	0.99	0.94	0.01	0.01	0.95
G445C	0.94	0.02	0.86	0.97	0.01	0.01	0.86
G445A	0.96	0.01	0.95	0.95	0.00	0.00	0.94
T446C	0.95	0.01	0.94	0.88	0.01	0.00	1.00
T446A	0.96	0.02	0.79	0.90	0.01	0.01	0.90
A447T	0.96	0.02	0.97	0.96	0.01	0.01	0.93
A447G	0.97	0.03	0.92	0.90	0.01	0.01	0.96
G448A	0.68	0.97	0.78	0.90	1.00	1.00	0.92
G449T	0.76	0.10	0.98	0.87	0.04	0.04	0.91
G449A	0.90	0.08	0.84	0.85	0.04	0.03	0.94
C450T	0.62	0.89	0.81	0.86	1.00	0.96	0.92
C450A	0.64	0.85	0.72	0.84	1.00	1.00	0.86
A451T	0.60	0.85	0.70	0.83	1.00	1.00	0.84
A451G	0.60	0.67	0.81	0.90	0.84	0.83	0.93
A451C	0.68	0.84	0.76	0.85	1.00	0.98	0.87
G452T	0.58	0.82	0.70	0.80	1.00	1.00	0.81
G452A	0.65	0.85	0.70	0.85	1.00	1.00	0.86
GC453G	0.67	0.60	0.53	0.73	0.80	0.71	0.81
C453T	0.65	0.74	0.72	0.83	0.96	0.97	0.83
C453G	0.59	0.72	0.69	0.79	0.96	0.97	0.79
C453A	0.69	0.72	0.64	0.82	0.95	0.98	0.80
C454T	0.53	0.66	0.83	0.87	0.84	0.86	0.88
C454G	0.65	0.61	0.80	0.97	0.76	0.78	0.96
C454A	0.63	0.75	0.70	0.80	0.99	0.98	0.82
C455T	0.62	0.68	0.72	0.82	0.92	0.90	0.85
C455CA	0.53	0.84	0.76	0.80	1.00	0.98	0.85
CA456C	0.51	0.77	0.42	0.60	0.49	0.55	0.52
A456T	0.64	0.80	0.76	0.84	0.99	0.98	0.86
A456G	0.62	0.81	0.67	0.81	1.00	1.00	0.82
A456C	0.61	0.88	0.72	0.84	1.00	1.00	0.85
G457T	0.61	0.84	0.74	0.83	1.00	1.00	0.85
G457C	0.58	0.63	0.84	0.92	0.80	0.78	0.96
G457A	0.64	0.84	0.71	0.84	1.00	0.99	0.85
C458T	0.63	0.84	0.75	0.84	1.00	0.97	0.88
C458G	0.62	0.79	0.71	0.81	0.98	1.00	0.81
C458A	0.61	0.85	0.67	0.82	1.00	1.00	0.83
T459G	0.53	0.87	0.82	0.83	1.00	0.99	0.87
T459C	0.58	0.78	0.72	0.80	0.99	0.99	0.82
T459A	0.67	0.64	0.80	0.98	0.78	0.79	0.98
TG460T	0.77	0.30	0.87	0.89	0.13	0.14	0.83
G460T	0.72	0.55	0.70	0.94	0.72	0.71	0.96

G460C	0.76	0.14	0.60	0.90	0.06	0.07	0.67
G460A	0.69	0.20	0.93	0.89	0.08	0.09	0.82
G461T	0.62	0.54	0.85	0.96	0.70	0.69	0.99
G461C	0.85	0.08	0.98	0.93	0.03	0.08	0.93
G461A	0.60	0.50	0.90	0.93	0.50	0.54	0.89
A462T	0.60	0.75	0.84	0.90	0.90	0.97	0.86
A462G	0.59	0.68	0.75	0.83	0.90	0.89	0.86
A462C	0.88	0.51	0.95	1.00	0.72	0.73	1.00
AC463A	0.72	0.63	0.76	0.98	0.78	0.77	1.00
C463T	0.56	0.83	0.73	0.81	0.99	1.00	0.83
C464T	0.57	0.83	0.75	0.81	1.00	0.99	0.84
C464A	0.62	0.82	0.72	0.82	1.00	0.98	0.85
CT465C	0.69	0.60	0.69	0.90	0.79	0.75	0.96
T465G	0.66	0.82	0.68	0.83	1.00	0.99	0.84
T465C	0.64	0.69	0.76	0.91	0.85	0.89	0.88
T465A	0.57	0.73	0.71	0.78	0.97	0.98	0.78
TC466T	0.63	0.63	0.65	0.80	0.89	0.87	0.82
C466T	0.57	0.54	0.90	0.97	0.69	0.70	0.97
C466G	0.92	0.15	0.76	0.85	0.06	0.06	0.90
C466A	0.71	0.25	0.79	0.77	0.11	0.10	0.87
C467T	0.80	0.32	0.79	0.83	0.15	0.15	0.86
C467G	0.99	0.17	0.51	0.82	0.09	0.08	0.79
C467A	0.66	0.27	0.74	0.78	0.11	0.11	0.79
C468T	0.63	0.75	0.76	0.82	0.98	0.99	0.83
CT469C	0.58	0.82	0.61	0.78	1.00	1.00	0.78
T469G	0.62	0.82	0.62	0.80	0.99	1.00	0.81
T469C	0.55	0.75	0.77	0.79	0.98	0.97	0.82
T469A	0.66	0.70	0.69	0.85	0.91	0.93	0.84
T469TG	0.68	0.70	0.84	0.98	0.82	0.83	0.99
G470A	0.61	0.60	0.56	0.67	0.50	0.42	0.80
G471T	0.64	0.52	0.66	0.69	0.36	0.30	0.87
G471C	0.59	0.53	0.69	0.73	0.34	0.32	0.80
G471A	0.61	0.59	0.63	0.83	0.69	0.74	0.78
G472A	0.59	0.66	0.55	0.69	0.89	0.87	0.71
GA473G	0.45	0.71	0.86	0.75	0.97	0.91	0.84
A473T	0.58	0.79	0.64	0.78	0.99	0.99	0.80
A473G	0.61	0.74	0.78	0.83	0.96	0.98	0.84
A473C	0.65	0.51	0.69	0.74	0.35	0.31	0.85
A474T	0.61	0.78	0.76	0.82	0.98	1.00	0.83
A474G	0.56	0.78	0.73	0.79	0.99	1.00	0.81
A474C	0.50	0.70	0.88	0.83	0.91	0.89	0.88
A475T	0.56	0.77	0.67	0.77	0.99	1.00	0.77
A475G	0.59	0.80	0.70	0.80	1.00	0.99	0.82
C476T	0.61	0.84	0.70	0.82	1.00	1.00	0.84
C476G	0.58	0.82	0.79	0.82	1.00	0.99	0.85
C476A	0.67	0.78	0.85	0.98	0.85	0.88	0.96
C476CA	0.72	0.76	0.77	0.92	0.91	0.91	0.93
A477T	0.59	0.79	0.69	0.80	1.00	1.00	0.81
A477G	0.57	0.81	0.78	0.81	1.00	1.00	0.83
AC478A	0.71	0.75	0.75	0.95	0.87	0.94	0.88
C478T	0.60	0.80	0.71	0.81	0.99	1.00	0.83
C478G	0.65	0.70	0.92	1.00	0.82	0.84	0.99
C478A	0.64	0.82	0.79	0.88	0.95	1.00	0.86

G479A	0.61	0.61	0.63	0.82	0.73	0.76	0.79
G481C	0.57	0.83	0.43	0.67	0.94	0.92	0.66
C482T	0.68	0.82	0.73	0.85	1.00	1.00	0.86
C482G	0.48	0.74	0.63	0.66	0.99	1.00	0.67
C482A	0.74	0.84	0.87	0.92	0.96	0.91	0.98
A483T	0.59	0.88	0.69	0.83	1.00	1.00	0.85
A483G	0.57	0.86	0.85	0.86	0.97	1.00	0.87
A483C	0.88	0.98	0.44	0.89	1.00	1.00	0.85
G484T	0.62	0.82	0.63	0.81	0.99	1.00	0.81
G484C	0.67	0.87	0.44	0.85	0.93	1.00	0.75
G484A	0.57	0.81	0.75	0.80	1.00	0.99	0.83
A485T	0.63	0.77	0.78	0.83	0.99	0.98	0.85
A485G	0.60	0.78	0.90	0.92	0.91	0.90	0.95
A485C	0.57	0.82	0.63	0.78	1.00	1.00	0.79
G486T	0.61	0.73	0.87	0.95	0.85	0.87	0.96
G486A	0.55	0.80	0.63	0.76	1.00	1.00	0.78
G487T	0.54	0.85	0.63	0.78	1.00	1.00	0.80
G487A	0.51	0.81	0.52	0.71	0.96	1.00	0.69
G488T	0.49	0.82	0.79	0.78	1.00	1.00	0.81
G488C	0.54	0.79	0.58	0.73	0.99	0.98	0.74
C489T	0.64	0.76	0.84	0.92	0.90	0.92	0.92
C490T	0.64	0.75	0.87	0.98	0.85	0.90	0.94
C490A	0.60	0.80	0.79	0.83	0.99	0.98	0.85
T491C	0.63	0.77	0.66	0.80	0.99	0.99	0.80
T491A	0.67	0.79	0.68	0.82	1.00	1.00	0.83
A492T	0.62	0.76	0.76	0.81	0.99	0.97	0.84
A492G	0.60	0.81	0.68	0.80	0.99	0.99	0.82
A492C	0.66	0.82	0.77	0.85	0.99	1.00	0.86
C493T	0.62	0.79	0.71	0.81	1.00	0.95	0.86
C493G	0.66	0.80	0.73	0.84	0.99	0.98	0.85
C493A	0.65	0.78	0.79	0.87	0.96	0.97	0.87
A494T	0.64	0.81	0.64	0.81	1.00	0.99	0.82
A494G	0.58	0.81	0.79	0.82	1.00	0.99	0.85
A494C	0.63	0.75	0.76	0.81	1.00	0.95	0.86
G495T	0.59	0.77	0.69	0.79	0.99	0.99	0.80
G495A	0.70	0.80	0.74	0.85	1.00	0.98	0.87
G496T	0.60	0.77	0.62	0.77	1.00	0.99	0.78
G496A	0.56	0.78	0.82	0.81	0.99	0.98	0.85
C497T	0.70	0.84	0.44	0.77	1.00	0.99	0.75
C497G	0.78	0.81	0.36	0.75	0.98	1.00	0.70
C497A	0.61	0.84	0.71	0.83	0.99	1.00	0.83
T498G	0.59	0.85	0.64	0.80	1.00	0.99	0.82
T498C	0.57	0.75	0.55	0.73	0.97	0.97	0.72
T498A	0.62	0.82	0.73	0.83	0.99	1.00	0.84
G499T	0.54	0.80	0.64	0.79	0.96	1.00	0.77
G499A	0.58	0.71	0.74	0.80	0.95	0.96	0.81
G500T	0.63	0.75	0.83	0.88	0.93	0.93	0.90
G500C	0.60	0.84	0.68	0.82	1.00	0.99	0.83
G500A	0.60	0.63	0.92	0.99	0.77	0.78	0.99
G501T	0.56	0.76	0.94	0.93	0.87	0.89	0.95
G501A	0.62	0.75	0.83	0.89	0.92	0.91	0.92
C502T	0.60	0.79	0.97	0.97	0.86	0.89	0.98
C502A	0.60	0.80	0.99	0.96	0.88	0.89	0.99

Best Fit Values of Model Parameters

G505T	0.59	0.84	0.56	0.78	0.99	1.00	0.78
G505A	0.54	0.78	0.85	0.80	1.00	0.99	0.84
G507T	0.65	0.75	0.98	1.00	0.84	0.87	1.00
G507C	0.70	0.68	0.98	1.00	0.82	0.84	1.00
G507A	0.57	0.69	0.94	0.98	0.80	0.83	0.98
T508C	0.65	0.81	0.62	0.81	0.99	0.99	0.81
T508A	0.64	0.77	0.61	0.78	1.00	0.99	0.79
T509C	0.60	0.75	0.67	0.80	0.97	1.00	0.78
T509A	0.63	0.80	0.60	0.79	1.00	0.99	0.80
G510T	0.64	0.83	1.00	1.00	0.86	0.91	1.00
G510C	0.64	0.82	0.56	0.78	1.00	0.99	0.78
G510A	0.64	0.79	0.76	0.85	0.97	1.00	0.84
GC511G	0.61	0.87	0.61	0.82	1.00	1.00	0.83
C511T	0.61	0.79	0.95	0.97	0.87	0.91	0.96
C511G	0.65	0.79	0.55	0.77	0.99	0.99	0.77
C511A	0.63	0.80	0.81	0.84	0.99	0.98	0.87
C512T	0.67	0.81	0.79	0.86	0.98	0.99	0.87
C512A	0.59	0.79	0.78	0.82	1.00	0.99	0.84
A513T	0.60	0.75	0.88	0.91	0.89	0.90	0.93
A513G	0.64	0.80	0.64	0.80	1.00	1.00	0.80
C514T	0.63	0.76	0.94	0.99	0.84	0.87	0.99
C514A	0.58	0.70	0.63	0.78	0.92	0.91	0.80
C515T	0.66	0.70	0.98	1.00	0.82	0.84	1.00
C515G	0.92	0.12	0.54	0.92	0.04	0.05	0.69
C515A	0.59	0.74	0.72	0.79	0.98	0.97	0.81
T516C	0.60	0.80	0.67	0.79	0.99	1.00	0.80
G517T	0.63	0.67	1.00	1.00	0.77	0.83	1.00
G517C	0.61	0.69	0.97	1.00	0.80	0.83	1.00
G517A	0.60	0.77	0.82	0.84	0.97	0.99	0.84
G517GC	0.62	0.74	0.92	0.97	0.84	0.86	0.99
C518T	0.57	0.75	0.90	0.93	0.87	0.93	0.90
C519T	0.51	0.82	0.60	0.73	1.00	0.99	0.75
C520T	0.56	0.78	0.78	0.80	0.99	0.98	0.83
C520A	0.57	0.79	0.53	0.72	0.99	1.00	0.72
C521T	0.61	0.82	0.71	0.83	0.98	1.00	0.83
C521G	0.57	0.77	0.87	0.90	0.90	0.96	0.86
C521A	0.60	0.73	0.99	1.00	0.81	0.85	1.00
C522T	0.58	0.78	0.88	0.85	0.96	0.97	0.87
C527T	0.56	0.82	0.56	0.75	0.99	0.99	0.75
C527G	0.66	0.83	0.28	0.46	0.98	0.75	0.54
C527A	0.63	0.87	0.50	0.79	1.00	1.00	0.77
T528G	0.60	0.71	0.64	0.78	0.95	0.99	0.75
T528C	0.60	0.79	0.70	0.80	1.00	0.99	0.82
T528A	0.51	0.80	0.48	0.63	0.92	0.93	0.63
G529T	0.63	0.79	0.73	0.82	1.00	0.94	0.89
G529C	0.74	0.84	0.86	0.93	0.96	0.98	0.92
G529A	0.57	0.74	0.68	0.76	0.99	0.99	0.78
C530T	0.59	0.83	0.54	0.76	0.99	1.00	0.76
G531T	0.68	0.71	0.39	0.79	0.64	0.89	0.53
G531C	0.40	0.83	1.00	0.97	0.77	0.89	0.98
G531A	0.68	0.77	0.68	0.82	1.00	0.99	0.83
T532C	0.62	0.70	0.93	0.99	0.81	0.83	1.00
T532A	0.51	0.70	0.92	0.91	0.84	0.88	0.91

Best Fit Values of Model Parameters

A533T	0.63	0.72	0.85	0.93	0.87	0.83	0.99
A533G	0.55	0.70	0.91	0.94	0.83	0.86	0.94
G534T	0.68	0.82	0.61	0.83	1.00	1.00	0.83
G534C	0.62	0.76	0.68	0.80	0.98	0.98	0.80
G534A	0.66	0.83	0.63	0.82	1.00	1.00	0.82
A535T	0.57	0.80	0.51	0.74	0.95	0.97	0.72
A535G	0.60	0.83	0.72	0.82	1.00	0.99	0.85
T536C	0.66	0.77	0.72	0.83	0.98	0.98	0.84
T536A	0.65	0.85	0.59	0.82	1.00	1.00	0.82
TG537T	0.77	0.80	0.77	0.93	0.93	0.93	0.93
G537T	0.59	0.82	0.49	0.75	0.98	0.99	0.74
G537C	0.55	0.78	0.83	0.81	0.99	0.98	0.85
G537A	0.49	0.90	0.35	0.39	1.00	0.79	0.47
G538T	0.64	0.84	0.60	0.81	1.00	1.00	0.81
G538C	0.60	0.76	0.76	0.82	0.97	0.99	0.83
G538A	0.59	0.80	0.63	0.80	0.97	1.00	0.79
T539G	0.79	0.89	0.40	0.82	1.00	1.00	0.78
T539C	0.57	0.77	0.82	0.81	0.99	1.00	0.83
T539A	0.68	0.77	0.65	0.86	0.94	1.00	0.81
G540T	0.60	0.89	0.40	0.72	0.99	0.99	0.69
G540A	0.56	0.87	0.35	0.56	0.94	0.97	0.52
A541T	0.59	0.82	0.60	0.78	1.00	0.99	0.80
A541G	0.59	0.77	0.77	0.82	0.98	0.97	0.84
A541C	0.64	0.83	0.68	0.83	1.00	1.00	0.84
A542G	0.61	0.81	0.55	0.77	0.99	0.99	0.77
T543G	0.49	0.54	1.00	0.96	0.62	0.67	0.96
T543C	0.54	0.75	0.96	0.91	0.89	0.88	0.96
T543A	0.61	0.79	0.66	0.80	0.99	0.99	0.82
G544T	0.60	0.88	0.57	0.81	1.00	1.00	0.81
G544C	0.58	0.78	0.70	0.80	0.99	1.00	0.81
G544A	0.55	0.82	0.69	0.78	1.00	1.00	0.81
T545G	0.56	0.83	0.83	0.84	0.99	1.00	0.86
T545C	0.63	0.81	0.70	0.82	0.99	1.00	0.83
T545A	0.54	0.76	0.82	0.80	0.99	0.97	0.83
C546T	0.60	0.86	0.55	0.78	1.00	1.00	0.78
C546A	0.55	0.84	0.50	0.72	1.00	0.97	0.74
A547T	0.62	0.83	0.65	0.81	1.00	1.00	0.82
A547G	0.54	0.76	0.92	0.92	0.87	0.94	0.90
A547C	0.69	0.73	0.86	0.99	0.84	0.85	0.99
T548C	0.58	0.72	0.87	0.93	0.85	0.89	0.91
T548A	0.60	0.77	0.75	0.81	0.99	0.98	0.84
A549G	0.63	0.77	0.74	0.82	0.99	0.99	0.83
A549C	0.59	0.86	0.64	0.80	1.00	1.00	0.81
AT550A	0.73	0.75	0.63	0.82	0.99	0.98	0.82
T550C	0.63	0.80	0.69	0.82	0.99	0.99	0.83
T550A	0.58	0.84	0.59	0.79	1.00	1.00	0.79
TC551T	0.68	0.84	0.57	0.82	0.99	1.00	0.80
C551T	0.64	0.85	0.56	0.81	1.00	1.00	0.81
C551G	0.40	0.73	0.64	0.61	0.79	0.84	0.60
C551A	0.75	0.90	0.55	0.87	1.00	0.98	0.86
C552G	0.65	0.82	0.76	0.84	1.00	0.99	0.86
C552A	0.54	0.83	0.59	0.77	0.99	1.00	0.77
T553G	0.60	0.83	0.71	0.82	1.00	0.99	0.83

Best Fit Values of Model Parameters

T553C	0.60	0.82	0.78	0.85	0.97	1.00	0.85
T553A	0.59	0.82	0.64	0.79	1.00	0.99	0.81
TG554T	0.70	0.73	0.92	1.00	0.84	0.85	1.00
G555C	0.56	0.76	0.95	0.96	0.84	0.88	0.96
G555A	0.57	0.76	0.90	0.91	0.89	0.93	0.91
G556C	0.62	0.79	0.89	0.89	0.94	0.95	0.91
G556A	0.58	0.69	0.97	0.99	0.80	0.83	0.99
T557C	0.60	0.75	0.87	0.89	0.91	0.89	0.94
T557A	0.61	0.69	0.96	1.00	0.80	0.83	1.00
A558T	0.67	0.76	0.73	0.83	0.98	0.97	0.85
A558G	0.62	0.75	0.72	0.80	0.99	0.99	0.80
G559T	0.67	0.84	0.61	0.83	1.00	0.99	0.83
G559A	0.61	0.79	0.74	0.81	1.00	0.99	0.84
A560T	0.60	0.83	0.68	0.81	1.00	1.00	0.82
A560C	0.52	0.89	0.73	0.81	1.00	1.00	0.84
G561C	0.63	0.77	0.70	0.80	1.00	0.99	0.82
G561A	0.59	0.85	0.67	0.81	1.00	0.99	0.83
T562C	0.61	0.75	0.83	0.86	0.94	0.93	0.89
T562A	0.63	0.82	0.75	0.83	1.00	0.99	0.86
TG563T	0.81	0.85	0.75	0.90	0.99	0.99	0.89
G563T	0.52	0.80	0.74	0.78	0.99	0.99	0.81
G563C	0.78	0.73	0.85	1.00	0.85	0.86	1.00
G563A	0.56	0.88	0.54	0.78	1.00	1.00	0.78
G564C	0.69	0.71	0.81	0.99	0.83	0.85	0.97
G564A	0.56	0.68	0.92	0.97	0.80	0.83	0.96
T565G	0.73	0.94	0.23	0.65	1.00	0.98	0.58
T565C	0.59	0.75	0.82	0.84	0.96	0.92	0.89
T565A	0.57	0.85	0.74	0.82	1.00	1.00	0.84
G566T	0.59	0.43	0.88	0.88	0.21	0.27	0.75
G566A	0.63	0.77	0.66	0.81	0.97	1.00	0.80
GC567G	0.75	0.89	0.48	0.85	1.00	1.00	0.81
C567T	0.61	0.81	0.63	0.79	1.00	1.00	0.80
C567G	0.63	0.92	0.25	0.51	0.81	0.92	0.43
C567A	0.61	0.54	0.70	0.79	0.64	0.57	0.90
G568T	0.61	0.87	0.75	0.84	1.00	1.00	0.87
G568A	0.63	0.80	0.70	0.82	0.99	0.99	0.83
G569T	0.60	0.78	0.83	0.84	0.98	0.97	0.87
G569C	0.55	0.68	0.81	0.84	0.89	0.88	0.87
G569A	0.55	0.72	0.85	0.86	0.90	0.91	0.88
GC570G	0.74	0.78	0.82	0.97	0.88	0.90	0.96
C570T	0.54	0.83	0.48	0.71	0.96	0.97	0.70
C570G	0.64	0.91	0.27	0.52	0.97	0.88	0.51
C570A	0.51	0.80	0.75	0.78	1.00	0.99	0.81
C571T	0.58	0.88	0.60	0.80	1.00	1.00	0.81
C571G	0.69	0.73	0.88	0.99	0.83	0.84	1.00
C571A	0.63	0.85	0.87	0.88	0.98	0.99	0.89
CA572C	0.68	0.66	0.97	1.00	0.80	0.81	1.00
A572T	0.57	0.81	0.81	0.81	1.00	0.99	0.84
A572G	0.63	0.82	0.61	0.80	1.00	1.00	0.80
A572C	0.56	0.69	0.90	0.95	0.81	0.85	0.94
A572AG	0.83	0.79	0.90	1.00	0.88	0.88	1.00
G573T	0.63	0.80	0.88	0.89	0.95	0.95	0.91
G573A	0.53	0.77	0.87	0.80	1.00	0.98	0.84

Best Fit Values of Model Parameters

G574T	0.70	0.83	0.77	0.87	0.99	0.99	0.88
G574C	0.61	0.80	0.82	0.84	0.99	0.99	0.86
G574A	0.56	0.70	0.96	0.99	0.79	0.83	0.98
G575T	0.51	0.69	0.98	0.97	0.79	0.82	0.98
G575C	0.62	0.74	0.84	0.92	0.88	0.89	0.93
G575A	0.62	0.75	0.85	0.88	0.93	0.86	0.98
GC576G	0.86	0.90	0.49	0.87	1.00	1.00	0.84
C576T	0.61	0.82	0.62	0.80	1.00	0.99	0.81
C576G	0.66	0.86	0.62	0.83	1.00	0.99	0.84
C576A	0.60	0.86	0.63	0.82	1.00	1.00	0.82
C577T	0.56	0.87	0.47	0.73	1.00	0.99	0.72
C577G	0.45	0.51	1.00	0.90	0.50	0.56	0.89
C577A	0.54	0.85	0.68	0.82	0.97	1.00	0.81
A578T	0.64	0.78	0.70	0.81	1.00	0.99	0.82
A578G	0.62	0.75	0.86	0.92	0.89	0.89	0.95
A578C	0.67	0.61	0.80	0.98	0.76	0.77	0.98
G579T	0.67	0.83	0.66	0.84	1.00	1.00	0.84
G579C	0.64	0.79	0.78	0.84	0.99	0.98	0.86
G579A	0.62	0.71	0.61	0.76	0.97	0.97	0.76
A580T	0.61	0.81	0.65	0.80	0.99	0.99	0.82
A580G	0.62	0.85	0.49	0.77	0.99	0.99	0.76
T581G	0.67	0.95	0.68	0.88	1.00	1.00	0.88
T581C	0.55	0.76	0.79	0.81	0.97	0.99	0.82
T581A	0.60	0.77	0.80	0.83	0.97	0.97	0.85
T581TC	0.47	0.79	0.69	0.73	1.00	1.00	0.75
T581TA	0.59	0.90	0.58	0.82	1.00	1.00	0.82
TG582T	0.74	0.83	0.88	0.97	0.91	0.94	0.95
G582T	0.65	0.79	0.65	0.81	0.99	0.97	0.84
G582A	0.52	0.83	0.44	0.59	0.91	0.91	0.58
G583T	0.43	0.78	0.76	0.72	0.99	0.98	0.77
G583A	0.55	0.72	0.84	0.85	0.92	0.93	0.87
G584T	0.72	0.73	0.73	0.87	0.93	0.83	0.99
G584C	0.43	0.70	1.00	0.92	0.79	0.81	0.95
G584A	0.58	0.71	0.99	1.00	0.80	0.84	1.00
G585T	0.47	0.80	0.77	0.77	0.99	0.99	0.81
G585C	0.54	0.78	0.64	0.75	1.00	0.99	0.78
G585A	0.62	0.74	0.79	0.82	0.97	0.97	0.84
T586G	0.58	0.75	0.76	0.79	0.98	0.94	0.85
T586C	0.60	0.77	0.77	0.84	0.96	0.98	0.83
T586A	0.57	0.74	0.92	0.93	0.87	0.88	0.95
TC587T	0.71	0.77	0.80	0.95	0.89	0.91	0.94
C587T	0.61	0.78	0.68	0.80	0.99	1.00	0.81
C587G	0.43	1.00	1.00	0.86	0.97	0.99	0.97
C587A	0.62	0.86	0.65	0.82	1.00	1.00	0.83
C588T	0.62	0.85	0.70	0.83	1.00	1.00	0.85
C588A	0.50	0.77	0.79	0.77	0.99	1.00	0.80
C589T	0.57	0.82	0.73	0.82	0.98	1.00	0.83
C589G	0.58	0.69	0.75	0.84	0.89	0.97	0.78
C589A	0.57	0.78	0.74	0.80	0.99	0.99	0.82
A590T	0.60	0.77	0.66	0.78	0.99	0.99	0.79
A590G	0.59	0.79	0.74	0.80	1.00	0.98	0.84
A590C	0.48	0.60	0.74	0.86	0.67	0.81	0.72
C591T	0.59	0.85	0.62	0.80	1.00	1.00	0.81

C591G	0.58	0.78	0.72	0.81	0.98	1.00	0.81
C591A	0.59	0.85	0.63	0.81	1.00	1.00	0.81
A592T	0.53	0.82	0.78	0.80	1.00	1.00	0.83
A592G	0.59	0.84	0.56	0.77	1.00	1.00	0.77
A592C	0.49	0.74	0.84	0.78	0.98	1.00	0.80
G593T	0.58	0.77	0.64	0.76	1.00	0.99	0.78
G593A	0.63	0.79	0.75	0.83	0.99	0.99	0.84
A594T	0.56	0.78	0.65	0.77	0.99	0.99	0.78
A594G	0.51	0.85	0.42	0.56	0.94	0.93	0.56
A594C	0.46	0.75	0.81	0.75	0.98	0.99	0.78
G595T	0.59	0.78	0.77	0.82	0.98	0.99	0.83
G595C	0.55	0.67	0.77	0.85	0.85	0.84	0.86
G595A	0.53	0.73	0.93	0.97	0.81	0.91	0.90
C596T	0.62	0.79	0.68	0.80	1.00	0.99	0.82
C596A	0.64	0.76	0.79	0.86	0.95	0.91	0.91
A597T	0.63	0.81	0.78	0.84	0.99	0.98	0.87
A597G	0.58	0.76	0.76	0.81	0.97	0.98	0.82
A597C	0.65	0.70	0.64	0.77	0.99	0.96	0.80
C598T	0.65	0.83	0.68	0.83	1.00	1.00	0.84
C598G	0.59	0.86	0.51	0.77	0.99	1.00	0.76
C598A	0.62	0.80	0.55	0.77	1.00	0.99	0.78
G599A	0.61	0.80	0.72	0.81	1.00	0.98	0.84
C600T	0.41	0.77	0.95	0.77	0.98	0.97	0.83
C600A	0.61	0.79	0.70	0.81	0.99	1.00	0.82
T601C	0.55	0.81	0.64	0.77	0.99	1.00	0.78
T601A	0.62	0.85	0.59	0.81	1.00	1.00	0.81
TC602T	0.77	0.79	0.79	0.96	0.89	0.90	0.96
C602T	0.63	0.82	0.82	0.84	1.00	0.96	0.90
C602G	0.69	0.78	0.68	0.83	0.98	1.00	0.82
C603T	0.52	0.81	0.58	0.73	0.98	0.99	0.73
C603G	0.61	0.79	0.77	0.82	0.99	0.99	0.84
C603A	0.57	0.79	0.66	0.78	0.99	1.00	0.79
CT604C	0.72	0.68	0.90	1.00	0.82	0.83	1.00
T604G	0.63	0.87	0.59	0.82	1.00	1.00	0.82
T604C	0.55	0.78	0.75	0.79	0.99	0.99	0.80
T604A	0.58	0.79	0.74	0.81	0.99	1.00	0.83
T605G	0.61	0.84	0.63	0.81	1.00	1.00	0.81
T605C	0.59	0.80	0.81	0.82	1.00	1.00	0.85
T605A	0.65	0.84	0.56	0.81	1.00	1.00	0.80
TG606T	0.73	0.71	0.80	0.99	0.83	0.83	0.99
G606T	0.63	0.76	0.68	0.81	0.98	0.99	0.82
G606A	0.56	0.83	0.56	0.75	1.00	1.00	0.76
G607T	0.68	0.65	0.56	0.75	0.92	0.86	0.80
G607C	0.60	0.82	0.60	0.78	0.99	0.99	0.78
G607A	0.58	0.79	0.71	0.79	1.00	0.98	0.82
T608C	0.58	0.74	0.70	0.77	0.99	0.99	0.79
T608A	0.63	0.71	0.87	0.98	0.82	0.84	0.98
A609T	0.70	0.85	0.75	0.87	0.99	1.00	0.87
A609G	0.64	0.79	0.75	0.83	0.99	0.98	0.85
T610G	0.71	0.80	0.63	0.83	0.99	0.99	0.82
T610C	0.59	0.83	0.55	0.77	1.00	1.00	0.77
T610A	0.58	0.82	0.69	0.81	0.99	1.00	0.82
C611T	0.61	0.77	0.72	0.80	1.00	0.99	0.82

Best Fit Values of Model Parameters

C611G	0.65	0.87	0.63	0.83	1.00	1.00	0.83
C611A	0.58	0.81	0.64	0.79	1.00	1.00	0.80
C612T	0.59	0.85	0.60	0.79	1.00	1.00	0.80
C612G	0.57	0.83	0.54	0.76	0.99	0.99	0.76
C612A	0.62	0.84	0.61	0.80	1.00	1.00	0.81
CT613C	0.87	0.79	0.91	1.00	0.89	0.90	1.00
T613C	0.65	0.82	0.70	0.83	1.00	0.99	0.84
T613A	0.63	0.78	0.67	0.80	0.99	0.97	0.83
G614T	0.61	0.84	0.59	0.80	1.00	1.00	0.81
G614C	0.72	0.80	0.66	0.84	0.99	1.00	0.83
G614A	0.58	0.83	0.59	0.79	0.99	1.00	0.79
C615T	0.58	0.83	0.60	0.78	0.99	0.99	0.79
C615G	0.64	0.77	0.63	0.79	0.99	0.99	0.80
C615A	0.62	0.78	0.68	0.80	0.99	0.99	0.81
T616C	0.64	0.82	0.69	0.83	1.00	0.99	0.84
G617T	0.76	0.75	0.61	0.83	0.97	0.96	0.84
G617C	0.58	0.81	0.71	0.80	1.00	0.99	0.83
G617A	0.60	0.80	0.71	0.80	1.00	0.97	0.84
GC618G	0.71	0.73	0.97	1.00	0.84	0.85	1.00
C618T	0.59	0.75	0.86	0.89	0.91	0.93	0.89
C618G	0.43	0.77	1.00	0.88	0.86	0.88	0.94
C618A	0.63	0.76	1.00	1.00	0.84	0.86	1.00
C619T	0.66	0.83	0.79	0.85	0.99	0.98	0.88
C619G	0.60	0.77	0.88	0.88	0.94	0.93	0.91
C619A	0.59	0.80	0.86	0.90	0.92	1.00	0.86
C619CT	0.74	0.78	0.96	1.00	0.87	0.89	1.00
CT620C	0.77	0.65	0.86	1.00	0.80	0.81	1.00
T620G	0.65	0.77	0.81	0.87	0.95	0.98	0.87
T620C	0.52	0.74	0.82	0.78	0.99	0.94	0.84
T620A	0.57	0.78	0.73	0.79	0.99	0.98	0.82
T621G	0.61	0.69	0.70	0.80	0.93	0.95	0.80
T621C	0.69	0.81	0.72	0.86	0.98	0.99	0.86
T621A	0.55	0.78	0.83	0.82	0.98	0.98	0.85
T622C	0.70	0.82	0.77	0.86	1.00	0.99	0.88
T622A	0.60	0.81	0.67	0.80	1.00	1.00	0.81
G623T	0.49	0.89	0.31	0.36	1.00	0.84	0.41
G623A	0.60	0.78	0.85	0.83	0.99	0.95	0.89
C624T	0.61	0.79	0.80	0.83	0.98	0.98	0.85
C624G	0.54	0.81	0.65	0.77	0.99	1.00	0.78
C624A	0.67	0.70	0.83	0.98	0.82	0.83	0.98
T625G	0.55	0.78	0.72	0.80	0.98	0.99	0.80
T625C	0.62	0.83	0.68	0.82	1.00	1.00	0.83
T625A	0.53	0.76	0.56	0.71	0.95	0.96	0.71
G626T	0.65	0.66	0.82	0.97	0.80	0.81	0.97
G626A	0.62	0.79	0.69	0.80	1.00	0.99	0.82
C627T	0.59	0.78	0.72	0.80	0.99	0.99	0.82
C627G	0.60	0.82	0.66	0.80	0.99	0.99	0.81
C627A	0.50	0.73	0.92	0.83	0.93	0.89	0.91
T628G	0.51	0.76	0.75	0.75	1.00	0.98	0.78
T628C	0.62	0.84	0.71	0.83	1.00	1.00	0.85
T628A	0.57	0.83	0.63	0.78	1.00	1.00	0.80
TG629T	0.68	0.84	0.74	0.86	0.99	1.00	0.86
G629T	0.60	0.77	0.70	0.79	1.00	0.99	0.81

Best Fit Values of Model Parameters

G629C	0.60	0.78	0.67	0.80	0.99	0.99	0.81
G629A	0.57	0.78	0.65	0.77	0.99	0.99	0.79
C630T	0.58	0.77	0.71	0.82	0.95	1.00	0.80
C630G	0.58	0.83	0.77	0.82	0.99	1.00	0.84
C630A	0.55	0.79	0.75	0.79	0.99	0.99	0.82
T631G	0.49	0.74	0.95	0.86	0.91	0.89	0.92
T631C	0.68	0.81	0.72	0.84	1.00	0.99	0.85
T631A	0.54	0.79	0.78	0.79	0.99	0.99	0.82
T632C	0.62	0.80	0.75	0.82	1.00	0.99	0.84
T632A	0.65	0.83	0.63	0.82	1.00	1.00	0.82
G633T	0.56	0.85	0.61	0.79	1.00	1.00	0.80
G633C	0.62	0.75	0.92	0.98	0.84	0.87	0.97
G633A	0.62	0.79	0.65	0.79	1.00	0.99	0.80
T634C	0.54	0.74	0.75	0.78	0.98	0.98	0.79
T634A	0.53	0.76	0.79	0.78	0.99	0.98	0.82
TG635T	0.74	0.76	0.91	1.00	0.86	0.87	1.00
G635T	0.59	0.72	0.80	0.84	0.94	0.93	0.86
G635C	0.57	0.86	0.52	0.77	0.99	1.00	0.76
G635A	0.62	0.85	0.68	0.83	1.00	1.00	0.84
G636C	0.66	0.80	0.75	0.90	0.92	1.00	0.84
G636A	0.50	0.75	0.93	0.86	0.92	0.92	0.90
C637T	0.59	0.80	0.67	0.79	1.00	1.00	0.80
C637G	0.59	0.74	1.00	1.00	0.81	0.86	1.00
C637A	0.65	0.71	0.91	0.99	0.82	0.84	0.99
T638C	0.62	0.83	0.67	0.82	1.00	1.00	0.83
T638A	0.55	0.83	0.68	0.79	0.99	0.99	0.81
G639T	0.59	0.78	0.83	0.83	0.98	0.98	0.85
G639C	0.57	0.79	0.71	0.79	0.99	0.98	0.82
G639A	0.61	0.76	0.87	0.91	0.90	0.90	0.94
C640T	0.74	0.84	0.73	0.88	0.99	0.99	0.88
C640G	0.88	0.72	0.40	0.78	0.98	0.95	0.75
C640A	0.67	0.81	0.57	0.80	1.00	1.00	0.79
A641T	0.54	0.82	0.85	0.83	0.99	1.00	0.85
A641G	0.65	0.77	0.75	0.87	0.94	0.99	0.83
A641C	0.72	0.87	0.72	0.87	1.00	1.00	0.88
C642T	0.61	0.79	0.70	0.81	0.99	0.99	0.82
C642G	0.68	0.83	0.70	0.85	1.00	0.99	0.86
C642A	0.64	0.85	0.69	0.83	1.00	0.99	0.85
T643G	0.62	0.77	0.65	0.79	0.99	0.99	0.80
T643C	0.63	0.78	0.83	0.85	0.98	0.97	0.87
T643A	0.64	0.79	0.69	0.83	0.99	0.99	0.83
G644T	0.56	0.79	0.81	0.81	0.99	0.99	0.84
G644C	0.58	0.75	0.85	0.86	0.94	0.95	0.87
G644A	0.57	0.78	0.76	0.80	0.99	0.99	0.82
G645T	0.51	0.75	0.84	0.79	0.99	0.99	0.81
G645A	0.60	0.75	0.91	0.97	0.85	0.89	0.95
C646T	0.66	0.89	0.56	0.83	1.00	0.99	0.83
C646G	0.62	0.88	0.69	0.84	1.00	1.00	0.85
C646A	0.55	0.86	0.73	0.82	1.00	1.00	0.84
G647T	0.34	0.83	0.72	0.65	0.99	0.98	0.70
G647C	0.62	0.85	0.51	0.78	1.00	0.99	0.78
G647A	0.62	0.83	0.66	0.82	1.00	1.00	0.82
A648T	0.58	0.76	0.71	0.80	0.98	0.99	0.81

Best Fit Values of Model Parameters

A648G	0.59	0.87	0.54	0.78	1.00	1.00	0.79
A648C	0.57	0.80	0.68	0.79	1.00	1.00	0.82
C649T	0.61	0.81	0.67	0.81	1.00	0.99	0.83
C649G	0.72	0.80	0.76	0.88	0.97	0.99	0.87
C649A	0.67	0.78	0.79	0.87	0.96	0.93	0.91
T650G	0.54	0.71	0.80	0.79	0.96	0.93	0.84
T650C	0.61	0.84	0.55	0.79	1.00	1.00	0.78
T650A	0.56	0.80	0.66	0.78	1.00	0.99	0.80
G651T	0.66	0.80	0.76	0.85	0.98	1.00	0.85
G651C	0.59	0.68	0.63	0.76	0.92	0.95	0.74
G651A	0.57	0.79	0.72	0.79	0.99	0.98	0.82
C652T	0.58	0.81	0.65	0.79	1.00	1.00	0.80
C652G	0.62	0.81	0.93	0.93	0.92	0.93	0.95
C652A	0.50	0.81	0.93	0.82	0.99	0.98	0.86
A653T	0.65	0.75	0.66	0.82	0.96	1.00	0.80
A653G	0.66	0.89	0.44	0.79	1.00	1.00	0.76
A653C	0.61	0.80	0.56	0.77	0.99	0.99	0.77
C654T	0.49	0.75	0.90	0.85	0.91	0.96	0.84
C654G	0.61	0.87	0.59	0.82	1.00	1.00	0.82
C654A	0.57	0.81	0.75	0.82	0.98	1.00	0.83
T655G	0.49	0.72	0.92	0.87	0.88	0.90	0.89
T655C	0.60	0.81	0.69	0.81	0.99	1.00	0.82
T655A	0.61	0.80	0.70	0.81	1.00	0.99	0.83
TG656T	0.57	0.64	0.99	1.00	0.74	0.78	1.00
G656T	0.60	0.79	0.72	0.81	0.99	0.98	0.83
G656C	0.63	0.84	0.76	0.84	1.00	0.99	0.87
G656A	0.61	0.80	0.64	0.80	0.99	1.00	0.80
G657C	0.60	0.79	0.82	0.83	0.98	0.96	0.87
G657A	0.59	0.77	0.79	0.82	0.98	0.98	0.84
T658G	0.56	0.91	0.57	0.79	1.00	1.00	0.80
T658C	0.61	0.80	0.70	0.81	1.00	0.99	0.82
T658A	0.49	0.75	0.81	0.77	0.99	0.99	0.79
C659T	0.65	0.83	0.61	0.82	1.00	1.00	0.82
C659A	0.70	0.78	0.57	0.80	1.00	0.99	0.80
T660C	0.62	0.81	0.61	0.79	1.00	0.99	0.80
T660A	0.57	0.78	0.67	0.78	0.99	0.99	0.79
T661G	0.81	0.80	0.60	0.86	0.98	0.99	0.83
T661C	0.65	0.81	0.65	0.82	1.00	1.00	0.82
T661A	0.62	0.79	0.74	0.82	0.99	1.00	0.83
C662T	0.63	0.87	0.45	0.76	0.99	0.99	0.74
C662A	0.63	0.90	0.51	0.82	1.00	1.00	0.80
A663T	0.60	0.83	0.64	0.80	1.00	1.00	0.81
A663G	0.61	0.80	0.76	0.82	0.99	0.99	0.84
A663C	0.59	0.78	0.54	0.73	0.99	1.00	0.73
G664T	0.64	0.82	0.70	0.83	1.00	1.00	0.84
G664C	0.62	0.81	0.58	0.79	0.99	1.00	0.79
G664A	0.54	0.70	0.81	0.82	0.91	0.91	0.85
C665T	0.61	0.82	0.63	0.80	1.00	0.99	0.81
C665G	0.64	0.87	0.69	0.84	1.00	0.99	0.86
C665A	0.61	0.78	0.66	0.80	0.98	0.99	0.80
T666G	0.71	0.83	0.41	0.78	0.98	1.00	0.73
T666C	0.68	0.81	0.57	0.80	1.00	1.00	0.80
T666A	0.57	0.77	0.77	0.80	0.99	0.98	0.83

Best Fit Values of Model Parameters

A667T	0.59	0.74	0.75	0.81	0.97	0.97	0.83
A667G	0.57	0.81	0.68	0.79	1.00	1.00	0.81
C668T	0.62	0.82	0.68	0.82	1.00	1.00	0.83
C668A	0.59	0.86	0.67	0.82	1.00	1.00	0.83
T669G	0.65	0.63	0.66	0.83	0.86	0.85	0.85
T669C	0.63	0.81	0.63	0.81	0.99	1.00	0.81
T669A	0.60	0.82	0.76	0.83	1.00	0.99	0.86
TG670T	0.74	0.66	0.96	1.00	0.81	0.83	1.00
G670T	0.61	0.83	0.68	0.81	1.00	0.99	0.83
G670C	0.54	0.80	0.79	0.80	0.99	1.00	0.83
G670A	0.67	0.78	0.66	0.82	1.00	1.00	0.82
G671T	0.73	0.74	0.96	1.00	0.84	0.86	1.00
G671A	0.54	0.76	0.76	0.79	0.98	0.99	0.81
GT672G	0.81	0.94	0.98	0.94	0.99	0.98	0.98
T672G	0.71	0.86	0.62	0.87	0.99	1.00	0.85
T672C	0.64	0.75	0.75	0.83	0.97	0.98	0.83
T672A	0.57	0.79	0.73	0.80	0.99	0.98	0.83
TG673T	0.76	0.83	0.73	0.87	1.00	0.99	0.88
G673T	0.63	0.78	0.75	0.82	0.99	0.99	0.84
G673C	0.42	0.77	0.79	0.72	0.98	0.99	0.75
G673A	0.62	0.78	0.63	0.79	0.99	0.98	0.80
G674T	0.59	0.77	0.73	0.79	1.00	0.93	0.87
G674C	0.64	0.84	0.59	0.82	0.99	1.00	0.81
G674A	0.51	0.77	0.86	0.80	0.99	0.98	0.84
C675T	0.62	0.83	0.72	0.83	1.00	0.99	0.85
C675G	0.72	0.84	0.59	0.84	1.00	1.00	0.83
C675A	0.61	0.75	0.70	0.80	0.98	0.98	0.81
G676T	0.63	0.85	0.59	0.82	1.00	1.00	0.81
G676C	0.48	0.76	0.82	0.77	0.99	0.99	0.80
G676A	0.66	0.83	0.62	0.82	1.00	1.00	0.82
G677T	0.74	0.85	0.61	0.86	1.00	1.00	0.85
G677A	0.58	0.62	0.65	0.73	0.86	0.74	0.86
A678T	0.65	0.80	0.66	0.81	0.99	0.99	0.81
A678G	0.62	0.83	0.59	0.80	0.99	1.00	0.79
AG679A	0.79	0.82	0.93	1.00	0.89	0.90	1.00
G679T	0.59	0.76	0.75	0.80	0.99	0.99	0.82
G679A	0.58	0.80	0.81	0.82	0.99	1.00	0.85
G680T	0.55	0.73	0.71	0.78	0.96	1.00	0.76
G680A	0.66	0.80	0.72	0.84	0.99	1.00	0.84
GA681G	0.80	0.87	0.83	0.93	0.97	1.00	0.91
A681T	0.66	0.80	0.57	0.79	1.00	1.00	0.78
A681G	0.64	0.87	0.72	0.85	1.00	1.00	0.86
A682T	0.60	0.81	0.71	0.81	0.99	0.99	0.83
A682G	0.67	0.84	0.63	0.83	1.00	0.99	0.84
G683T	0.64	0.76	0.82	0.87	0.94	0.90	0.94
G683C	0.64	0.69	0.77	0.91	0.86	0.86	0.92
G683A	0.49	0.75	0.80	0.76	0.98	0.99	0.79
C684T	0.65	0.80	0.70	0.82	0.99	0.99	0.83
C684G	0.66	0.91	0.53	0.85	1.00	1.00	0.83
C684A	0.56	0.79	0.75	0.81	0.98	1.00	0.82
A685T	0.61	0.79	0.71	0.81	1.00	0.99	0.82
A685G	0.61	0.79	0.71	0.81	0.99	0.98	0.83
A685C	0.49	0.78	0.60	0.71	0.98	0.99	0.72

Best Fit Values of Model Parameters

G686T	0.55	0.79	0.76	0.81	0.98	1.00	0.82
G686C	0.72	0.78	0.70	0.85	0.98	0.98	0.85
G686A	0.56	0.75	0.75	0.78	1.00	0.99	0.80
C687T	0.65	0.77	0.62	0.82	0.97	0.99	0.80
C687G	0.61	0.78	0.57	0.76	0.99	0.98	0.77
C687A	0.62	0.85	0.68	0.83	1.00	1.00	0.85
T688G	0.61	0.78	0.69	0.80	1.00	0.99	0.81
T688C	0.55	0.76	0.68	0.78	0.97	1.00	0.77
T688A	0.60	0.79	0.63	0.80	0.97	1.00	0.78
A689T	0.66	0.78	0.70	0.82	1.00	0.99	0.83
A689G	0.63	0.78	0.74	0.83	0.99	0.99	0.84
A689C	0.66	0.80	0.76	0.83	1.00	1.00	0.85
G690T	0.79	0.89	0.57	0.90	0.97	1.00	0.85
G690C	0.78	0.91	0.69	0.90	1.00	1.00	0.90
G690A	0.62	0.91	0.33	0.64	0.96	0.93	0.61
G691T	0.93	0.79	0.07	0.64	0.51	0.50	0.28
G691A	0.60	0.89	0.07	0.37	0.58	0.29	0.27
T692G	0.79	0.86	0.04	0.53	0.55	0.48	0.16
T692C	0.66	0.81	0.11	0.36	0.61	0.22	0.49
T692A	0.69	0.84	0.05	0.27	0.83	0.10	0.67
G693T	0.43	0.84	0.16	0.28	0.53	0.17	0.47
G693C	0.86	0.90	0.25	0.76	1.00	0.99	0.68
G693A	0.50	0.75	0.79	0.78	0.98	0.99	0.80
A694T	0.60	0.90	0.14	0.52	0.46	0.52	0.27
A694G	0.57	0.90	0.28	0.43	0.92	0.94	0.37
A694C	0.59	0.96	0.32	0.69	0.99	0.98	0.65
G695T	0.54	0.90	0.29	0.61	0.54	0.84	0.34
G695A	0.66	0.88	0.12	0.46	0.58	0.44	0.34
T696C	0.72	0.88	0.44	0.81	1.00	1.00	0.78
T696A	0.74	0.87	0.64	0.87	1.00	0.97	0.89
T697G	0.91	0.79	0.78	1.00	0.89	0.87	1.00
T697C	0.66	0.83	0.63	0.83	1.00	0.99	0.83
T697A	0.49	0.72	0.78	0.75	0.97	0.96	0.79
C698T	0.64	0.80	0.71	0.83	0.98	0.99	0.84
C698A	0.53	0.74	0.71	0.75	0.98	0.99	0.76
T699C	0.55	0.77	0.77	0.78	1.00	0.98	0.82
T699A	0.57	0.81	0.69	0.79	1.00	0.99	0.81
C700T	0.53	0.79	0.74	0.78	1.00	1.00	0.80
C700G	0.66	0.79	0.68	0.87	0.94	1.00	0.83
C700A	0.60	0.78	0.59	0.77	0.99	1.00	0.77
T701G	0.37	0.91	0.96	0.80	0.98	1.00	0.87
T701C	0.61	0.78	0.66	0.79	0.99	0.99	0.80
T701A	0.58	0.81	0.73	0.81	1.00	1.00	0.83
TG702T	0.80	0.72	0.82	1.00	0.84	0.84	1.00
G702T	0.64	0.79	0.87	0.90	0.93	0.92	0.94
G702C	0.55	0.83	0.68	0.79	0.99	1.00	0.81
G702A	0.60	0.81	0.73	0.82	1.00	1.00	0.83
C703T	0.53	0.78	0.80	0.80	0.99	0.99	0.83
C703G	0.39	0.65	0.96	0.80	0.83	0.81	0.89
C703A	0.61	0.78	0.61	0.78	0.99	1.00	0.78
CT704C	0.69	0.77	0.77	0.87	0.96	0.93	0.91
T704G	0.72	0.80	0.84	0.96	0.90	0.92	0.96
T704C	0.54	0.77	0.76	0.78	1.00	0.96	0.84

Best Fit Values of Model Parameters

T704A	0.64	0.77	0.70	0.81	1.00	1.00	0.82
T704TC	0.35	0.78	1.00	0.79	0.90	0.89	0.91

The following tables were obtained with the Human Splicing Finder, Version 3.1

ESE Finder matrices for SRp40, SC35, SF2/ASF and SRp55 proteins

Sequence Position	cDNA Position	Linked SR protein	Enhancer motif
+3	SRp40	TGAGAGG	84.79
+11	SC35	AGCTTCCA	76.46
+12	SC35	GCTTCCAG	76.34
+16	SRp40	CCAGAGC	82.46
+17	SF2/ASF (IgM-BRCA1)	CAGAGCA	80.54
+17	SF2/ASF	CAGAGCA	80.02
+20	SRp55	AGCAGC	74.95
+23	SRp55	AGCAGC	74.95
+25	SF2/ASF (IgM-BRCA1)	CAGCTGT	76.00
+25	SF2/ASF	CAGCTGT	76.06
+31	SRp55	TGCCGC	76.16
+33	SF2/ASF (IgM-BRCA1)	CCGCCTT	72.77
+42	SRp55	TGAATA	76.10
+51	SC35	GGTCCGAG	84.63
+58	SC35	GACCCCCA	91.09
+60	SF2/ASF (IgM-BRCA1)	CCCCCAG	72.38
+61	SRp40	CCCCAGG	83.47
+61	SF2/ASF (IgM-BRCA1)	CCCCAGG	71.38
+62	SF2/ASF (IgM-BRCA1)	CCCAGGG	87.62
+62	SF2/ASF	CCCAGGG	82.18
+74	SRp40	TGGCAGG	79.46
+75	SF2/ASF (IgM-BRCA1)	GGCAGGG	72.77
+75	SF2/ASF	GGCAGGG	80.37
+85	SF2/ASF (IgM-BRCA1)	CTGAGTG	74.69
+86	SRp40	TGAGTGC	78.20
+90	SC35	TGCCCGAG	75.54
+90	SF2/ASF (IgM-BRCA1)	TGCCCGA	73.00
+90	SF2/ASF	TGCCCGA	74.43
+93	SF2/ASF (IgM-BRCA1)	CCGAGGG	84.69
+93	SF2/ASF	CCGAGGG	80.72
+105	SC35	AGCTGCTG	82.36
+107	SRp40	CTGCTGG	78.86
+107	SF2/ASF (IgM-BRCA1)	CTGCTGG	71.15

+116	SRp40	TTACACT	82.04
+118	SRp40	ACACTGC	87.13
+121	SF2/ASF (IgM-BRCA1)	CTGCCTG	73.15
+122	SRp40	TGCCTGG	79.22
+127	SC35	GGCTTTCG	79.41
+133	SRp55	CGCTTC	76.04
+134	SC35	GCTTCCTA	79.84
+139	SRp40	CTACCCC	78.62
+140	SC35	TACCCCCA	78.49
+145	SRp40	CCACCCC	80.48
+146	SF2/ASF (IgM-BRCA1)	CACCCCA	81.92
+146	SF2/ASF	CACCCCA	79.27
+155	SF2/ASF (IgM-BRCA1)	CACCCAG	77.62
+155	SF2/ASF	CACCCAG	75.01
+157	SF2/ASF (IgM-BRCA1)	CCCAGTG	75.69
+158	SRp40	CCAGTGC	80.96
+173	SC35	TTCCACTG	80.52
+175	SRp40	CCACTGA	82.10
+184	SRp40	CCTGAGG	81.26
+185	SF2/ASF (IgM-BRCA1)	CTGAGGA	89.92
+185	SF2/ASF	CTGAGGA	88.47
+186	SRp55	TGAGGA	74.82
+205	SRp40	TTTGAGG	81.56
+216	SRp40	TGTAAGG	79.40
+229	SF2/ASF (IgM-BRCA1)	GGCAGGG	72.77
+229	SF2/ASF	GGCAGGG	80.37
+262	SF2/ASF (IgM-BRCA1)	CAGCCTA	79.77
+262	SF2/ASF	CAGCCTA	80.43
+264	SC35	GCCTACTG	83.22
+266	SRp40	CTACTGG	94.49
+275	SC35	GGTCCTCA	79.23
+278	SRp40	CCTCATG	79.46
+279	SF2/ASF (IgM-BRCA1)	CTCATGA	80.54
+279	SF2/ASF	CTCATGA	78.80
+289	SRp40	TCTCTGC	87.13
+292	SRp40	CTGCAGG	80.36
+293	SRp55	TGCAGG	75.65
+293	SF2/ASF (IgM-BRCA1)	TGCAGGA	74.54
+293	SF2/ASF	TGCAGGA	76.65
+297	SC35	GGATATTG	78.92
+309	SC35	GGGCGCTG	80.33
+315	SRp55	TGTGGC	80.97
+320	SF2/ASF (IgM-BRCA1)	CTGACTG	76.31

+320	SF2/ASF	CTGACTG	75.42
+321	SRp40	TGACTGT	79.34
+325	SRp55	TGTGTG	74.82
+329	SRp55	TGGGTA	74.12
+341	SC35	TGACCGTG	75.60
+344	SF2/ASF (IgM-BRCA1)	CCGTGGG	71.92
+354	SRp40	TGAGAGC	79.70
+358	SC35	AGCTGCCA	75.66
+360	SF2/ASF (IgM-BRCA1)	CTGCCAG	71.38
+365	SF2/ASF (IgM-BRCA1)	AGCACGA	75.92
+365	SF2/ASF	AGCACGA	82.76
+375	SF2/ASF (IgM-BRCA1)	CCGGGGG	71.46
+376	SF2/ASF (IgM-BRCA1)	CGGGGGG	78.92
+390	SRp40	TGTCTGC	82.22
+395	SC35	GCCCCCTG	87.52
+396	SF2/ASF (IgM-BRCA1)	CCCCCTG	74.15
+401	SC35	TGCCCCCA	80.70
+403	SF2/ASF (IgM-BRCA1)	CCCCCAT	73.92
+407	SC35	CATCCCTG	81.81
+409	SRp40	TCCCTGC	79.04
+413	SRp55	TGCAGC	86.98
+422	SF2/ASF	GCCAGGA	77.23
+426	SC35	GGATGGTG	81.32
+431	SC35	GTGCCCCA	75.11
+439	SRp40	TTGCAGG	82.51
+440	SRp55	TGCAGG	75.65
+440	SF2/ASF (IgM-BRCA1)	TGCAGGT	72.77
+440	SF2/ASF	TGCAGGT	74.61
+450	SF2/ASF (IgM-BRCA1)	CAGCCCA	79.00
+450	SF2/ASF	CAGCCCA	77.81
+453	SF2/ASF (IgM-BRCA1)	CCCAGCT	76.46
+455	SF2/ASF (IgM-BRCA1)	CAGCTGG	74.46
+455	SF2/ASF	CAGCTGG	73.85
+461	SC35	GACCTCCC	75.29
+464	SF2/ASF (IgM-BRCA1)	CTCCCTG	76.08
+465	SRp40	TCCCTGG	84.13
+466	SF2/ASF (IgM-BRCA1)	CCCTGGG	74.85
+473	SRp40	AAACACG	78.32
+474	SF2/ASF	AACACGG	81.13
+475	SRp40	ACACGGG	78.44
+476	SF2/ASF (IgM-BRCA1)	CACGGGC	72.00
+482	SF2/ASF (IgM-BRCA1)	CAGAGGG	89.92
+482	SF2/ASF	CAGAGGG	90.74

+487	SC35	GGCCTACA	80.82
+488	SC35	GCCTACAG	76.95
+490	SRp40	CTACAGG	95.99
+500	SC35	GGCCTGAG	83.47
+503	SF2/ASF (IgM-BRCA1)	CTGAGTT	76.23
+503	SF2/ASF	CTGAGTT	74.08
+516	SC35	TGCCCCCA	80.70
+517	SC35	GCCCCCAG	81.25
+518	SF2/ASF (IgM-BRCA1)	CCCCCAG	72.38
+519	SRp40	CCCCAGG	83.47
+519	SF2/ASF (IgM-BRCA1)	CCCCAGG	71.38
+520	SF2/ASF (IgM-BRCA1)	CCCAGGT	89.15
+520	SF2/ASF	CCCAGGT	84.39
+524	SC35	GGTCTGCG	82.30
+527	SF2/ASF (IgM-BRCA1)	CTGCGTA	74.85
+528	SRp55	TGCGTA	93.71
+547	SC35	ATATCCTG	77.63
+553	SRp55	TGGGTA	74.12
+565	SRp55	TGCGGC	90.89
+567	SF2/ASF (IgM-BRCA1)	CGGCCAG	76.92
+568	SC35	GGCCAGGG	77.26
+577	SF2/ASF (IgM-BRCA1)	CAGATGG	77.62
+577	SF2/ASF	CAGATGG	79.62
+583	SC35	GGGTCCCA	77.69
+584	SC35	GGTCCCAC	76.34
+585	SC35	GTCCCACA	81.50
+587	SF2/ASF (IgM-BRCA1)	CCCACAG	75.54
+588	SRp40	CCACAGA	83.59
+589	SRp55	CACAGA	75.40
+589	SF2/ASF (IgM-BRCA1)	CACAGAG	79.15
+589	SF2/ASF	CACAGAG	77.23
+590	SRp40	ACAGAGC	78.32
+591	SF2/ASF (IgM-BRCA1)	CAGAGCA	80.54
+591	SF2/ASF	CAGAGCA	80.02
+598	SF2/ASF (IgM-BRCA1)	CGCTCCT	72.77
+607	SC35	GTATCCTG	88.38
+613	SRp55	TGCTGC	76.16
+615	SF2/ASF (IgM-BRCA1)	CTGCCTT	74.69
+622	SRp55	TGCTGC	76.16
+622	SC35	TGCTGCTG	80.52
+625	SRp55	TGCTGC	76.16
+628	SC35	TGCTTGTG	75.72
+632	SRp55	TGTGGC	80.97

+639	SRp40	GCACTGG	83.53
+640	SF2/ASF (IgM-BRCA1)	CACTGGC	72.46
+642	SF2/ASF (IgM-BRCA1)	CTGGCGA	78.31
+642	SF2/ASF	CTGGCGA	75.13
+644	SC35	GGCGACTG	80.58
+646	SRp40	CGACTGC	86.35
+651	SRp40	GCACTGG	83.53
+652	SF2/ASF (IgM-BRCA1)	CACTGGT	81.62
+652	SF2/ASF	CACTGGT	80.14
+657	SC35	GTCTTCAG	83.65
+659	SRp40	CTTCAGC	84.61
+663	SC35	AGCTACTG	84.94
+665	SRp40	CTACTGG	94.49
+675	SF2/ASF (IgM-BRCA1)	CGGAGGA	95.46
+675	SF2/ASF	CGGAGGA	92.37
+682	SRp55	AGCAGC	74.95
+695	SC35	GTTCTCTG	87.83
+697	SRp40	TCTCTGC	87.13

RESCUE ESE hexamers

Fairbrother WG, Yeh RF, Sharp PA, Burge CB. Predictive identification of exonic splicing enhancers in human genes. Science. 2002 Aug 9;297(5583):1007-13

Sequence Position	cDNA Position	Enhancer motif
40	+40	CCTGAA
100	+100	GATGGA
177	+177	ACTGAA
178	+178	CTGAAG
179	+179	TGAAGC
187	+187	GAGGAG
248	+248	CTGAAA
249	+249	TGAAAG
321	+321	TGACTG
335	+335	TCAACG
471	+471	GGAAAC
472	+472	GAAACA
482	+482	CAGAGG
658	+658	TCTTCA
659	+659	CTTCAG
676	+676	GGAGGA
677	+677	GAGGAA
678	+678	AGGAAG

680	+680	GAAGCA
681	+681	AAGCAG

Predicted PESE Octamers from Zhang & Chasin.

Zhang XH, Chasin LA. Computational definition of sequence motifs governing constitutive exon splicing. Genes Dev. 2004 Jun 1;18(11):1241-50

Sequence Position	cDNA Position	Enhancer motif	Motif value (0-100)
9	+9	GCAGCTTC	30.44
21	+21	GCAGCAGC	10.87
24	+24	GCAGCTGT	39.34
25	+25	CAGCTGTG	38.37
57	+57	AGACCCCC	38.13
81	+81	GAATCTGA	30.83
101	+101	ATGGAGCT	30.38
156	+156	ACCCAGTG	26.53
176	+176	CACTGAAG	38.12
177	+177	ACTGAAGC	37.74
184	+184	CCTGAGGA	44.48
185	+185	CTGAGGAG	48.52
186	+186	TGAGGAGC	40.81
187	+187	GAGGAGCA	57.89
188	+188	AGGAGCAT	33.2
245	+245	GATCTGAA	36.71
268	+268	ACTGGCTG	31.31
338	+338	ACGTGACC	31.54
360	+360	CTGCCAGC	47.59
454	+454	CCAGCTGG	42.69
455	+455	CAGCTGGA	49.24
457	+457	GCTGGACC	40.48
505	+505	GAGTTGCC	30.64
508	+508	TTGCCACC	24.19
511	+511	CCACCTGC	26.78
513	+513	ACCTGCCC	55
609	+609	ATCCTGCT	23.21
610	+610	TCCTGCTG	44.28
618	+618	CCTTTGCT	32.21
622	+622	TGCTGCTG	34.72
657	+657	GTCTTCAG	34.58
673	+673	GGCGGAGG	1.21
676	+676	GGAGGAAG	47.57
677	+677	GAGGAAGC	42.39

Ratio PESE/PESS: 6.8

Silencer motifs from Sironi et al.

Sironi M, Menozzi G, Riva L, Cagliani R, Comi GP, Bresolin N, Giorda R, Pozzoli U. Silencer elements as possible inhibitors of pseudoexon splicing. Nucleic Acids Res. 2004 Mar 19;32(5):1783-91

Sequence Position	cDNA Position	Sironi's motif	Silencer motif
+1	Motif 2 - [T/G]G[T/A]GGGG	TGTGAGAG	72.42
+3	Motif 1 - CTAGAGGT	TGAGAGGC	80.93
+3	Motif 2 - [T/G]G[T/A]GGGG	TGAGAGGC	80.20
+5	Motif 2 - [T/G]G[T/A]GGGG	AGAGGCAG	62.54
+12	Motif 3 - TCTCCCAA	GCTTCCAG	76.97
+16	Motif 1 - CTAGAGGT	CCAGAGCA	79.23
+29	Motif 2 - [T/G]G[T/A]GGGG	TGTGCCGC	66.35
+36	Motif 3 - TCTCCCAA	CCTTCCTG	69.14
+46	Motif 2 - [T/G]G[T/A]GGGG	TATGTGGT	66.35
+48	Motif 2 - [T/G]G[T/A]GGGG	TGTGGTCC	73.23
+51	Motif 3 - TCTCCCAA	GGTCCGAG	62.64
+55	Motif 1 - CTAGAGGT	CGAGACCC	64.72
+59	Motif 3 - TCTCCCAA	ACCCCCAG	77.56
+63	Motif 1 - CTAGAGGT	CCAGGGAT	68.31
+67	Motif 2 - [T/G]G[T/A]GGGG	GGATGGGT	86.07
+68	Motif 2 - [T/G]G[T/A]GGGG	GATGGGTG	68.12
+70	Motif 2 - [T/G]G[T/A]GGGG	TGGGTGGC	70.71
+71	Motif 2 - [T/G]G[T/A]GGGG	GGGTGGCA	66.56
+72	Motif 2 - [T/G]G[T/A]GGGG	GGTGGCAG	69.35
+75	Motif 2 - [T/G]G[T/A]GGGG	GGCAGGGA	69.39
+76	Motif 2 - [T/G]G[T/A]GGGG	GCAGGGAA	66.30
+86	Motif 2 -	TGAGTGCC	70.18

		[T/G]G[T/A]GGGG		
+92		Motif 1 - CTAGAGGT	CCCGAGGG	72.64
+94		Motif 1 - CTAGAGGT	CGAGGGGA	73.01
+94		Motif 2 - [T/G]G[T/A]GGGG	CGAGGGGA	87.24
+99		Motif 2 - [T/G]G[T/A]GGGG	GGATGGAG	75.24
+100		Motif 2 - [T/G]G[T/A]GGGG	GATGGAGC	63.28
+101		Motif 1 - CTAGAGGT	ATGGAGCT	68.62
+103		Motif 2 - [T/G]G[T/A]GGGG	GGAGCTGC	60.23
+108		Motif 2 - [T/G]G[T/A]GGGG	TGCTGGCT	69.63
+120		Motif 3 - TCTCCCAA	ACTGCCTG	66.29
+134		Motif 3 - TCTCCCAA	GCTTCCTA	71.27
+135		Motif 3 - TCTCCCAA	CTTCCTAC	66.41
+138		Motif 3 - TCTCCCAA	CCTACCCC	67.86
+140		Motif 3 - TCTCCCAA	TACCCCCA	65.38
+141		Motif 3 - TCTCCCAA	ACCCCCAC	77.98
+145		Motif 3 - TCTCCCAA	CCACCCCA	73.01
+146		Motif 3 - TCTCCCAA	CACCCCAT	63.78
+150		Motif 3 - TCTCCCAA	CCATCCAC	63.64
+153		Motif 3 - TCTCCCAA	TCCACCCA	61.63
+154		Motif 3 - TCTCCCAA	CCACCCAG	80.41
+158		Motif 1 - CTAGAGGT	CCAGTGCC	65.60
+160		Motif 3 - TCTCCCAA	AGTGCCAA	65.08
+171		Motif 3 - TCTCCCAA	AGTTCCAC	61.79
+184		Motif 1 - CTAGAGGT	CCTGAGGA	72.58
+186		Motif 2 - [T/G]G[T/A]GGGG	TGAGGAGC	80.20
+193		Motif 3 - TCTCCCAA	CATGCCAT	61.93
+205		Motif 1 - CTAGAGGT	TTTGAGGT	74.76
+205		Motif 2 - [T/G]G[T/A]GGGG	TTTGAGGT	66.35
+207		Motif 2 - [T/G]G[T/A]GGGG	TGAGGTAA	69.37
+216		Motif 2 - [T/G]G[T/A]GGGG	TGTAAGGG	68.11
+217		Motif 2 - [T/G]G[T/A]GGGG	GTAAGGGA	61.98
+218		Motif 1 - CTAGAGGT	TAAGGGAT	60.88
+218		Motif 2 - [T/G]G[T/A]GGGG	TAAGGGAT	69.37
+222		Motif 1 - CTAGAGGT	GGATAGGG	62.30

+222	Motif 2 - [T/G]G[T/A]GGGG	GGATAGGG	69.17
+223	Motif 2 - [T/G]G[T/A]GGGG	GATAGGGG	65.03
+224	Motif 1 - CTAGAGGT	ATAGGGGC	71.07
+224	Motif 2 - [T/G]G[T/A]GGGG	ATAGGGGC	73.38
+225	Motif 2 - [T/G]G[T/A]GGGG	TAGGGGCA	60.69
+229	Motif 2 - [T/G]G[T/A]GGGG	GGCAGGGA	69.39
+230	Motif 2 - [T/G]G[T/A]GGGG	GCAGGGAC	66.30
+238	Motif 2 - [T/G]G[T/A]GGGG	AGTTGGGG	85.37
+239	Motif 2 - [T/G]G[T/A]GGGG	GTTGGGGA	80.18
+253	Motif 2 - [T/G]G[T/A]GGGG	AGTAGGGG	78.18
+254	Motif 1 - CTAGAGGT	GTAGGGGC	68.44
+254	Motif 2 - [T/G]G[T/A]GGGG	GTAGGGGC	77.13
+255	Motif 2 - [T/G]G[T/A]GGGG	TAGGGGCC	60.69
+266	Motif 1 - CTAGAGGT	CTACTGGC	60.99
+271	Motif 2 - [T/G]G[T/A]GGGG	GGCTGGTC	64.52
+283	Motif 3 - TCTCCCAA	TGACCCTC	62.90
+287	Motif 3 - TCTCCCAA	CCTCTCTG	69.14
+293	Motif 2 - [T/G]G[T/A]GGGG	TGCAGGAT	61.64
+300	Motif 2 - [T/G]G[T/A]GGGG	TATTGGGC	75.30
+301	Motif 2 - [T/G]G[T/A]GGGG	ATTGGGCT	66.40
+305	Motif 2 - [T/G]G[T/A]GGGG	GGCTGGGC	76.58
+306	Motif 2 - [T/G]G[T/A]GGGG	GCTGGGCG	70.15
+308	Motif 2 - [T/G]G[T/A]GGGG	TGGGCGCT	60.69
+313	Motif 2 - [T/G]G[T/A]GGGG	GCTGTGGC	63.28
+315	Motif 2 - [T/G]G[T/A]GGGG	TGTGGCTG	71.20
+325	Motif 2 - [T/G]G[T/A]GGGG	TGTGTGGG	83.25

+327	Motif 2 - [T/G]G[T/A]GGGG	TGTGGGTA	88.10
+345	Motif 2 - [T/G]G[T/A]GGGG	CGTGGGTG	78.23
+347	Motif 2 - [T/G]G[T/A]GGGG	TGGGTGGT	70.71
+348	Motif 2 - [T/G]G[T/A]GGGG	GGGTGGTG	64.52
+349	Motif 2 - [T/G]G[T/A]GGGG	GGTGGTGA	80.18
+351	Motif 2 - [T/G]G[T/A]GGGG	TGGTGAGA	62.75
+352	Motif 2 - [T/G]G[T/A]GGGG	GGTGAGAG	69.35
+354	Motif 1 - CTAGAGGT	TGAGAGCT	78.48
+354	Motif 2 - [T/G]G[T/A]GGGG	TGAGAGCT	70.18
+359	Motif 3 - TCTCCCAA	GCTGCCAG	76.97
+367	Motif 1 - CTAGAGGT	CACGAGTT	69.74
+374	Motif 2 - [T/G]G[T/A]GGGG	TCCGGGGG	70.71
+375	Motif 2 - [T/G]G[T/A]GGGG	CCGGGGGG	60.84
+376	Motif 2 - [T/G]G[T/A]GGGG	CGGGGGGA	77.74
+377	Motif 2 - [T/G]G[T/A]GGGG	GGGGGGAC	73.71
+387	Motif 2 - [T/G]G[T/A]GGGG	GGTTGTCT	62.20
+392	Motif 3 - TCTCCCAA	TCTGCCCC	73.67
+395	Motif 3 - TCTCCCAA	GCCCCTG	69.41
+399	Motif 3 - TCTCCCAA	CCTGCCCC	67.86
+401	Motif 3 - TCTCCCAA	TGCCCCA	64.49
+402	Motif 3 - TCTCCCAA	GCCCCAT	75.65
+407	Motif 3 - TCTCCCAA	CATCCCTG	72.88
+417	Motif 2 - [T/G]G[T/A]GGGG	GCTTGGCC	62.20
+426	Motif 2 - [T/G]G[T/A]GGGG	GGATGGTG	74.01
+427	Motif 2 - [T/G]G[T/A]GGGG	GATGGTGC	63.28
+432	Motif 3 - TCTCCCAA	TGCCCCAT	68.71
+440	Motif 2 - [T/G]G[T/A]GGGG	TGCAGGTA	60.41
+444	Motif 2 - [T/G]G[T/A]GGGG	GGTAGGCA	71.91

+450	Motif 3 - TCTCCCAA	CAGCCCAG	66.96
+456	Motif 2 - [T/G]G[T/A]GGGG	AGCTGGAC	62.00
+463	Motif 3 - TCTCCCAA	CCTCCCTG	86.32
+467	Motif 2 - [T/G]G[T/A]GGGG	CCTGGGAA	62.55
+481	Motif 1 - CTAGAGGT	GCAGAGGG	78.78
+481	Motif 2 - [T/G]G[T/A]GGGG	GCAGAGGG	60.23
+483	Motif 2 - [T/G]G[T/A]GGGG	AGAGGGCC	80.25
+490	Motif 1 - CTAGAGGT	CTACAGGC	76.59
+495	Motif 2 - [T/G]G[T/A]GGGG	GGCTGGGC	76.58
+496	Motif 2 - [T/G]G[T/A]GGGG	GCTGGGCC	70.15
+502	Motif 1 - CTAGAGGT	CCTGAGTT	67.52
+504	Motif 2 - [T/G]G[T/A]GGGG	TGAGTTGC	63.30
+507	Motif 3 - TCTCCCAA	GTTGCCAC	64.83
+514	Motif 3 - TCTCCCAA	CCTGCCCC	67.86
+516	Motif 3 - TCTCCCAA	TGCCCCCA	64.49
+517	Motif 3 - TCTCCCAA	GCCCCCAG	78.83
+519	Motif 1 - CTAGAGGT	CCCCAGGT	64.15
+526	Motif 3 - TCTCCCAA	TCTGCGTA	61.48
+531	Motif 1 - CTAGAGGT	GTAGATGG	65.22
+533	Motif 2 - [T/G]G[T/A]GGGG	AGATGGTG	70.26
+534	Motif 2 - [T/G]G[T/A]GGGG	GATGGTGA	63.28
+550	Motif 2 - [T/G]G[T/A]GGGG	TCCTGGGT	62.75
+551	Motif 2 - [T/G]G[T/A]GGGG	CCTGGGTA	61.33
+555	Motif 2 - [T/G]G[T/A]GGGG	GGTAGAGT	65.03
+556	Motif 1 - CTAGAGGT	GTAGAGTG	68.59
+558	Motif 1 - CTAGAGGT	AGAGTGGT	74.65
+558	Motif 2 - [T/G]G[T/A]GGGG	AGAGTGGT	73.38
+560	Motif 2 - [T/G]G[T/A]GGGG	AGTGGTGC	76.43
+562	Motif 2 - [T/G]G[T/A]GGGG	TGGTGCGG	62.75
+563	Motif 2 - [T/G]G[T/A]GGGG	GGTGCGGC	80.18

+565	Motif 2 - [T/G]G[T/A]GGGG	TGCGGCCA	60.69
+566	Motif 3 - TCTCCCAA	GCGGCCAG	61.64
+570	Motif 1 - CTAGAGGT	CCAGGGCC	65.60
+570	Motif 2 - [T/G]G[T/A]GGGG	CCAGGGCC	60.31
+576	Motif 1 - CTAGAGGT	CCAGATGG	71.33
+578	Motif 2 - [T/G]G[T/A]GGGG	AGATGGGG	82.32
+579	Motif 2 - [T/G]G[T/A]GGGG	GATGGGGT	80.18
+581	Motif 2 - [T/G]G[T/A]GGGG	TGGGGTCC	60.69
+584	Motif 3 - TCTCCCAA	GGTCCCAC	80.25
+586	Motif 3 - TCTCCCAA	TCCCACAG	69.03
+590	Motif 1 - CTAGAGGT	ACAGAGCA	72.40
+599	Motif 3 - TCTCCCAA	GCTCCTTG	67.56
+614	Motif 3 - TCTCCCAA	GCTGCCTT	64.38
+630	Motif 1 - CTAGAGGT	CTTGTGGC	62.30
+632	Motif 2 - [T/G]G[T/A]GGGG	TGTGGCTG	71.20
+665	Motif 1 - CTAGAGGT	CTACTGGT	67.50
+668	Motif 1 - CTAGAGGT	CTGGTGGC	62.30
+669	Motif 2 - [T/G]G[T/A]GGGG	TGGTGGCG	69.63
+670	Motif 2 - [T/G]G[T/A]GGGG	GGTGGCGG	80.18
+672	Motif 2 - [T/G]G[T/A]GGGG	TGGCGGAG	61.64
+673	Motif 2 - [T/G]G[T/A]GGGG	GGCGGAGG	67.64
+674	Motif 1 - CTAGAGGT	GCGGAGGA	63.13
+676	Motif 2 - [T/G]G[T/A]GGGG	GGAGGAAG	66.30
+690	Motif 2 - [T/G]G[T/A]GGGG	GGTGAGTT	68.12

ESS decamers from Wang et al.

Wang Z, Rolish ME, Yeo G, Tung V, Mawson M, Burge CB. Systematic identification and analysis of exonic splicing silencers. Cell. 2004 Dec 17;119(6):831-45

Sequence Position	cDNA Position	Silencer motif
210	+210	GGTAAGTGTA

Predicted PESS Octamers from Zhang & Chasin.

Zhang XH, Chasin LA. Computational definition of sequence motifs governing constitutive exon splicing. Genes Dev. 2004 Jun 1;18(11):1241-50

Sequence Position	cDNA Position	Silencer motif	Motif value (0-100)
68	+68	GATGGGTG	26.14
97	+97	GGGGATGG	33.2
375	+375	CCGGGGGG	2.24
493	+493	CAGGCTGG	3.81
533	+533	AGATGGTG	32.13